CHROMOPHORE SHIELDING ON METAL OXIDE SURFACES

by

Yongyi Zhang

A Dissertation submitted to the

Graduate School-Newark

Rutgers, The State University of New Jersey

in partial fulfillment of the requirements

for the degree of

Doctor of Philosophy

Graduate Program in Chemistry

written under the direction of

Professor Elena Galoppini

and approved by

_____

_____

_____

_____

Newark, New Jersey

October, 2010

ABSTRACT OF THE DISSERTATION

Chromophore Shielding on Metal Oxide Surfaces

By Yongyi Zhang

Dissertation Director:
Professor Elena Galoppini

The work present in this thesis is divided into two parts. The common theme is the development of methods to shield chromophores on heterogeneous metal oxide surfaces; and study the effects of shielding on their surface properties.

Part A describes the synthesis of homoleptic ruthenium polypyridine star-shaped complexes with conjugated oligophenylenethylene linkers on each bipyridine ligand to fix the distance between a ruthenium metal center and metal oxide surfaces in all three dimensions. Star complexes did bind covalently to the metal oxide surfaces with bidentate mode. The photophysical properties were influenced by the length of the rigid linkers. On basic TiO_2 films, the injection yields decreased as the linker length increased. The injection process was on 100-150 ns time scale. Recombination rate was largely reduced (10^5 s^{-1} order) compared to the value of rigid-rods (10^7 s^{-1} order) due to well-controlled distance separation.

Part B describes the aggregation study of dye@cyclodextrins on metal oxide surface. Cyclodextrins bound to TiO_2 surface by –OH group. Suitable-sized cyclodextrins were found to separate pyrene and perylene derivative on ZrO_2 surface. Reduced excimer band and enhanced monomer band were observed in fluorescence emission spectra.

Acknowledgement

I would like to express my deep appreciation to my advisor Professor Elena Galoppini for her intelligent suggestion and continuing encouragement during my doctoral research and studies. My appreciation also extends to my colleagues in the group: Dr. Massimiliano Lamberto, Dr Jonathan Rochford, Dr. Olena Taratula, Dr. Sujatha Rochford, Dr. Alfred Lee, Mr. Zhiyong Wu, Ms. Marina Freitag, Mr. Andrew Kopecky, Mr. Keyur Chitre, Ms.Yan Cao, and Ms. Agnieszka Klimczak, for their support and encouragement.

I am very grateful to our collaborator, Professor Gerald. J. Meyer and his students, Dr. Maria Abrahamsson, and Mr. Patrik Johansson in Johns Hopkins University for their great help on photophysical and electrochemical studies. I thank Professor Richard Mendelsohn and Dr. Carol Flach for the generosity on the usage of IR instrument.

Special thank go to my family, especially my wife, Guangru Mao, for their unconditionally support and patient love during my entire graduate study.

Table of Contents

List of Figures

Lists of Tables

List of illustrations

CHAPTER A-1: INTRODUCTION

Light-induced electron transfer from chromophore molecules into the conduction band of wide band gap semiconductor nanoparticles has been intensely studied. This process has been employed in photocatalysis,[1,2] molecular electronics,[3] sensors,[4,5] and dye-sensitized solar cell (DSSC).[6] DSSC was originally developed by O'Regan and Grätzel in early 1990s' with covalent attachment of ruthenium polypyridine complexes to metal oxide nanoparticles through the carboxylic acid anchoring groups.[6] The energy conversion efficiency was ~7%. Since then, a large number of chromophores were designed and tested to improve this device. Part A of this thesis focuses on the kinetics and mechanistic study of charge transfer processes on the nanocrystalline metal oxide thin films by using a novel class of homoleptic ruthenium star complexes developed in our lab and their potential use in DSSC application.

A-1-1. Ruthenium Complexes in DSSC Application

A general configuration of a DSSC is shown in Figure A-1-1.1. The chromophore molecule acts as the photo-sensitizer attached onto metal oxide semiconductor, which is coated on a transparent conductive glass electrode. When combined with a counter-electrode, it forms a sandwich-shape cell filled with electrolyte between two electrodes.

A wide variety of inorganic transition metal complexes and organic chromophores have been used as sensitizers. The most efficient inorganic sensitizers include transition metal complexes of polypyridines, porphyrins, and phthalocyanines.[7] Ruthenium (II) is the metal ion commonly used in polypyridine complexes. In the case of metalloporphyins and metallophthalocyanines, the preferred metal ions are those with full or half-filled d-

orbitals, such as Zn (II), Mg (II) and Al (III). Organic dyes, such as pyrene,[8] perylene,[9] coumarin,[10] anthracene,[11] and other conjugated organic dyes,[12-19] have also been anchored to metal oxide semiconductor surfaces for sensitization purposes due to their higher extinction coefficient, higher quantum yield, and the ability to tune their properties by synthetic modifications.

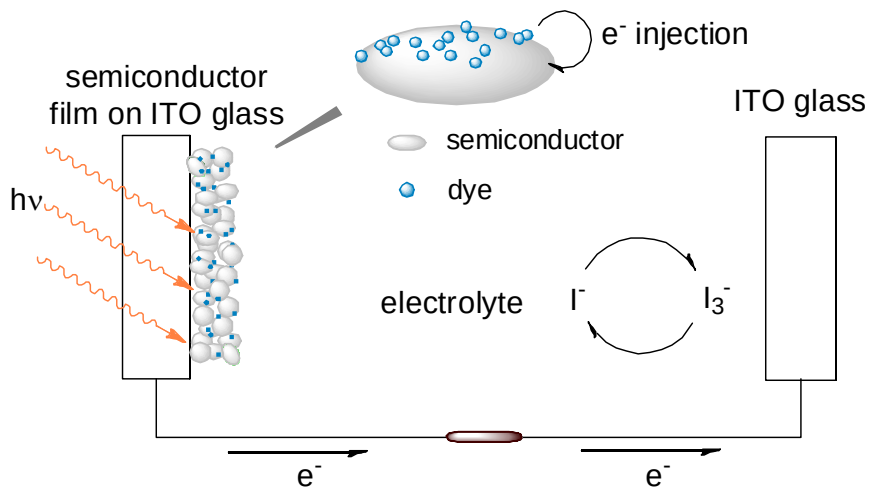

Figure A-1-1.1. A typical DSSC with its components.

Until now the most efficient sensitizers for DSSC application are ruthenium polypyridine complexes N3 and black dye in Figure A-1-1.2. Selected ruthenium complexes for DSSC application are shown in Figure A-1-1.2.

Many of the ruthenium polypyridine sensitizers employed in champion DSSCs are of the form cis-$Ru(LL)_2X_2$, where LL is a 2,2'-bipyridine (bpy) -like ligand and X is a non-chromophoric ligand. The most efficient sensitizer by now is called N3, where LL = 4,4'-dicarboxylic acid bipyridine (dcb) and X = SCN^-, with overall conversion efficiency ~10%.[20] The $Ru^{III/II}$ reduction potential of N3 is more negative as compared to $Ru(bpy)_3^{2+}$, and the absorption and emission maxima shifts to red.[21] The electron density of the

highest occupied molecular orbital (HOMO) shifts from the ruthenium metal center to the isothiocyanate ligands.[22] The metal to ligand charge transfer (MLCT) excited state is localized on the ligand substituted with the –COOH group.[20,23] A similarly successful ruthenium based sensitizer, which based on terpyridine rather than bpy is called 'black dye'. It extends the spectral sensitivity of solar cell significantly towards the red along with a lower extinction coefficient compared to N3.[24]

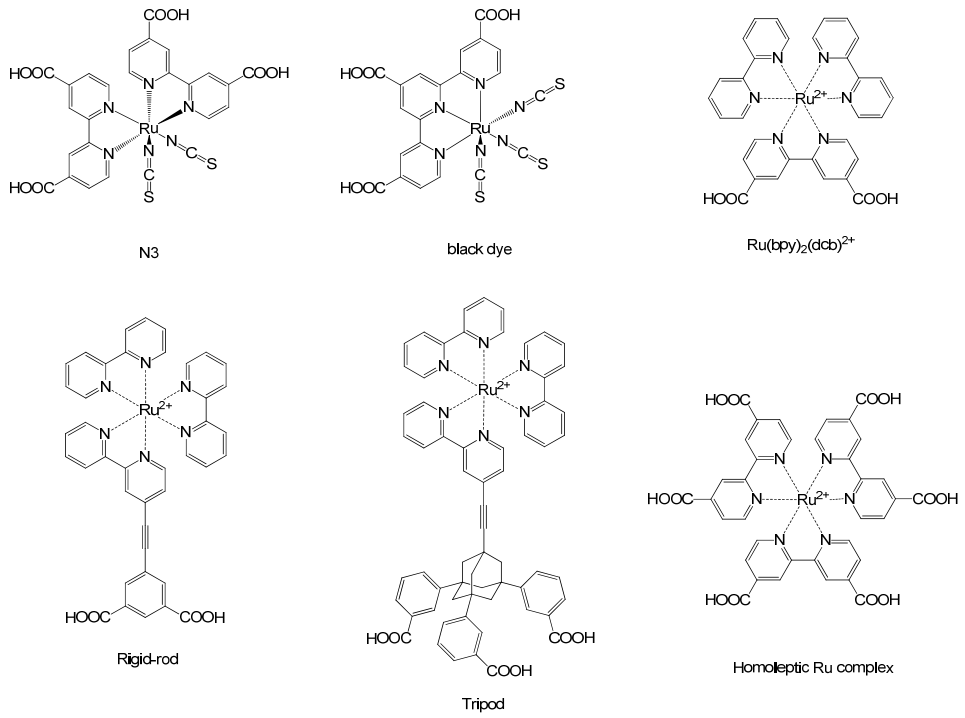

Figure A-1-1.2. Chemical structures of ruthenium polypyridine complexes

Although N3 and closely related analogues give highest solar cell performance, $Ru(bpy)_2(dcb)^{2+}$ derivatives still remain of interest, since the presence of the NCS groups results in lower stability when dye is in its oxidized form.[25] $Ru(bpy)_2(dcb)^{2+}$ has three bpy derivative ligands coordinated to the ruthenium metal center. Upon absorbing a photon, electron is promoted into the lowest unoccupied molecular orbital (LUMO). Fast

intersystem crossing to triplet[26] results in a long lived excited state, which is preferred for the electron injection into the conduction band of semiconductor.

A recent area of interest in electron transfer studies on dye-sensitized semiconductor is the development of anchor-bridge containing linkers. These well-designed linkers are useful to tune the properties of dyes and fundamentally elucidate the electron transfer process at the chromophore-semiconductor interface. Meyer and coworkers for instance, studied the ruthenium polypyridine complexes with flexible hydrocarbon chains terminated with a group for binding.[27,28] Decreased electron injection and recombination rates were observed in these cases. Rigid linkers have later been employed with conjugated π units to separate the ruthenium metal center and semiconductor surface.[29] Our group also focuses the interfacial charge transfer study by using ruthenium polypyridine complexes as well as organic chromophores with rigid linkers (tripods[30-36] and rigid-rods[8,37-42]).

All the complexes mentioned above, including N3 derivatives, black dye, $Ru(bpy)_2(dcb)^{2+}$, and the linker-contained ruthenium polypyridine complexes, are heteroleptic, meaning that more than one type of ligands are coordinated to the ruthenium metal center. Thus the MLCT state is normally delocalized in one of the ligands, for instance the bpy-OPE units in the rigid-rod or tripod systems. As a contrast, ruthenium metal center with all ligands identical is called homoleptic ruthenium complex. A simple example of homoleptic ruthenium complex in DSSC application is $Ru(dcb)_3^{2+}$. After photoexcitation, the electron is promoted to the LUMO. The initial excited state possesses the same structural symmetry as the ground state, and a delocalized electronic

wavefunction on all three ligands each formally possessing 1/3 of an electron charge has been invoked.[21]

A-1-2. Homoleptic Ruthenium Complexes

A common drawback in the syntheses of heteroleptic ruthenium complexes is the multistep-reaction pathway needed for sequential chelation of the appropriate ligands around the metal center. Homoleptic ruthenium complexes appear more attractive by offering a one-step access to highly symmetric dyes. There are numerous examples of applications involving homoleptic complexes of Ru.

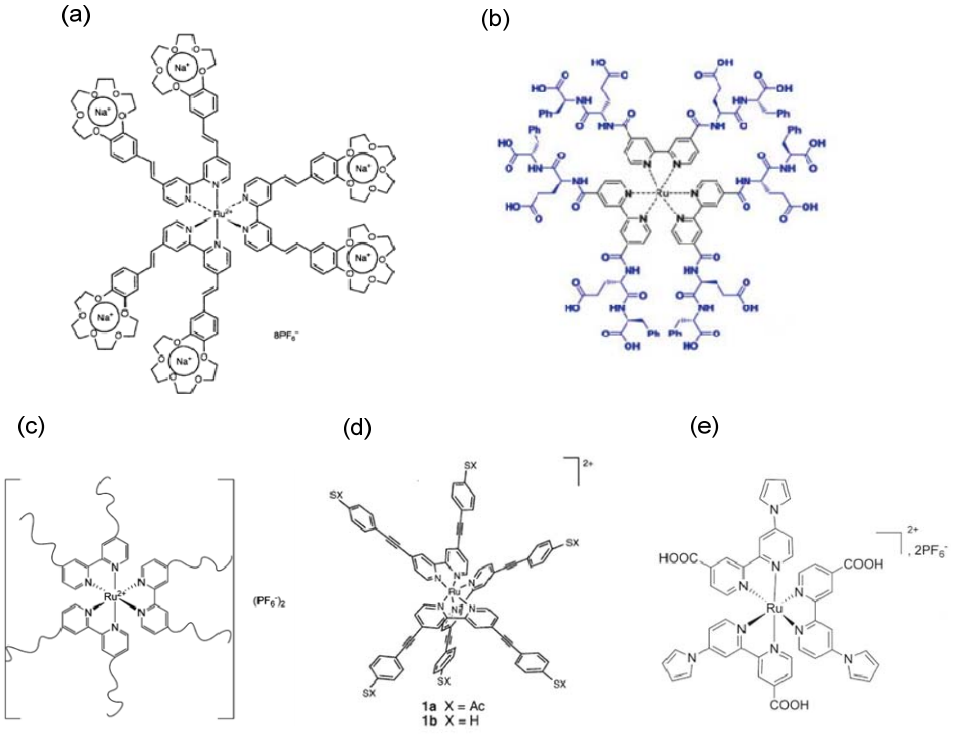

Figure A-1-2-1. (a) Chemical structure of vinyl-linked benzo-crown ether-bpy Ru complex. (b) Chemical structure of dendritic homoleptic Ru complex.[43] (c) Representative Ru tris(bpy)-centered polystyrene complex.[44] (d) Chemical structure of Ru tris(bpy) with rigid linkers. (e) Ru tris(bpy) complex with pyrrolo units.[25]

Beer and coworkers prepared homoleptic ruthenium complexes carrying macrocyclic binding site (Figure A-1-2.1(a)[45,46]) for recognition of Group IA and IIA metal cations as a chemical sensor. The complex was prepared and electropolymerised onto platinum and optically transparent conducting glass electrodes. The alkaline or alkali cation coordinates at the crown ether recognition site resulting in a red-shift of emission maxima.

Homoleptic ruthenium complexes have also been used as a dendrimer core for protein surface recognition.[43,47,48] They carry functional groups in all three dimensions, thus making a diverse array of noncovalent interactions with target protein (Figure A-1-2.1(b)[43]).

Demas and coworkers designed and synthesized ruthenium tris(bpy)-centered polystyrene complex to develop oxygen sensors. The polymer chains provided a homogeneous environment for the sensing moiety and avoided or minimized problems associated with multicomponent sensors. Moreover, the polymer chain can avoid precipitation or aggregation (Figure A-1-2.1(c)[44]).

Otsuki and coworkers synthesized ruthenium homoleptic complexes with fully conjugated OPE ligand (Figure A-1-2.1(d)[49]). The complexes were bound onto gold by the thiol anchoring groups. Single molecules were observed by using scanning tunneling microscopy (STM).

Homoleptic ruthenium complexes, however, have not gained much attention for DSSC application compared to the heteroleptic ones as their MLCT bands are sharper and occur at higher energy.[50] Recently Gros and coworkers reported ruthenium tris(bpy)

complexes containing pyrrolo unites (Figure A-1-2.1(e)[25]) with 65% Incident-Photon-to-electron Conversion Efficiency (IPCE) value.

The homoleptic ruthenium star complexes studied in this thesis were designed with rigid linkers attached on the bipyridine ligand to provide distance and orientation control. This is explained in the following section together with a description of the DSSC.

A-1-3. The Mechanism of Dye-Sensitized Solar Cells

The general mechanism for light to electrical power conversion in DSSC is depicted in Figure A-1-3.1. Briefly: light is absorbed by a sensitizer to promote an electron from the HOMO to the LUMO of the sensitizing dye, following an excited state molecule (S*);[7] the electron in the excited state can either decay to the ground state (relaxation) or inject into the conduction band of the semiconductor, resulting in charge separation (injection); the oxidized sensitizer (S^+) is regenerated by an external electron donor in the electrolyte, normally a redox mediator, iodine/iodide couple (regeneration); the injected electron moves through the nanocrystalline semiconductor network to the external circuit and returns to the counter electrode where it reduces the oxidized electron donor. Thus all oxidation chemistry at the dye-sensitized electrode is reversed at the counter electrode, no net chemical reactions occur and for this reason, the DSSC is also called regenerative.[21]

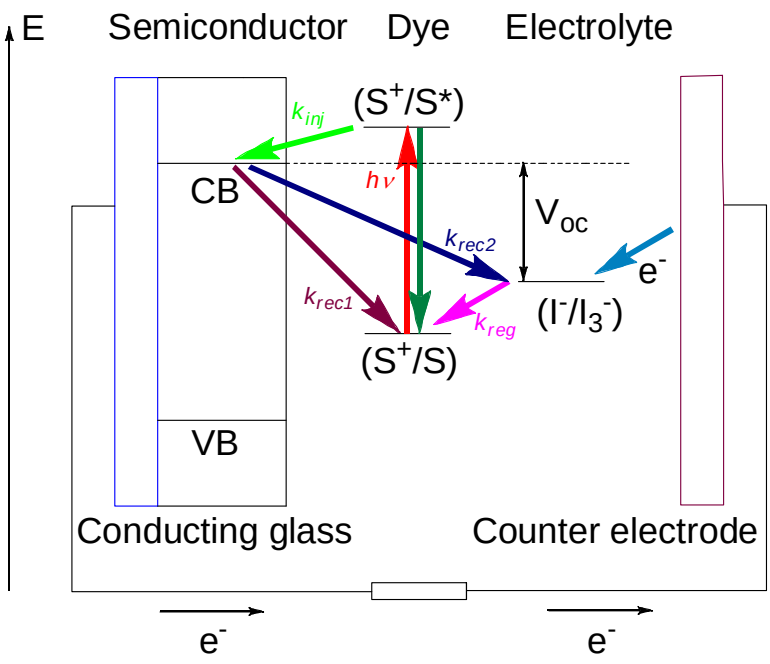

Figure A-1-3.1. The main charge transfer processes of the DSSCs: k_{inj}, injection; k_{reg}, regeneration; k_{rec1} and k_{rec2}, recombination; CB, conduction band; VB, valence band; V_{oc}, open-circuit photovoltage

Some electron transfer process may compete with the processes described above, resulting in lower solar cell efficiency. As shown in the Figure A-1-3.1, after the charge separation step, the electron may recombine with the oxidized sensitizer or the oxidized donor in the electrolyte (recombination). These competitive processes combined with the sensitizer excited state decay or self-quenching can cause energy loss and reduce the solar cell performance. To achieve a high light-to-energy conversion, a DSSC should have significant overlap between dye absorption and solar spectrum, rapid charge separation, efficient dye regeneration and minimum charge recombination. Thus the time scale of the key electronic processes involved in the conversion of light to electricity should be compared and considered for a DSSC. Figure A-1-3.2 shows the area normalized electron transfer rate.[51]

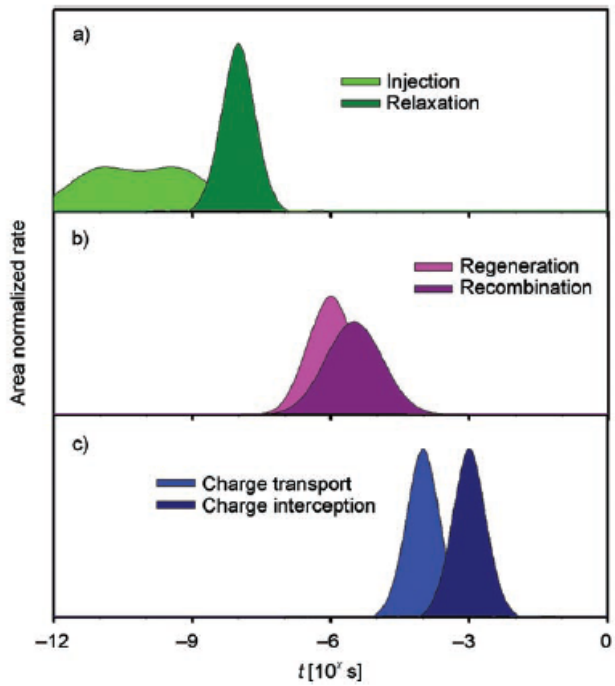

Figure A-1-3.2. Area normalized electron transfer rates for the main charge transfer processes illustrated in figure A-1-3.1[51]

The electron injection rate (k_{inj}) is ultrafast and occurs in the femtosecond and picosecond time domain. Many research groups reported injection in the < 200 fs range[30,52-56] with multiexponential kinetics.[57-61] As an example of Ru complexes, two injection kinetics (< 200 fs and 14-3 ps) have been reported by McCusker and coworkers. The femtosecond injection was attributed to injection from the nonthermalized ^{1}MLCT excited state, and the picosecond injection was attributed to injection from the lowest-energy ^{3}MLCT excited state.[62,63] For example, Willig and coworkers observed different electron injection constant for the same chromophore but with carboxylic and phosphonate anchoring groups.[64,65] Since the excited state is normally in the nanosecond domain, the injection (in the fs to ps range) will dominate and the electron transfer reactions can produce near unity quantum yields for the initial charge separation.

The competitive process charge recombination (k_{rec}), occurs between an electron in metal oxide semiconductor and oxidized center, is in the micro-millisecond domain.[66] This process has been explained by electron trapping within the metal oxide semiconductor film.[67] Although the k_{rec} is slower than the k_{inj}, it still lowers the efficiency of the DSSCs. Thus, minimizing this process while maintaining efficient injection is an attractive way to modify the DSSC. This can be achieved by increase the distance, for instance, by using a bridge unit, between dye metal center and TiO_2 surface, thereby decreasing the rate of recombination, or by stepwise charge transfer processes, by using anchor-donor$_1$-donor$_2$ systems.

A-1-4. Homoleptic Ruthenium Star Complexes Design

Our group has employed oligophenylenethynylene (OPE) units as the rigid linker with isophthalic (Ipa) anchoring group in one end and chromophores in other end to form rigid-rods model dyes. Two carboxylic acid functional groups on the Ipa unit provide strong electronic coupling with metal oxide semiconductor surface.[68] The main purpose to employ the rigid linkers was to develop good to study the charge injection and recombination dynamics. Piotrowiak and coworkers studied the influence of the OPE bridge length on the electron transfer at the sensitizer/semiconductor interface (Figure A-1-4.1[69]). A weak linker length dependence of the injection rates was observed. The injection rate comparison data is shown in Table A-1-4.1.[69] The recombination rates for these series of sensitizers, however, were found to be independent of the linker's length.[39]

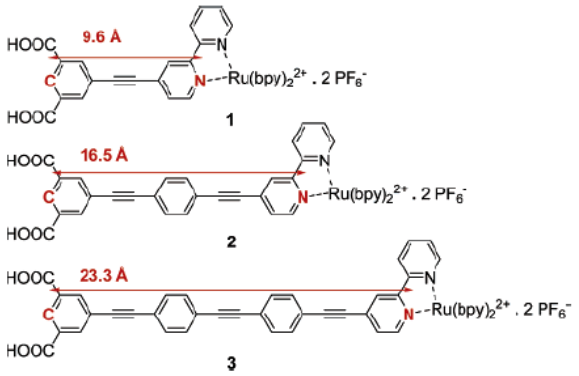

Figure A-1-4.1. Chemical structure of rigid-rods with various bridge lengths[69]

Table A-1-4.1. Electron injection time constants (τ) and amplitudes (A) for rigid-rods[69]

rod	λ_{abs},[a] nm (ϵ, $M^{-}1cm^{-}1$)	C to N length,[b] Å	τ_1,[c] ps (A)	τ_2, ps (A)
1	462 (1.6×10^4)	9.6	7.1 (0.35)	56.2 (0.65)
2	465 (2.0×10^4)	16.5	8.7 (0.28)	66.2 (0.72)
3	465 (2.0×10^4)	23.3	12.9 (0.44)	101.4 (0.56)

a. MLCT band, in CH_3CN solutions. b. Calculated using Spartan'02 (PM3 minimization). c. Probe at 670 nm.

The explanation of the weak distance-dependent of electron injection and recombination rate in these rigid-rod ruthenium (II) complexes is summarized from two aspects according to the recently reported literature as follows:

1) *Distance Control* Diau and coworkers recently reported that the electron injection from a porphyrin-rigid-rod sensitizer can occur not only through the π-conjugated linker (the linker with the anchoring group is similar with the rigid rod studied in our research group) to the anchored metal oxide nanoparticle but also through space to an adjacent nanoparticle (Scheme A-1-4.1). The electron transfer of the localized electrons in dye/TiO_2 nanoparticles films is widely reported not single-exponential. A

rapid back electron transfer component was observed.[70-72] Thus the rigid-rod type sensitizers can't fully separate the dye unit with the metal oxide semiconductor nanoparticle.

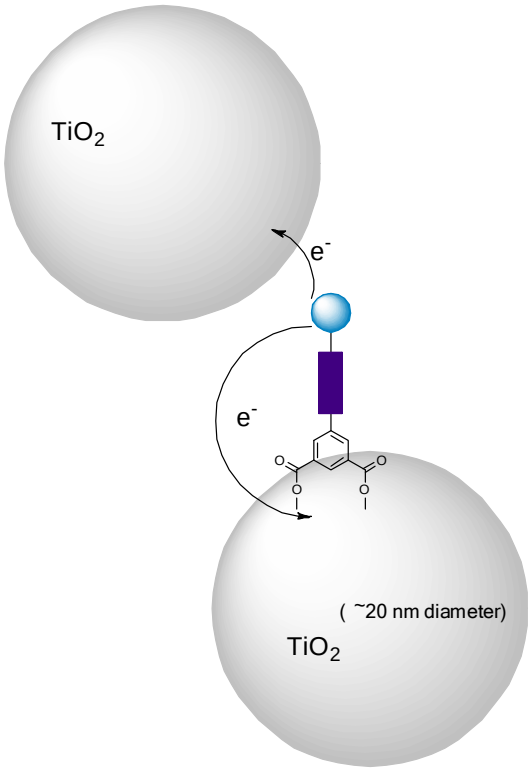

Scheme A-1-4.1. Schematic representation of the role of morphology on electron transfer events at the Dye/TiO_2 interface (not in scale)

2) <u>Orientation Control</u> Orientation on the TiO_2 surface must be considered for the rigid-rods.[41,64,73,74] Persson and coworkers, by using full quantum chemical (B3LYP/VDZ) geometry optimizations, indicated that the energetically preferred anchoring mode of the Ipa linker was by both carboxylic acid anchor groups to a model TiO_2 nanocrystal than a single carboxylic acid anchor group. The surface attachment chemistry causes the rigid rod sensitizers to tilt by approximately 45° relative but not perpendicular to the surface

normal.[41] Thus the real distance between the dye unit and the metal oxide semiconductor surface is not the length of the rigid linker.

To improve both the distance and orientation control of the rigid linkers, homoleptic ruthenium (II) polypyridine star complexes were. The schematic representation of the star sensitizer/TiO_2 interface is shown in Scheme A-1-4.2. The star sensitizers have the rigid linkers attached on each bipyridine ligand to fix the distance between the ruthenium metal center and the metal oxide semiconductor nanoparticles in all three dimensions. The distance between the ruthenium metal center and the metal oxide semiconductor surface is controlled by the length of the rigid linker. The homoleptic ruthenium star complexes shield the ruthenium metal center from the heterogeneous interface. The heterogeneity, surface traps and complexity of nanostructured semiconductors are known to greatly complicate the charge injection and recombination dynamics studies.[21,58] The following chapters of Part A of this thesis will focus on the synthesis of the star sensitizers and their photophysical property studies.

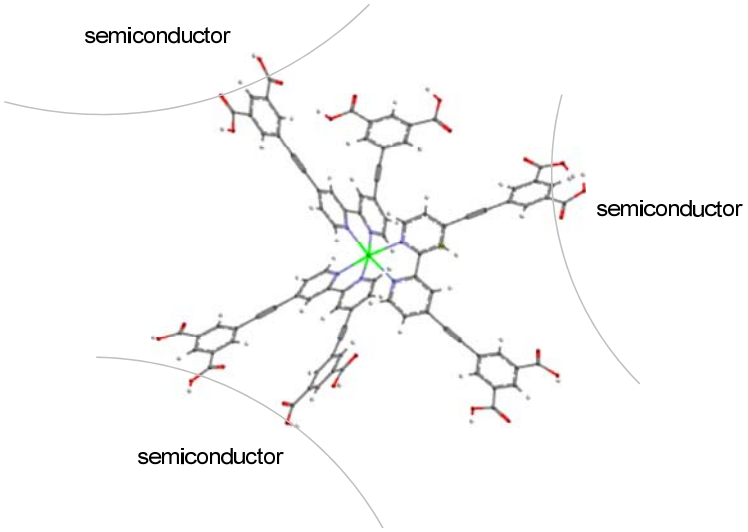

Scheme A-1-4.2. Schematic representation of star sensitizer/TiO_2 interface.

A-1-5. References

1. Serpone, N.; Pelizzetti, E. *Photocatalysis. Fundamentals and Applications.*; John Wiley & Sons: New York, 1989.

2. Kamat, P. V.; Meisel, D. *Semiconductor Nanoclusters: Physical, Chemical and Catalytic Aspects.*; Elsevier: Amsterdam, 1997.

3. Jortner, J.; Ratner, M. *Molecular Electronics*; Blackwell: London, 1997.

4. Manera, M. G.; Leo, G.; Curri, M. L.; Cozzoli, P. D.; Rella, R.; Siciliano, P.; Agostiano, A.; Vasanelli, L. Investigation on Alcohol Vapours/TiO_2 Nanocrystal Thin Films Interaction by SPR Technique for Sensing Application. *Sensors and Actuators B* **2004**, *100*, 75.

5. Comini, E.; Baratto, C.; Faglia, G.; Ferroni, M.; Sberveglieri, G. Single Crystal ZnO Nanowires as Optical and Conductometric Chemical Sensor. *J. Phys. D: Appl. Phys.* **2007**, *40*, 7255.

6. O'Regan, B.; Grätzel, M. A Low-cost, High-efficiency Solar Cell Based on Dye-sensitized Colloidal TiO_2 Films. *Nature* **1991**, *353*, 737.

7. Kalyanasundaram, K.; Grätzel, M. Applications of Functionalized Transition Metal Complexes in Photonic and Optoelectronic Devices. *Coord. Chem. Rev.* **1998**, *177*, 347.

8. Taratula, O.; Rochford, J.; Piotrowiak, P.; Galoppini, E.; Carlisle, R. A.; Meyer, G. J. Pyrene-Terminated Phenylenethynylene Rigid Linkers Anchored to Metal Oxide Nanoparticles. *J. Phys. Chem. B* **2006**, *110*, 15734.

9. Zimmermann, C.; Willig, F.; Ramakrishna, S.; Burfeindt, B.; Pettinger, B.; Eichberger, R.; Storck, W. Experimental Fingerprints of Vibrational Wave-Packet Motion during Ultrafast Heterogeneous Electron Transfer. *J. Phys. Chem. B* **2001**, *105*, 9245.

10. Hara, K.; Sayama, K.; Arakawa, H.; Ohga, Y.; Shinpo, A.; Suga, S. A Coumarin-derivative Dye Sensitized Nanocrystalline TiO_2 Solar Cell Having a High Solar-energy Conversion Efficiency up to 5.6%. *Chem. Commun.* **2001**, 569.

11. Martini, I.; Hodak, J. H.; Hartland, G. V. Effect of Structure on Electron Transfer Reactions between Anthracene Dyes and TiO_2 Nanoparticles. *J. Phys. Chem. B* **1998**, *102*, 9508.

12. Kamat, P. V.; Fox, M. A. Photosensitization of TiO_2 Colloids by Erythrosin B in Acetonitrile. *Chem. Phys. Lett.* **1983**, *102*, 379.

13. Rossetti, R.; Brus, L. E. Time-resolved Raman Scattering Study of Adsorbed, Semioxidized Eosin Y Formed by Excited-state Electron Transfer into Colloidal Titanium(IV) Oxide Particles. *J. Am. Chem. Soc.* **1984**, *106*, 4336.

14. Pelet, S.; Grätzel, M.; Moser, J. Femtosecond Dynamics of Interfacial and Intermolecular Electron Transfer at Eosin-Sensitized Metal Oxide Nanoparticles. *J. Phys. Chem. B* **2003**, *107*, 3215.

15. Kitamura, T.; Ikeda, M.; Shigaki, K.; Inoue, T.; Anderson, N. A.; Ai, X.; Lian, T. Q.; Yanagida, S. Phenyl-Conjugated Oligoene Sensitizers for TiO_2 Solar Cells. *Chem. Mater.* **2004**, *16*, 1806.

16. Ito, S.; Zakeeruddin, S. M.; Humphry-Baker, R.; Liska, P.; Comte, P.; Nazeeruddin, M. K.; Péchy, P.; Takata, M.; Miura, H.; Uchida, S.; Grätzel, M. High-Efficiency Organic-Dye-Sensitized Solar Cells Controlled by Nanocrystalline-TiO_2 Electrode Thickness. *Adv. Mater.* **2006**, *18*, 1202.

17. Hara, K.; Kurashige, M.; Ito, S.; Shinpo, A.; Suga, S.; Sayama, K.; Arakawa, H. Novel Polyene Dyes for Highly Efficient Dye-sensitized Solar Cells. *Chem. Commun.* **2003**, 252.

18. Li, S.-L.; Jiang, K.-J.; Shao, K.-F.; Yang, L.-M. Novel Organic Dyes for Efficient Dye-Sensitized Solar Cells. *Chem. Commun.* **2006**, 2792.

19. Yum, J.-H.; Hagberg, D. P.; Moon, S.-J.; Karlsson, K. M.; Marinado, T.; Sun, L.; Hagfeldt, A.; Nazeeruddin, M. K.; Grätzel, M. A Light-Resistant Organic Sensitizer for Solar-Cell Applications. *Angew. Chem. Int. Ed.* **2009**, *48*, 1576.

20. Nazeeruddin, M. K.; Kay, A.; Rodicio, I.; Humphry-Baker, R.; Mueller, E.; Liska, P.; Vlachopoulos, N.; Grätzel, M. Conversion of Light to Electricity by cis-X_2bis(2,2'-bipyridyl-4,4'-dicarboxylate) Ruthenium(II) Charge-transfer Sensitizers (X = Cl^-, Br^-, I^-,

CN^-, and SCN^-) on Nanocrystalline Titanium Dioxide Electrodes. *J. Am. Chem. Soc.* **1993**, *115*, 6382.

21. Ardo, S.; Meyer, G. J. Photodriven Heterogeneous Charge Transfer with Transition-metal Compounds Anchored to TiO_2 Semiconductor Surfaces. *Chem. Soc. Rev.* **2009**, *38*, 115.

22. Persson, P.; Bergström, R.; Ojamäe, L.; Lunell, S. Quantum-Chemical Studies of Metal Oxides for Photoelectrochemical Applications. *Adv. Quantum Chem.* **2002**, *41*, 203.

23. Nazeeruddin, M. K.; Péchy, P.; Renouard, T.; Zakeeruddin, S. M.; Humphry-Bakery, R.; Comte, P.; Liska, P.; Cevery, L.; Costa, E.; Shklover, V.; Spiccia, L.; Deacon, G. B.; Kay, A.; Bignozzi, C. A.; Grätzel, M. Engineering of Efficient Panchromatic Sensitizers for Nanocrystalline TiO_2-Based Solar Cells. *J. Am. Chem. Soc.* **2001**, *123*, 1613.

24. Nazeeruddin, M. K.; Péchy, P.; Grätzel, M. Efficient Panchromatic Sensitization of Nanocrystalline TiO_2 Films by a Black Dye Based on a Trithiocyanato–Ruthenium Complex. *Chem. Commun.* **1997**, 1705.

25. Grabulosa, A.; Beley, M.; Gros, P. C.; Cazzanti, S.; Caramori, S.; Bignozzi, C. A. Homoleptic Ruthenium Complex Bearing Dissymmetrical 4-Carboxy-40-pyrrolo-2,2'-bipyridine for Efficient Sensitization of TiO_2 in Solar Cells. *Inorg. Chem.* **2009**, *48*, 8030.

26. Alary, A.; Heully, J.-L.; Bijeire, L.; Vicendo, P. Is the ^{3}MLCT the Only Photoreactive State of Polypyridyl Complexes? *Inorg. Chem.* **2007**, *46*, 3154.

27. Heimer, T. A.; D'Arcangelis, S. T.; Farzad, F.; Stipkala, J. M.; Meyer, G. J. An Acetylacetonate-Based Semiconductor−Sensitizer Linkage. *Inorg. Chem.* **1996**, *35*, 5319.

28. Gillaizeau-Gauthier, I.; Odobel, F.; Alebbi, M.; Argazzi, R.; Costa, E.; Bignozzi, C. A.; Qu, P.; Meyer, G. J. Phosphonate-Based Bipyridine Dyes for Stable Photovoltaic Devices. *Inorg. Chem.* **2001**, *40*, 6073.

29. Kilså, K.; Mayo, E. I.; Kuciauskas, D.; Villahermosa, R.; Lewis, N. S.; Winkler, J. R.; Gray, H. B. Effects of Bridging Ligands on the Current−Potential Behavior and Interfacial Kinetics of Ruthenium-Sensitized Nanocrystalline TiO_2 Photoelectrodes. *J. Phys. Chem. A.* **2003**, 3379.

30. Piotrowiak, P.; Galoppini, E.; Wei, Q.; Meyer, G. J.; Wiewiòr, P. Subpicosecond Photoinduced Charge Injection from 'Molecular Tripods' into Mesoporous TiO_2 Over the Distance of 24 Angstroms. *J. Am. Chem. Soc.* **2003**, *125*, 5278.

31. Guo, W.; Galoppini, E.; Rydja, G. I.; Pardi, G. Synthesis of a Molecular Tripod to Anchor Molecular Coordination Compounds to Semiconductor Nanoparticles. *Tetrahedron Lett.* **2000**, *41*, 7419.

32. Galoppini, E.; Guo, W.; Qu, P.; Meyer, G. J. Long-Distance Electron Transfer Across Molecule-Nanocrystalline Semiconductor Interfaces. *J. Am. Chem. Soc.* **2001**, *123*, 4342.

33. Galoppini, E.; Guo, W.; Zhang, W.; Hoertz, P.; Qu, P.; Meyer, G. J. Long-Range Electron Transfer across Molecule-Nanocrystalline Semiconductor Interfaces Using Tripodal Sensitizers. *J. Am. Chem. Soc.* **2002**, *124*, 7801.

34. Wei, Q.; Galoppini, E. Tripodal Ru(II) Complexes with Conjugated and Non-conjugated Rigid-rod Bridges for Semiconductor Nanoparticles Sensitization. *Tetrahedron* **2004**, *60*, 8497.

35. Thyagarajan, S.; Liu, A.; Famoyin, O. A.; Lamberto, M.; Galoppini, E. Tripodal Pyrene Chromophores for Semiconductor Sensitization: New Footprint Design. *Tetrahedron* **2007**, *63*, 7550.

36. Lee, C.-H.; Zhang, Y.; Romayanantakit, A.; Galoppini, E. Modular Synthesis of Ruthenium Tripodal System with Variable Anchoring Groups Positions for Semiconductor Sensitization. *Tetrahedron* **2010**, *66*, 3897.

37. Wang, D.; Schlegel, J. M.; Galopppini, E. Synthesis of Rigid-rod Linkers to Anchor Chromophores to Semiconductor Nanoparticles. *Tetrahedron* **2002**, *58*, 6027.

38. Hoertz, P. G.; Carlisle, R.; Meyer, G. J.; Wang, D.; Piotrowiak, P.; Galoppini, E. Organic Rigid-Rod Linkers for Coupling Chromophores to Metal Oxide Nanoparticles. *Nano Lett.* **2003**, *3*, 325.

39. Wang, D.; Mendelsohn, R.; Galoppini, E.; Hoertz, P. G.; Carlisle, R. A.; Meyer, G. J. Excited State Electron Transfer from Ru(II) Polypyridyl Complexes Anchored to Nanocrystalline TiO2 through Rigid-Rod Linkers. *J. Phys. Chem. B* **2004**, *108*, 16642.

40. Lamberto, M.; Pagba, C.; Piotrowiak, P.; Galoppini, E. Synthesis of Novel Rigid-rod and Tripodal Azulene Chromophores. *Tetrahedron Lett.* **2005**, *46*, 4895.

41. Abrahamsson, M.; Taratula, O.; Persson, P.; Galoppini, E.; Meyer, G. J. Meta-substituted Ru^{II} Rigid Rods for Sensitization of TiO_2. *J. Photochem. Photobiol. A: Chem* **2009**, *206*, 155.

42. Abrahamsson, M.; Johansson, P. G.; Ardo, S.; Kopecky, A.; Galoppini, E.; Meyer, G. J. Decreased Interfacial Charge Recombination Rate Constants with N3-Type Sensitizers. *J. Phys. Chem. Lett.* **2010**, *1*, 1725.

43. Ohkanda, J.; Satohb, R.; Kato, N. Protein Surface Recognition by Dendritic Ruthenium(II) Tris(bipyridine) Complexes. *Chem. Commun.* **2009**, 6949.

44. Payne, S. J.; Fiore, G. L.; Fraser, C. L.; Demas, J. N. Luminescence Oxygen Sensor Based on a Ruthenium(II) Star Polymer Complex. *Anal. Chem.* **2010**, *82*, 917.

45. Beer, P. D.; Kocian, O.; Mortimer, R. J.; Ridgway, C. New Alkynyl- and Vinyl-linked Benzo- and Aza-crown Etherbipyridyl Ruthenium(II) Complexes which Spectrochemically Recognize Group IA and IIA Metal Cationst. *J. Chem. Soc. Dalton Trans.* **1993**, 2629.

46. Beer, P. D.; Kocian, O.; Mortimer, R. J.; Ridgway, C. Syntheses, Coordination, Spectroscopy and Electropolymerisation Studies of New Alkynyl and Vinyl Linked Benzo- and Aza-crown Ether-Bipyridyl Ruthenium(II) Complexes. Spectrochemical Recognition of Group IA/IIA Metal Cations. *J. Chem. Soc., Chem. Commun.* **1991**, 1460.

47. Muldoon, J.; Ashcroft, A. E.; Wilson, A. J. Selective Protein-Surface Sensing Using Ruthenium(II) Tris(bipyridine) Complexes. *Chem. Eur. J.* **2010**, *16*, 100.

48. Osawa, M.; Hoshino, M.; Horiuchi, S.; Wakatsuki, Y. Palladium-Mediated One-Step Coupling between Polypyridine Metal Complexes: Preparation of Rigid and Dendritic Nano-Sized Ruthenium Complexes. *Organometallics* **1999**, *18*, 112.

49. Otsuki, J.; Kameda, H.; Tomihira, S.; Sakaguchi, H.; Takido, T. Ruthenium Complexes Containing Fully Conjugated Ligands Terminated with Thiol Groups. *Chem. Lett.* **2002**, 610.

50. Wilson, G. J.; Will, G. D. Density-functional Analysis of the Electronic Structure of Tris-bipyridyl Ru(II) Sensitisers. *Inorg. Chim. Acta* **2010**, *363*, 1627.

51. Martinson, A. B. F.; Hamann, T. W.; Pellin, M. J.; Hupp, J. T. New Architectures for Dye-Sensitized Solar Cells. *Chem. Eur. J.* **2008**, *14*.

52. Rehm, J. M.; Mclendon, G. L.; Nagasawa, Y.; Yoshihara, K.; Moser, J.; Grätzel, M. Femtosecond Electron-Transfer Dynamics at a Sensitizing Dye−Semiconductor (TiO_2) Interface. *J. Phys. Chem.* **1996**, *100*, 9577.

53. Burfeindt, B.; Hannappel, T.; Storck, W.; Willig, F. Measurement of Temperature-Independent Femtosecond Interfacial Electron Transfer from an Anchored Molecular Electron Donor to a Semiconductor as Acceptor. *J. Phys. Chem.* **1996**, *100*, 16463.

54. Asbury, J. B.; Ellingson, R. J.; Ghosh, H. N.; Ferrere, S.; Nozik, A. J.; Lian, T. Femtosecond IR Study of Excited-State Relaxation and Electron-Injection Dynamics of $Ru(dcbpy)_2(NCS)_2$ in Solution and on Nanocrystalline TiO_2 and Al_2O_3 Thin Films. *J. Phys. Chem. B* **1999**, *103*, 3110.

55. Huber, R.; Spörlein, S.; Moser, J. E.; Grätzel, M.; Wachtveitl, J. The Role of Surface States in the Ultrafast Photoinduced Electron Transfer from Sensitizing Dye Molecules to Semiconductor Colloids. *J. Phys. Chem. B* **2000**, *104*, 8995.

56. Schnadt, J.; Brühwiler, B.; Patthey, L.; O'Shea, J.; Södergren, S.; Odelius, M.; Ahuja, R.; Karis, O.; Baessler, M.; Persson, P.; Siegbahn, H.; Lunell, S.; Martensson, N. Experimental Evidence for Sub-3-fs Charge Transfer from an Aromatic Adsorbate to a Semiconductor. *Nature* **2002**, *418*, 620.

57. Tachibana, Y.; Moser, J. E.; Gratzel, M.; Klug, D. R.; Durrant, J. R. Subpicosecond Interfacial Charge Separation in Dye-Sensitized Nanocrystalline Titanium Dioxide Films. *J. Phys. Chem.* **1996**, *100*, 20056.

58. Benko, G.; Kallioinen, J.; Korppi-Tommola, J. E. I.; Yartsev, A. P.; Sundstrom, V. Photoinduced Ultrafast Dye-to-Semiconductor Electron Injection from Nonthermalized and Thermalized Donor States. *J. Am. Chem. Soc.* **2002**, *124*, 489.

59. Heimer, T. A.; Heilweil, E. J.; Bignozzi, C. A.; Meyer, G. J. Electron Injection, Recombination, and Halide Oxidation Dynamics at Dye-Sensitized Metal Oxide Interfaces. *J. Phys. Chem. A.* **2000**, *104*, 4256.

60. Tachibana, Y.; Rubtsov, I. V.; Montanari, I.; Yoshihara, K.; Klug, D. R.; Durrant, J. R. Transient Luminescence Studies of Electron Injection in Dye Sensitised Nanocrystalline TiO_2 Films. *J. Photochem. Photobiol. A: Chem* **2001**, *142*, 215.

61. Tachibana, Y.; Haque, S. A.; Mercer, I. P.; Durrant, J. R.; Klug, D. R. Electron Injection and Recombination in Dye Sensitized Nanocrystalline Titanium Dioxide Films: A Comparison of Ruthenium Bipyridyl and Porphyrin Sensitizer Dyes. *J. Phys. Chem. B* **2000**, *104*, 1198.

62. Damrauer, N. H.; McCusker, J. K. Ultrafast Dynamics in the Metal-to-Ligand Charge Transfer Excited-State Evolution of $[Ru(4,4'\text{-diphenyl-}2,2'\text{-bipyridine})3]^{2+}$. *J. Phys. Chem. A.* **1999**, *103*, 8440.

63. Kuciauskas, D.; Monat, J. E.; Villahermosa, R.; Gray, H. B.; Lewis, N. S.; McCusker, J. K. Transient Absorption Spectroscopy of Ruthenium and Osmium Polypyridyl Complexes Adsorbed onto Nanocrystalline TiO_2 Photoelectrodes. *J. Phys. Chem. B* **2002**, *106*, 9347.

64. Gundlach, L.; Ernstorfer, R.; Willig, F. Pathway-Dependent Electron Transfer for Rod-Shaped Perylene-Derived Molecules Adsorbed in Nanometer-Size TiO_2 Cavities. *J. Phys. Chem. C* **2007**, *111*, 13586.

65. Ernstorfer, R.; Gundlach, L.; Felber, S.; Storck, W.; Eichberger, R.; Willig, F. Role of Molecular Anchor Groups in Molecule-to-Semiconductor Electron Transfer. *J. Phys. Chem. B* **2006**, *110*, 25383.

66. Hagfeldt, A.; Grätzel, M. Light-Induced Redox Reactions in Nanocrystalline Systems. *Chem. Rev.* **1995**, *95*, 49.

67. Nelson, J.; Haque, S. A.; Klug, D. R.; Durrant, J. R. Trap-limited Recombination in Dye-sensitized Nanocrystalline Metal Oxide Electrodes. *Phys. Rev. B* **2001**, *63*, 205321.

68. Li, J.; Nilsing, M.; Kondov, I.; Wang, H.; Persson, P.; Lunell, S.; Thoss, M. Dynamical Simulation of Photoinduced Electron Transfer Reactions in Dye-Semiconductor Systems with Different Anchor Groups. *J. Phys. Chem. C* **2008**, *112*, 12326.

69. Myahkostupov, M.; Piotrowiak, P.; Wang, D.; Galoppini, E. Ru(II)-Bpy Complexes Bound to Nanocrystalline TiO_2 Films through Phenyleneethynylene (OPE) Linkers:

Effect of the Linkers Length on Electron Injection Rates. *J. Phys. Chem. C* **2007**, *111*, 2827.

70. Luo, L.; Chang, C.-W.; Lin, C.-Y.; Diau, E. W.-G. Femtosecond Fluorescence Dynamics of Zinc Biphenylporphine in Nanocrystalline TiO_2 Films: Evidence for Interfacial Electron Transfer through Space. *Chem. Phys. Lett.* **2006**, *432*, 452.

71. Chang, C.-W.; Chou, C. K.; Chang, I.-J.; Lee, Y.-P.; Diau, E. W.-G. Relaxation Dynamics of Ruthenium Complexes in Solution, PMMA and TiO_2 Films: The Roles of Self-Quenching and Interfacial Electron Transfer. *J. Phys. Chem. C* **2007**, *111*, 13288.

72. Chang, C.-W.; Luo, L.; Chou, C.-K.; Lo, C.-F.; Lin, C.-Y.; Hung, C.-S.; Lee, Y.-P.; Diau, E. W.-G. Femtosecond Transient Absorption of Zinc Porphyrins with Oligo(phenylethylnyl) Linkers in Solution and on TiO_2 Films. *J. Phys. Chem. C* **2009**, *113*, 11524.

73. Gundlach, L.; Felber, S.; Storck, W.; Galoppini, E.; Wei, Q.; Willig, F. Femtosecond Two-photon Photoemission Probing Electron Injection from the Excited Singlet State of Perylene Attached to a Long Rigid Tripod Anchor-cum-spacer on Rutile TiO_2(110) *Res. Chem. Intermed.* **2005**, *31*, 39.

74. Nilsing, M.; Lunell, S.; Persson, P.; Ojamäe, L. Phosphonic Acid Adsorption at the TiO_2 anatase (101) Surface Investigated by Periodic Hybrid HF-DFT Computations. *Surf. Sci.* **2005**, *582*, 49.

CHAPTER A-2:

SYNTHESIS OF HOMOLEPTIC RUTHENIUM COMPLEXES

A-2-1. Introduction and Overview of Synthetic Strategies

A series of homoleptic ruthenium (II) star-shaped complexes were designed and synthesized. They are made of three identical bipyridine ligands each with two conjugated OPE rigid linkers in the 4,4' positions terminating with carboxylic ester anchoring groups. Figure A-2-1.1 shows the chemical structures of the target compounds: 3 Short Star Complex (3SSC), Short Star Complex (SSC), Long Star Complex (LSC), Soluble Long Star Complex (SLSC). Conjugated OPE rigid linkers were designed to separate the ruthenium metal center and the metal oxide semiconductor surface at a fixed distance and orientation. 3SSC had one rigid linker attached onto the 4 position of each bipyridine unit. As a result 3SSC has isomers that the geometry would lead to point of contacts. 3SSC is a reference compound. The other three star complexes had two rigid linkers attached onto the 4 and 4' positions of each bipyridine unit. One additional OPE unit was introduced in the LSC and SLSC star complexes to increase the length of the rigid linker compared to the SSC and 3SSC star complexes. To increase the solubility of the star complex, two side chain butoxy groups were attached onto the phenyl ring for the SLSC. All of the complexes used isophthalic anchoring unit (Ipa), with two carboxylic ester groups, to assure the covalent binding to the metal oxide semiconductor nanoparticle surfaces. The counter ion to the ruthenium (II) complexes was hexafluorophosphate in all cases. The diameter of the complexes is in 2.5 - 4 nm range (Figure A-2-1.2).

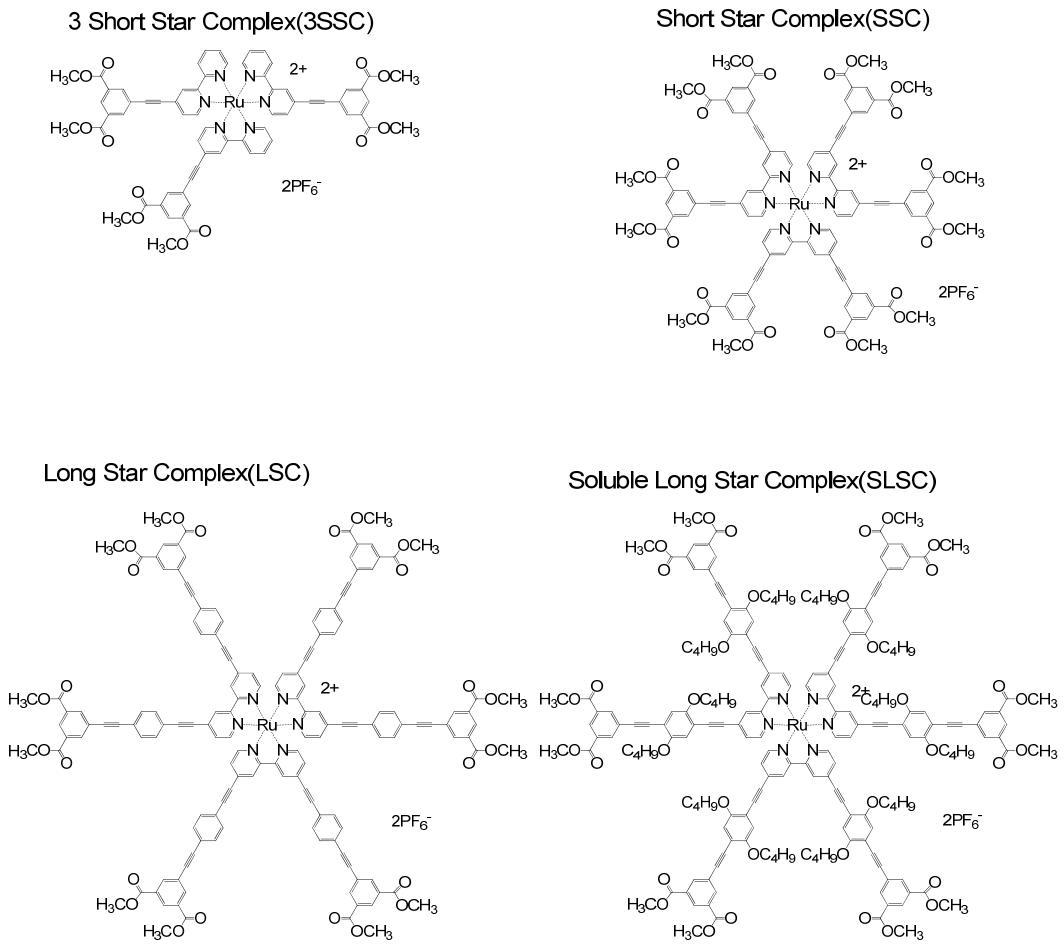

Figure A-2-1.1. Chemical structures of homoleptic ruthenium star complexes

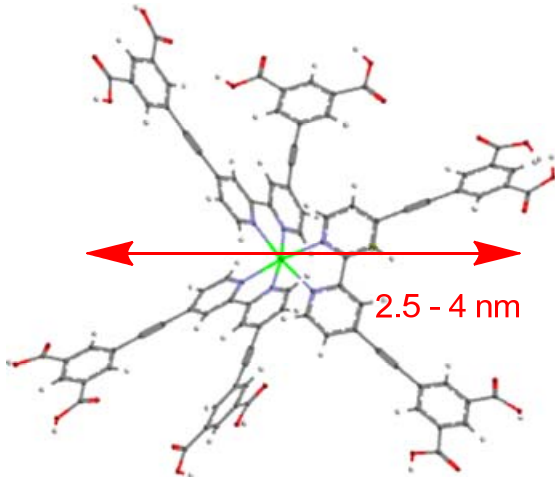

Figure A-2-1.2. Dimension of homoleptic ruthenium star complexes

The classical method to synthesize homoleptic ruthenium tris(bipyridine) derivatives involves the reaction between $RuCl_3$ and a bipyridine ligand.[1-4] Ruthenium (III) is reduced to ruthenium (II) in this reaction, and hypophosphorous acid is typically added as the reducing agent.[5] However, we found that this method was not suitable for the synthesis of ruthenium star complexes due to the low solubility of the target complexes. After two bipyridine ligands chelated with ruthenium metal center, the resulting complexes precipitated from the reaction mixture, preventing further coordination with the last ligand. Thus, two modified synthetic routes were used to synthesize the target complexes, as shown in Scheme A-2-1.1.

Method I was reported by Otsuki and coworkers to make a similar ruthenium complex.[6] $Ru(DMSO)_4(PF_6)_2$ was selected as the Ru(III) complex to chelate with the corresponding bipyridine ligands (Scheme A-2-1.1 Method I). The improved solubility of the ruthenium polypyridine, obtained by introducing hexafluorophosphate, a commonly used non-coordinating anion,[7] as the counter ion, prevented the ruthenium bis(bipyridine) precipitation from the reaction mixture. $Ru(DMSO)_4(PF_6)_2$ was prepared from commercially available chemical $Ru(DMSO)_4Cl_2$ by reaction with $AgPF_6$ in ethanol. The precipitation of insoluble silver chloride drove the reaction to completion. Since the $Ru(DMSO)_4Cl_2$ was expensive, it was also synthesized by heating DMSO solutions of ruthenium trichloride.[8] An alternative method (Scheme A-2-1.1 Method II) involved the Sonogashira cross-coupling reaction with halogenated (Bromo or Iodo) ruthenium tris(bipyridine) complexes[9-13] and the terminal alkyne linkers units. The mechanism of the cross-coupling reaction is described later in section A-2-2. Although the overall yield

was low and a large excess of terminal alkyne linker was required. This method led to high yields of the SSC and LSC complexes.

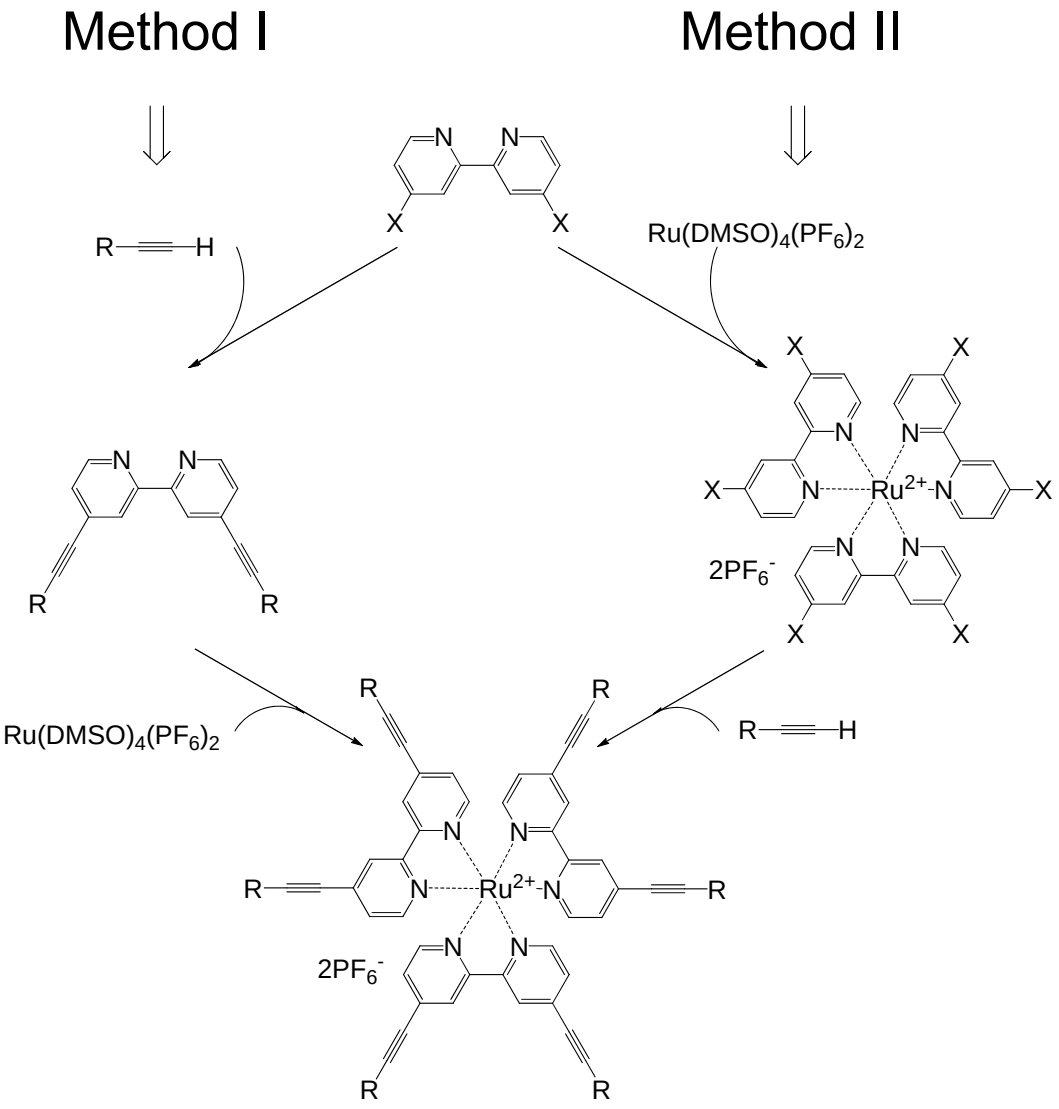

Scheme A-2-1.1. Synthetic routes to the star complexes

In this thesis, method I was selected to synthesize 3SSC and SLSC, while method II was preferred for SSC and LSC (Scheme A-2-1.1). Method I gave higher yield for soluble ligands. Although method II required a large excess of terminal alkyne, it was used because the solubility of SSC and LSC ligands is low. Both methods involved a

series of palladium-catalyzed cross-coupling reactions between aryl alkynes and aryl halides.

A-2-2. Palladium-Catalyzed Cross-Coupling Reactions

The coupling reactions employed in this study were Sonogashira coupling with or without copper. Both of the reactions were carried out in the presence of a palladium complex as the catalyst. The mechanism of both reactions is described in the following section.

Sonogashira Coupling with Copper Palladium-copper-catalyzed coupling reaction of terminal alkynes with aryl or vinyl halides leading to arylalkynes and conjugated enynes is termed Sonogashira coupling and was developed by Sonogashira et al. in 1975.[14,15] Heck[16] and Cassar[17] later reported a similar process, which did not involve copper catalyst but required harsher conditions. The general accepted mechanism of this cross-coupling reaction is depicted in Scheme A-2-2.1.[18]

The copper-co-catalyzed Sonogashira reaction is believed to take place through two independent catalytic cycles (palladium cycle and copper cycle), as shown in Scheme A-2-2-1. The catalytic cycle for the palladium catalysis (palladium cycle) is based on a usually fast oxidative addition of R_1-X (R_1 = aryl, X = I, Br) to the real catalyst generated from the initial palladium complex.

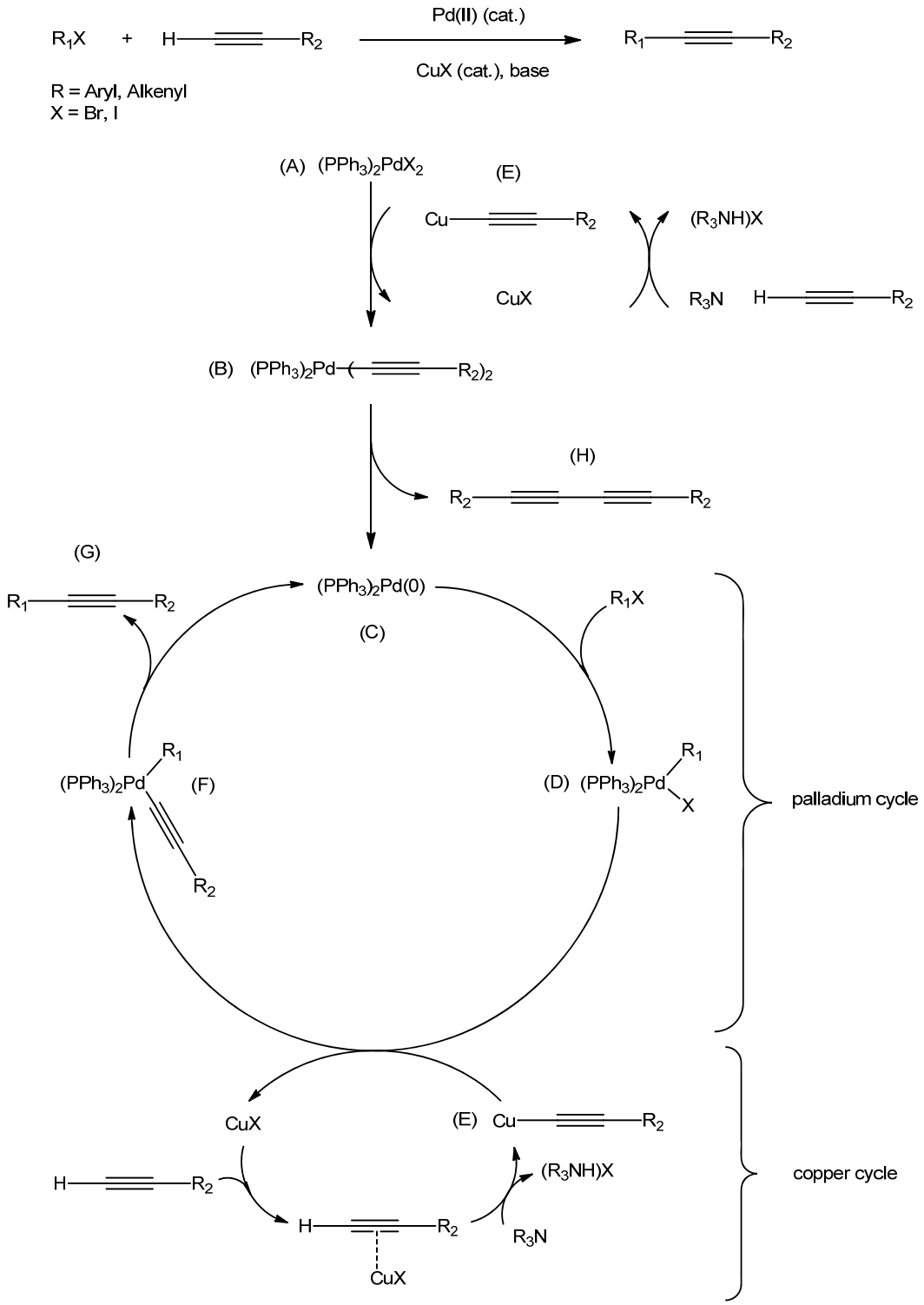

Scheme A-2-2.1. Reaction mechanism for Sonogashira coupling[18]

To initiate the catalytic cycle, the relatively acidic proton of terminal alkyne is deprotonated in catalytic amount by an amine, such as triethylamine or diisopropylamine. The resulting acetylide reacts with the copper halide to give catalytic amount of an alkynyl copper complex (E). In most cases, the commercially available Pd (II) is preferred to Pd (0) which is more air-sensitive. Pd in its oxidized form is inactive. It is generally believed that $Pd(PPh_3)_2X_2$ (A) transmetallates with the intermediate (alkynyl copper complex) to form the bis(triphenylphosphine)dialkynylpalladium(II) complex (B), which gives the active catalytic species $Pd(0)(PPh_3)_2$ (C). Subsequently, the Pd (0) compound reacts with aryl halide in an oxidative addition to form $Pd(II)(PPh_3)_2(aryl)X$ (D). This complex reacts with the alkynyl copper complex (E) produced in the copper cycle by transmetallation and trans-cis isomerization to give a $Pd(II)(PPh_3)_2(aryl)(alkynyl)$ complex (F). Finally, the resulting complex undergoes reductive elimination to produce the coupling product (G) and the $Pd(0)(PPh_3)_2$ (C) is regenerated. This Sonogashira coupling reaction was the preferred method to prepare the terminal alkyne linkers with OPE units varying length.

Sonogashira Coupling without Copper There are many factors that influence palladium-catalyzed cross-coupling reactions, including the type and amount of catalyst as well as the choice of solvent and base. One of the main side reactions is the formation of acetylene dimer (a 1,3-diene), which can be promoted by copper (I) and traces of oxygen. Although it is reported that using Pd (0) catalyst and THF as the solvent can inhibit the dimer formation,[19] we can still obtain the acetylene dimer, which is a loss of the multiple-steps-prepared terminal alkynes. Suzuki-type coupling has been used in our research group to minimize the dimer formation.[20] This method, however, required strict

moisture and oxygen free reaction condition and often gave low yield. Thus a modified Sonogashira coupling which does not employ copper (I) salts was chosen for the coupling reaction between a halogenated bipyridine and the terminal alkyne linker units. As an additional advantage, this modified cross-coupling reaction can avoid the possible chelation between the bipyridine ligand and the copper (I) salt to form a Cu (I) bpy complex. The mechanism of the copper-free Sonogashira Coupling reaction is shown in Scheme A-2-2.2.[21,22]

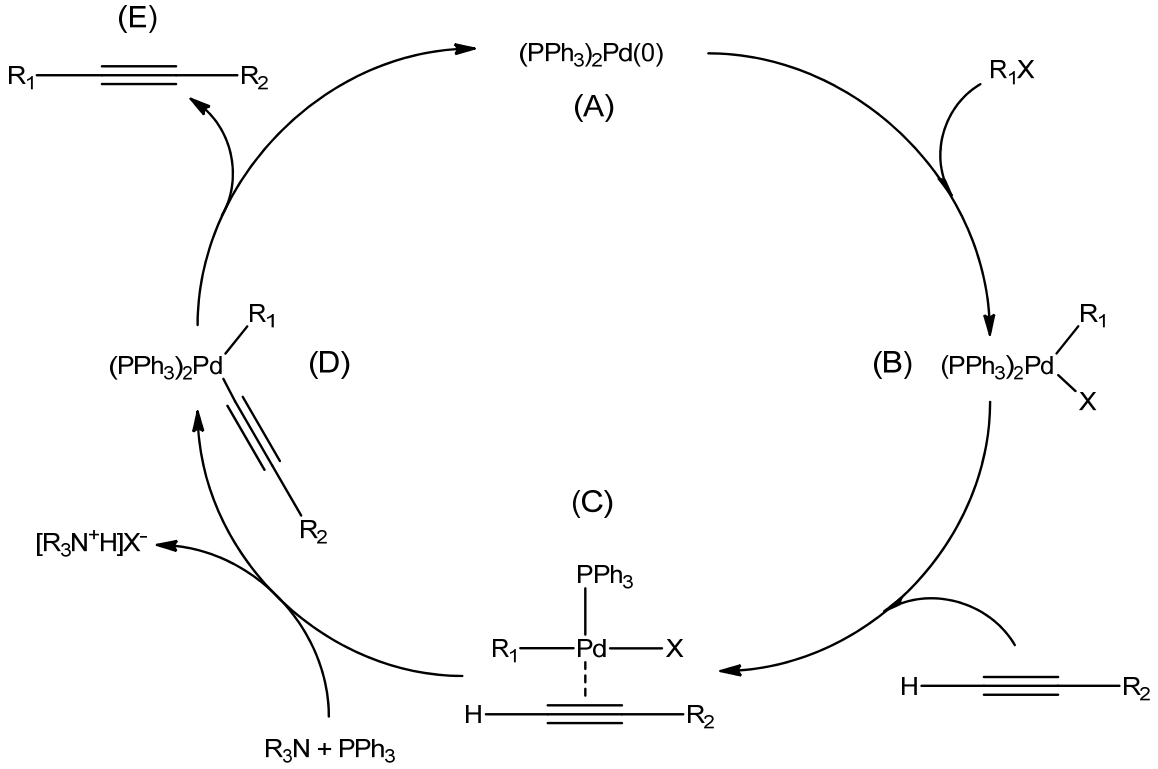

Scheme A-2-2.2. Reaction mechanism for copper-free Sonogashira coupling

The active catalytic compound $Pd(0)(PPh_3)_2$ (A) reacts with R_1X in an oxidative addition to give the $R_1Pd(PPh_3)_2X$ complex (B). The subsequent complexation of the alkyne is supposed to proceed first with displacement of one PPh_3 to give intermediate complex $(R_2C{\equiv}CH)R_1Pd(PPh_3)X$ (C). The ligated alkyne undergoes deprotonation by the

amine to form the new complex $(R_2C{\equiv}C)R_1Pd(PPh_3)_2$ (D), which gives the coupling product $R_2C{\equiv}CR_1$ (E) and regenerates the catalyst $Pd(0)(PPh_3)_2$ (A) by reductive elimination.

A-2-3. Synthesis of the Halogenated Bipyridines

4,4'-Dibromo-2,2'-bipyridine is commercially available. 4-Iodo-2,2'-bipyridine and 4,4'-diiodo-2,2'-bipyridine were synthesized in our laboratory. The purpose to use the iodo-substituted bipyridine is to increase the reactivity in the cross-coupling reactions. Since the bond dissociation energy of C-I is lower than that of C-Br.[18,23] Pd-catalyzed cross coupling reactions with aryl iodides usually take place readily at room temperature in high yields, while aryl bromides require higher temperatures. Aryl chlorides are not employed due to low reactivity.[24] The synthetic routes for 4-iodo-2,2'-bipyridine **(4)** and 4,4'-diiodo-2,2'-bipyridine **(8)** are shown in Schemes A-2-3.1 and A-2-3.2.

To synthesize the 4-iodo-2,2'-bipyridine **(4)**, reported procedures were used.[25-30] Commercially available 2,2'-bipyridine-N-oxide **(1)** was converted to 4-nitro-2,2'-bipyridine-N-oxide (**2)** by treatment with fuming nitric acid in concentrated sulfuric acid at 100°C. The yield of this nitration reaction was 68%. When potassium nitrate was used as the source of nitro group, yields were lower (~ 40%).[26] Compound 4-nitro-2,2'-bipyridine-N-oxide **(2)** was reduced by sodium borohydride with Pd/C to give 4-amino-2,2'-bipyridine **(3)** in 70% yield. Hydrazine with Pd/C was an alternate reducing reagent in this step that gave comparable yield. Finally, 4-iodo-2,2'-bipyridine **1** was prepared from 4-amino-2,2'-bipyridine **3** through Sandmeyer reaction in 60% yield. The low-

temperature (-6 to 0°C) and the vigorous stirring were key requirements in this step. Mechanical stirring was preferred to magnetic stirring.

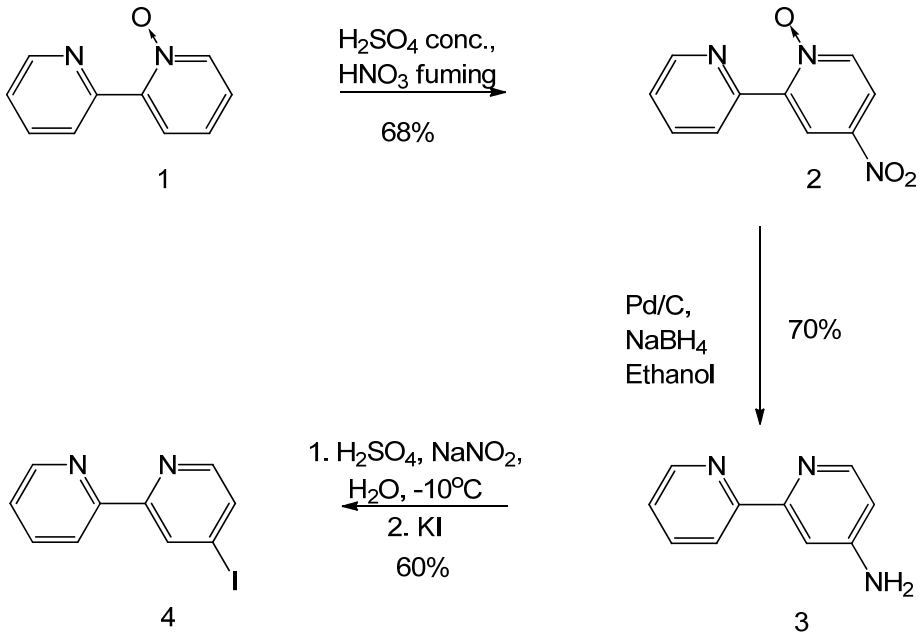

Scheme A-2-3.1. Synthetic route to 4,4'-diiodo-2,2'-bipyridine[25-30]

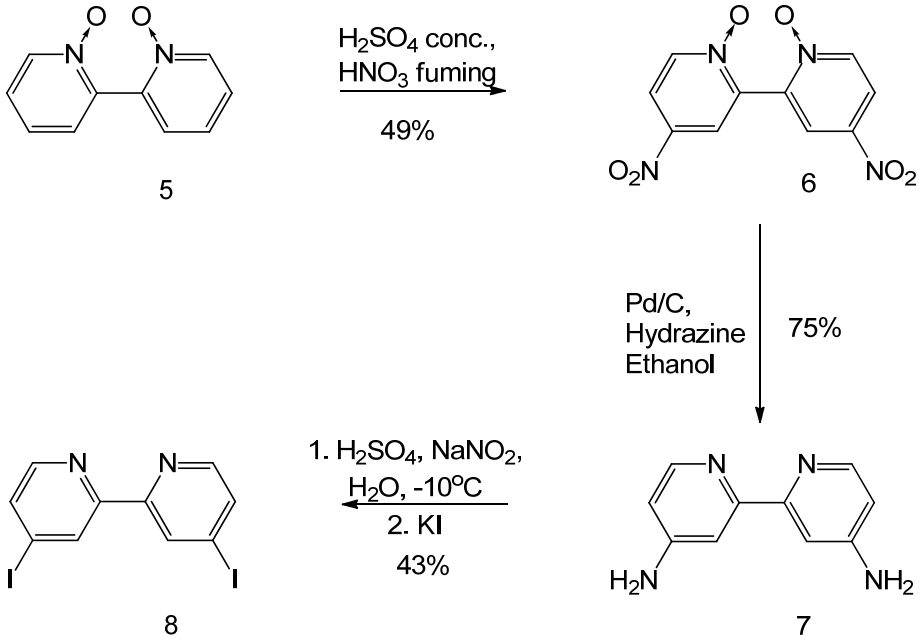

Scheme A-2-3.2. Synthetic route to 4,4'-diiodo-2,2'-bipyridine[27,28]

A similar synthetic route[27,28] was used to synthesize 4,4'-iodo-2,2'-bipyridine **(8)** starting from 2,2'-bipyridine-N, N'-dioxide **(5)**. The overall yield was lower than that of making mono-substituted bipyridine. The resulting compounds **4**, **8** and 4,4'-dibromo-2,2'-bipyridine were used as the aryl halides for further cross-coupling reactions with terminal alkyne linker units to prepare the ligands, as described in the next section.

A-2-4. Synthesis of the Bipyridine Ligands with Short Rigid Linkers

Two bipyridine ligands, **12** and **13**, with one OPE unit in the rigid linker were prepared. Compound **12** (ligand of 3SSC) had one short rigid linker in position 4 of the bipyridine, while compound **13** (ligand of SSC) had both bipyridine 4 and 4' positions attached with short rigid linkers. The synthetic route is shown in Scheme A-2-4.1.

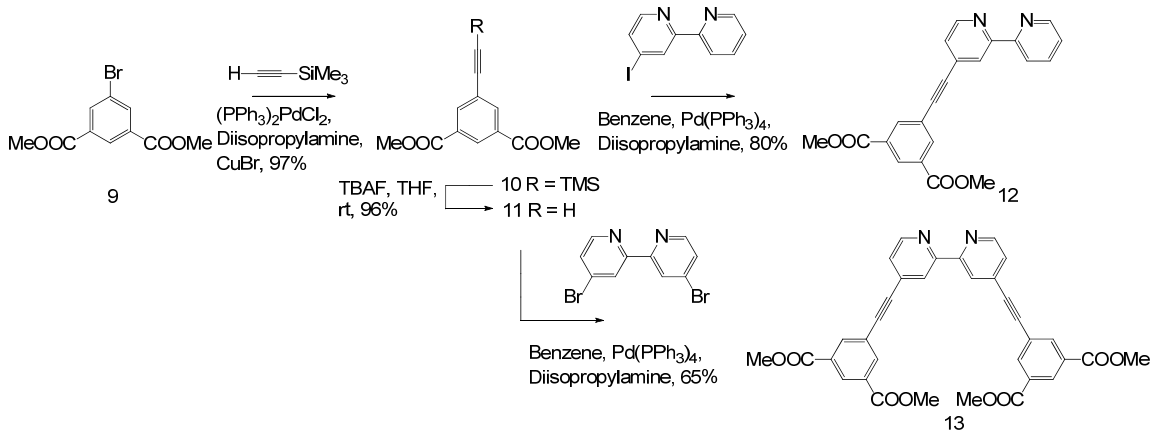

Scheme A-2-4.1. Synthetic routes to bipyridine ligands with short rigid linker

Dimethyl 5-bromoisophthalate **9** is commercially available. The synthesis of carboxylic esters was necessary to increase the solubility of the products and for easy purification purpose. Furthermore, carboxylic esters are suitable anchor groups to attach the sensitizers onto the metal oxide nanoparticle surfaces.[31,32] Dimethyl 5-

iodoisophthalate was also prepared using the Sandmeyer reaction[33] in a fair yield (30%). Although dimethyl 5-iodoisophthalate was not normally used in this work, it is a good alternative to the corresponding bromide since iodo-substituted aryl compounds are more reactive in the Pd-catalyzed cross-coupling reactions than bromo-substituted ones. The starting material, dimethyl 5-aminoisophthalate, is inexpensive compared to the dimethyl 5-bromoisophthalate. The synthetic route is shown in Scheme A-2-4.2. The low-temperature control in this step is crucial for the success of this reaction because the intermediate compound **28** decomposes above 0°C.

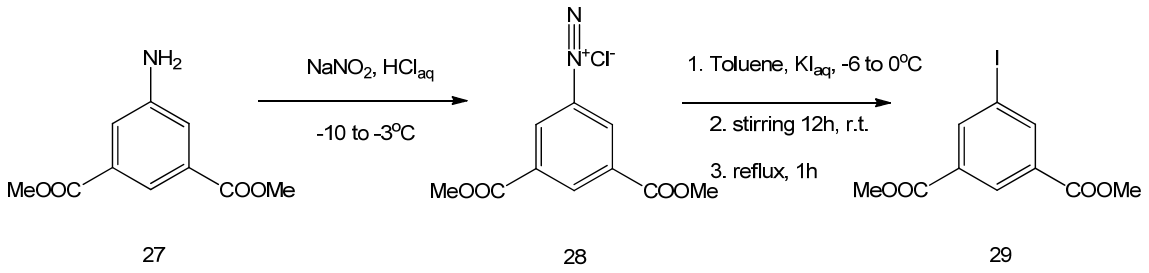

Scheme A-2-4.2. Synthetic route to dimethyl 5-iodoisophthalate.

Sonogashira cross-coupling[14,15,20,34,35] of trimethylsilylacetylene with dimethyl 5-bromoisophthalate (97% yield), followed by deprotection with tetrabutylammonium fluoride (TBAF), produced alkyne precursor **11** (overall 93% yield).[20] Copper-free Sonogashira coupling[35] of this precursor with 4-iodo-2,2'-bipyridine **4** and 4,4'-diiodo-2,2'-bipyidine **8** yielded **12** and **13**, respectively, in good yields (80% for **12** and 65% for **13**). The copper-free Sonogashira coupling was employed in this step to minimize the dimerization of the precursor alkyne **11** and to avoid the formation of copper-bipyridine complexes.

A-2-5. Synthesis of the Bipyridine Ligands with Long Rigid Linkers

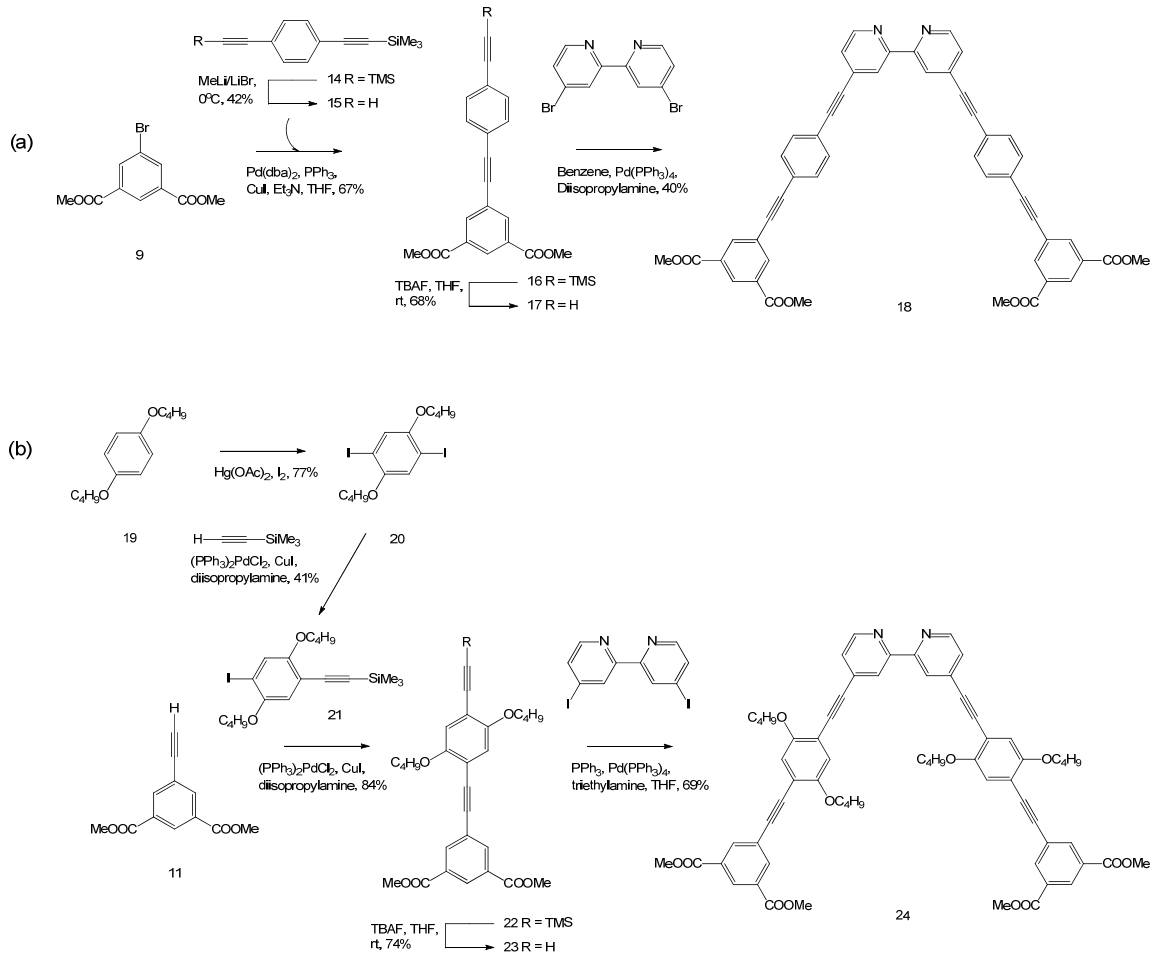

Scheme A-2-5.1. Synthetic routes to bipyridine ligands with long rigid linkers 18(a) and 24 (b)

The unsaturated rigid linker unit was readily prepared by iterative cross-coupling reactions.[20,32] The starting material, 1,4-bis(trimethylsilylethynyl)benzene **(14)**, is commercially available and used for coupling reaction after deprotection of one of the $SiMe_3$ groups at low temperature as shown in Scheme A-2-5.1. The mono-deprotected compound **15** cannot be separated from starting material **14** via silica gel column chromatography method. Reaction of **14** with one equivalent of MeLi·LiBr complex as the nucleophile[20] resulted in the formation of a 60:40 mixture of **14**:**15** (GC/MS). The

LiBr breaks aggregation of MeLi hexameric complexes to make the MeLi more nucleophilic.[20,36,37] The use of TBAF, a stronger nuclophile would result in complete deprotection of **14**.

The crude mixture of mono-deprotected compound **15** and un-reacted compound **14** was purified by column chromatography and then coupled with the anchoring unit dimethyl 5-bromoisophthalate. The remaining compound **14** was separated by silica gel column chromatography. The TMS-protected rigid linker **16** was deprotected with TBAF to give terminal alkyne **17** (overall yield 46%).

Star complex SLSC has two butoxy (-O-$(CH_2)_3CH_3$) substituents on the phenyl ring to improve the solubility. The commercially available 1,4-dibutoxybenzene **19** was selected as the starting material reagent.[38] After iodination at room temperature of compound **20**, one equivalent of trimethylsilylacetylene was used to obtain **21**. To prevent the cross-coupling of trimethylsilylacetylene with both iodo functional groups, trimethylsilylacetylene was added into the reaction mixture dropwise at low temperature before addition of the palladium catalyst with stirring. After adding the catalyst, the reaction mixture was heated to 40°C. The resulting compound **21**, a yellow oil, was coupled with precursor anchoring unit compound **11**, then deprotected with TBAF to give the rigid-rod linker terminal alkyne **23**.[20]

The terminal alkynes **17** and **23**, containing two phenylenethynylene groups with or without butoxy side chain on the phenyl unit, were employed in the copper-free Sonogashira coupling reaction with 4,4'-diiodo-2,2'-bipyidine **(8)** or commercially available 4,4'-dibromo-2,2'-bipyridine to give **18** and **24**, respectively (40% for **18** and

69% for **24**). Due to the solubility in organic solvents, SLSC ligand **24** gave higher yield compared to the value of LSC ligand **18**.

A-2-6. Synthesis of the Homoleptic Ruthenium Star Complexes

As described before, two methods were used to prepare the ruthenium star complexes. Method I was used for the **3SSC** and **SLSC**, and method II, was used for the **SSC** and **LSC**. The reason to select different methods is due to the solubility issue. Both the **3SSC** and **SLSC** ligands were soluble in the complexation reaction solvent system, while **SSC** and **LSC** ligands had much lower solubility, and consequently the complexation reaction yield much lower and the purification more difficult. Although the coupling reaction between compound **26** and terminal alkyne **11** and **17** yield 48% and 30% respectively, it is still higher than by using method I in the overall percentage yield.

As shown in Scheme A-2-6.1, $Ru(DMSO)_4(PF_6)_2$ was prepared by refluxing commercially available $Ru(DMSO)_4Cl_2$ and $AgPF_6$ in ethanol under nitrogen atmosphere to exchange the counter ion. The precipitation of insoluble silver chloride drove this reaction to completion. PF_6^- counter ion is a non-coordinating anion, and is believed to increase the solubility of ruthenium polypyridine complex without interrupting the chelating process.[39] After removing the formed precipitate AgCl by quick filtration, ethanol was removed slowly under nitrogen flow. The resulting orange product $Ru(DMSO)_4(PF_6)_2$ was highly hydroscopic at ambient condition. The product was stored in a vial protected with aluminum foil in a glove box under nitrogen atmosphere, and used shortly after the preparation.

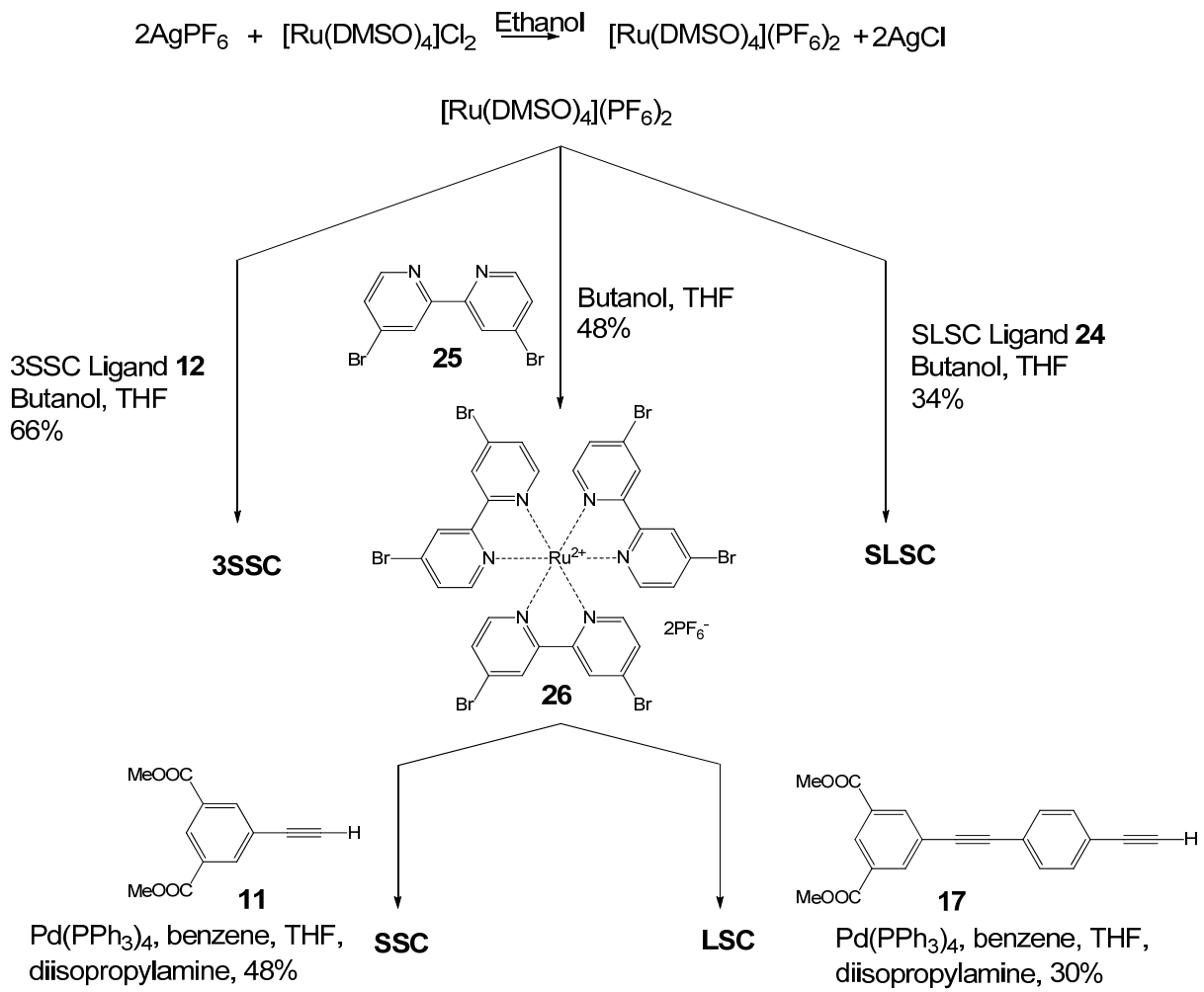

Scheme A-2-6.1. Synthetic routes to ruthenium star complexes

The same complexation conditions were employed to prepare **3SSC**, **SLSC**, and intermediate ruthenium complex **26**. The $Ru(DMSO)_4(PF_6)_2$ salt and the corresponding bipyridine ligand were stirred in a solvent mixture of 1-butanol and THF (2:1) at 120°C. THF improved the solubility of both the ligand and the homoleptic ruthenium complexes, while 1-butanol (b.p. 120°C) allowed using a higher reflux temperature for chelating reaction. UV-Vis absorption spectrum was used to monitor the reaction mixture. The reactions were stopped when no ruthenium bis(bipyridine) complex was observed. Visually this could be observed by color change of the reaction mixture as a purple color was indicated the existence of the partially chelated ruthenium bis(bipyridine) complex.

Figure A-2-6.1 shows the absorption spectra of reference compounds $Ru(bpy)_2Cl_2$ and $Ru(bpy)_2Cl_2$ in methanol. For the star complexes, the absorption band normally shifted to red, yet the existence of bi-chelated ruthenium is easily identified (two bands instead of one).

Compound **26** was quite soluble in the solvent used for cross-coupling conditions. The bromo functional groups were cross-coupled in the presence of a large excess (1:15 ratio) of terminal alkyne rigid linkers **11** and **17** via copper-free Sonogashira coupling method to yield **SSC** and **SLSC**. TLC was used to monitor the reaction mixture.

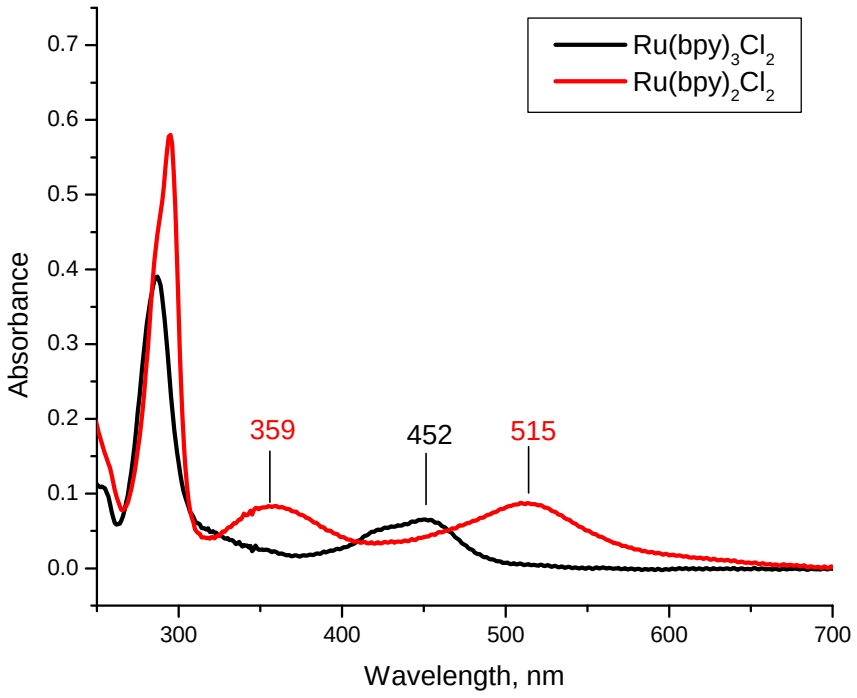

Figure A-2-6.1. Comparison of absorption spectra of standard ruthenium complexes

Carboxylic acid is the most commonly used anchoring group because of the strong covalent bonds with the TiO_2 nanoparticles and other MO_n semiconductor.[40] In the case

of star complexes, the anchoring group was not converted to carboxylic acid due to anticipated decrease in solubility. The carboxylic ester group was therefore used as the anchoring group to bind sensitizers onto metal oxide semiconductor surface with covalent bond. The binding is discussed in chapter A-3.

A-2-8. Experimental Section

General Procedure. All the air- and moisture sensitive reactions were performed under nitrogen atmosphere with glassware that was oven-dried and then flamed in vacuo. Column chromatography was performed using silica gel (Sorbent Technologies, 230-400 mesh). Thin Layer Chromatography (TLC) was performed on silica gel plates (Sorbent Technologies, w/UV254, aluminum backed, 200 μm), using UV light as the developing agent. "Standard workup" in the synthetic procedures refers to the following workup sequence: 1) the aqueous layer is extracted with the indicated solvent (typically 5 times); 2) the organic layers are collected and dried with anhydrous Na_2SO_4; c) the solvent is removed in vacuo on a rotary evaporator to give the crude product.

Instrumentation. NMR spectra were obtained on a Varian INOVA 500 spectrometer operating at 499.90 MHz for ^{1}H and 124.98 MHz for ^{13}C and collected in $CDCl_3$, unless otherwise specified. The ^{1}H spectra were referenced to tetramethylsilane or the central line of the solvent and the ^{13}C spectra to the central line of the solvent. Chemical shift (δ) are reported in ppm with a precision of ± 0.01 ppm. Coupling constant (*J*) are reported in Hz with a precision of ± 0.1 Hz. GC/MS data were obtained on a HP 6890 gas chromatograph equipped with a HP 5973 MS detector and a capillary column

(HP 19091s-433:30 m, phenylmethyl siloxane). Major ions were recorded to unit mass, and the intensity was parenthetically indicated as a percentage of the strongest peak. Melting points were measured with a Fisher melting point apparatus. IR data were collected on a Thermo Electron Corporation Nicolet 6700 FT-IR-ATR using ZnSe crystal. Atmosphere was selected as the background. Low resolution mass spectra (LRMS) were obtained by ESI method with apex-Qe series instrument, BRUKER.

Materials. Chloroform, ethyl acetate and dichloromethane (HPLC grade) were used as received. Deionized water was used from the in-house system. Hexane for column chromatography was distilled before use. THF was distilled from sodium/benzophenone under nitrogen atmosphere. Et_3N, diisopropylamine, benzene, and toluene were distilled from CaH_2 under nitrogen atmosphere prior to use. 1,4-Dibutoxybenzene was purchased from TCI. 4,4'-bromo-2,2'-bipyridine was purchased from Carbosynth. 2,2'-Bipyridine N,N'-dioxide, 2,2'-bipyridyl N-oxide, dimethyl 5-bromoisophthalate, 1,4-bis((trimethylsilyl)ethynyl)benzene, trimethylsilylacetylene, and $AgPF_6$ were purchased from Fisher-Acros or from Sigma-Aldrich. Palladium catalysts ($Pd(PPh_3)_2Cl_2$, $Pd(dba)_2$, and $Pd(PPh_3)_4$), and $Ru(DMSO)_4Cl_2$ were purchased from Strem and stored at 5-10°C. Organolithium reagents (MeLi/LiBr, 1.5 M solution in diethyl ether), copper catalysts (CuI and CuBr), tetrabutylammoniumfluoride trihydrate (TBAF), and all other commercially available chemicals and solvents were purchased from Fisher-Acros or from Sigma-Aldrich and were used as received.

Synthesis and Characterization Data

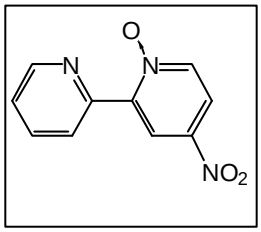

4-Nitro-2-(pyridin-2-yl)pyridine 1-oxide (2).[25] A round bottom flask with 2,2'-bipyridyl N-oxide (1, 2.24 g, MW 172, 13 mmol) was cooled in an ice bath at 0°C. Pre-cooled concentrated sulfuric acid (0°C, 32 mL) was added. Then the reaction mixture was heated to reflux. Nitric acid (fuming, 3.5 mL) was added through an addition funnel over 8 hours. Then additional nitric acid (red fuming, 3 mL) was added over 2 hours. The reaction mixture was refluxed for additional 2 hours. After cooling to room temperature, the reaction mixture was poured into crushed ice. Pre-cooled NaOH aqueous solution (20%, 0°C) was added dropwise to neutralize the acidic solution. A yellow precipitate formed as the pH was close to 7. The mixture was filtered and the precipitate was washed with cold distilled water to give the product **2** as yellow powder (1.93 g, Mw 217). Yield: 68%. ^{1}H NMR ($CDCl_3$): δ 9.16 (d, 1H, J = 3.0 Hz), δ 8.87-8.89 (d, 1H, J = 8.0 Hz), δ 8.78-8.79 (d, 1H, J = 4.5 Hz), δ 8.35-8.36 (d, 1H, J = 7.0 Hz), δ 8.05-8.07 (dd, 1H, J = 3.0, 7.0 Hz), δ 7.86-7.89 (m, 1H), δ 7.42-7.44 (m, 1H) ppm. The spectral data of the product were consistent with those reported in literature.[41]

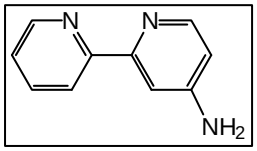

2,2'-Bipyridine-4-amine (3).[41] Under nitrogen atmosphere, 4-nitro-2,2'-bipyridyl N-oxide (**2**, 2.2 g, MW 217, 10 mmol) was added to pre-cooled methanol (0°C, 200 mL). Pd/C (0.5 g) was added. Then $NaBH_4$ (7.7 g, Mw 38, 200 mmol) was added in small portions to the solution with stirring. The flask was left under nitrogen flow to ensure all the hydrogen generated was removed. The resulting mixture was filtered to remove the catalyst, and the filtrate was dried under vacuum. Diluted HCl_{aq} (20%) was used to dissolve the crude product. The aqueous layer

was separated and saved. 40% NaOH aqueous solution was added dropwise to adjust to pH 10. Dichloromethane was used to do the standard workup to give product **3** as pale yellow powder (1.2 g, Mw 171). Yield: 70%. ^{1}H NMR ($CDCl_3$): δ 8.64-8.65 (d, 1H, J = 4.0 Hz), δ 8.35-8.37 (d, 1H, J = 8.0 Hz), δ 8.31-8.32 (d, 1H, J = 5.5 Hz), δ 7.77-7.81 (ddd, 1H, J = 1.5, 7.5 Hz), δ 7.68 (d, 1H, J = 2.5 Hz), δ 7.27-7.30 (m, 1H), δ 6.55-6.56 (dd, 1H, J = 2.5, 5.5 Hz), δ 4.26 (s, 2H) ppm. The spectral data of the product were consistent with those reported in literature.[41]

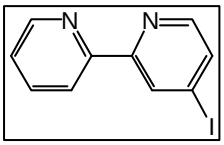

4-Iodo-2,2'-bipyridine (4).[41] 2,2'-Bipyridine-4-amine (**3**, 0.42 g, MW 171, 2.5 mmol) was suspended in 7.5 M aqueous H_2SO_4 (20 mL) and cooled to -10°C. A pre-cooled solution of $NaNO_2$ (0°C, 0.85 g, Mw 69, 12.3 mmol) in water (8 mL) was added dropwise over 1 hour with stirring. After an additional 15 minutes stirring, a pre-cooled solution of KI (0°C, 6.1 g, Mw 166, 37 mmol) in water (12 mL) was added dropwise over 1 hour. Then the reaction mixture was kept stirring for 30 minutes at -10°C and allowed to warm to room temperature. The resulting mixture was neutralized by sodium carbonate to pH 7-8. Sodium thiosulfate aqueous solution (10%) was used to decolorize the solution. After standard workup with dichloromethane, the resulting crude product was purified by silica gel column chromatography (ethyl acetate:hexane = 1:4, R_f = 0.31) to give the product **4** as white powder (0.41 g, Mw 282). Yield: 60%. ^{1}H NMR ($CDCl_3$): δ 8.83 (d, 1H, J = 1.0 Hz), δ 8.68 (d, 1H, J = 4.0 Hz), δ 8.37-8.38 (d, 1H, J = 8.0 Hz), δ 8.31-8.32 (d, 1H, J = 5.0 Hz), δ 7.80-7.84 (ddd, 1H, J = 2.0, 8.0 Hz), δ 7.68-7.69 (dd, 1H, J = 1.5, 5.5 Hz), δ 7.32-7.34 (m, 1H) ppm. The spectral data of the product were consistent with those reported in literature.[41]

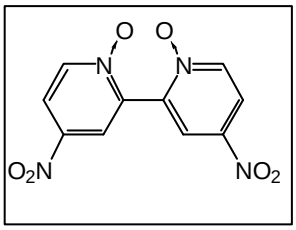

4,4'-Dinitro-2,2'-bipyridine 1,1'-dioxide (6).[26,27] Concentrated sulfuric acid (14 mL) was added to 2,2'-bipyridine N,N'-dioxide (**5**, 2.84 g, MW 188, 15.1 mmol) until all powder dissolved. The reaction mixture was cooled with an ice bath for 30 minutes, and nitric acid (fuming, 4.8 mL) was added dropwise via an addition funnel. The resulting solution was refluxed (100°C) for 24 hours. After the mixture was cooled to room temperature, the acidic mixture was poured into liquid nitrogen treated ice and let melt. A bright yellow precipitate formed. The mixture was filtered and the yellow precipitate was washed with water 3 times and allowed to air dry to give product **6** as yellow powder (2.05 g, Mw 278). Yield: 49%. ^{1}H NMR (DMSO)-d_6: δ 8.69 (d, 2H, J = 3.0 Hz), δ 8.59-8.60 (d, 2H, J = 7.5 Hz), δ 8.36-8.38 (dd, 2H, J = 3.0, 7.5 Hz) ppm. ^{13}C NMR (DMSO)-d_6: δ 142.55, 141.68, 140.92, 124.22, 122.40.

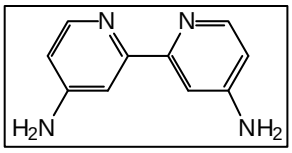

2,2'-Bipyridine-4,4'-diamine (7).[27] A mixture of 4,4'-dinitro-2,2'-bipyridine N,N'-dioxide (**6**, 3.5 g, MW 278, 12.6 mmol) and Pd/C (10%) (3.2 g) in absolute ethanol (390 mL) was purged with nitrogen for 30 minutes. The suspension was heated to reflux under nitrogen atmosphere. Hydrazine hydrate (28 mL) in absolute ethanol (130 mL) was added dropwise. The resulting solution was kept at reflux temperature overnight. The reaction mixture was immediately filtered, while hot, through Celite 521 and the pad was washed with boiling ethanol (4 x 50 mL). The combined ethanol solutions were reduced in volume to approximately 50 mL under vacuum. Distilled water (150 mL) was added into the solution. The resulting solution was kept at 2-8°C overnight. Compound **7** (1.75 g, MW 186) was obtained as pale yellow needle-like crystal. Yield: 75%. ^{1}H NMR (DMSO)-d_6: δ 8.01-8.03 (d, 2H, J

= 5.5 Hz), δ 7.53 (d, 2H, J = 2.0 Hz), δ 6.43-6.45 (dd, 2H, J = 2.5, 6.0 Hz), δ 6.02 (s, 4H, NH_2) ppm. ^{13}C NMR (DMSO)-d_6: δ 156.13, 154.91, 148.89, 108.61, 105.57.

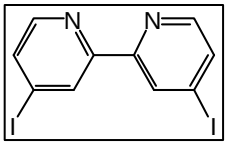

4,4'-Diiodo-2,2'-bipyridine (8).[41] 2,2'-Bipyridine-4,4'-diamine (**7**, 0.89 g, MW 186, 4.8 mmol) was suspended in 7.5 M aqueous H_2SO_4 (38 mL) and cooled to -10°C with an acetone/ice bath. A pre-cooled solution of $NaNO_2$ (0°C, 1.65 g, MW 69, 23.9 mmol) in water (15.3 mL) was added dropwise over 1 hour with stirring. After an additional 15 minutes, a pre-cooled solution of KI (0°C, 5.55 g, Mw 166, 33.4 mmol) in acetone/water (150 mL, v/v = 2:3) was added dropwise over 1 hour. The reaction mixture was kept stirring for 30 minutes at -10°C, allowed to warm to room temperature, then neutralized by sodium carbonate aqueous solution (10%). Sodium thiosulfate aqueous solution (10%) was used to decolorize the solution. After standard workup with dichloromethane, the compound **8** was recrystallized from ethanol as grey powder (0.84 g, MW 408). Yield: 43%. ^{1}H NMR (THF)-d_8: δ 8.85-8.86 (d, 2H, J = 1.5 Hz), δ 8.30-8.31 (d, 2H, J = 5.0 Hz), δ 7.78-7.79 (dd, 2H, J = 1.5, 5.0 Hz) ppm. ^{13}C NMR (THF)-d_8: δ 156.13, 150.51, 134.27, 131.12, 107.01.

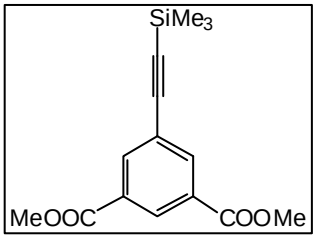

Dimethyl 5-((trimethylsilyl)ethynyl)isophthalate (10).[41] A flame-dried round bottom flask was charged with dimethyl 5-bromoisophthalate (**9**, 6.95 g, Mw 273, 25.5 mmol), diisopropylamine (160 mL), CuBr (360 mg, Mw 143, 2.52 mmol), trimethylsilylacetylene (25 g, Mw 98.22, 255 mmol), and $Pd(PPh_3)_2Cl_2$ (890 mg, Mw 701.89, 1.27 mmol),. The reaction mixture was stirred overnight at reflux

temperature under nitrogen atmosphere. After was cooled to room temperature, the resulting mixture was filtered, and the solvent was removed under vacuum. The remaining crude product was purified by silica gel column chromatography (ethyl acetate:hexane = 1:9, R_f = 0.32) to give the product **10** as white powder (7.19 g, MW 290). Yield: 97%. If dimethyl 5-iodoisophthalate was used instead of dimethyl 5-bromoisophthalate, the reaction was run at room temperature with 4 equivalents of trimethylsilylacetylene. The yield is similar. Mp: 100-102°C. ^{1}H NMR ($CDCl_3$): δ 8.60 (s, 1H), δ 8.29 (d, 2H, J = 1.5 Hz), δ 3.95 (s, 6H), δ 0.27 (s, 9H) ppm. The spectral data of the product were consistent with those reported in literature.[41]

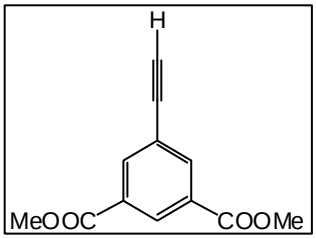

Dimethyl 5-ethynylisophthalate 11.[41] Tetrabutyl ammonium floride trihydrate (490 mg, Mw 315.5, 1.6 mmol) in THF (10 mL) was added to a THF (5 mL) solution of dimethyl 5-((trimethylsilyl)ethynyl)isophthalate (**10**, 400 mg, MW 290, 1.4 mmol) at -5°C in an acetone/ice bath. The reaction mixture was kept stirring at -5°C for 2 hours, monitored with TLC monitoring, and quenched by pouring into distilled water. After standard workup with chloroform, the crude product was purified by silica gel column chromatography (ethyl acetate:hexane = 1:9, R_f = 0.32) to give product **11** as white powder (290 mg, MW 218). Yield: 96%. Mp: 124-127°C. ^{1}H NMR ($CDCl_3$): δ 8.64 (s, 1H), δ 8.32 (d, 2H, J = 1.5 Hz), δ 3.96 (s, 6H), δ 3.17 (s, 1H) ppm. The spectral data of the product were consistent with those reported in literature.[41]

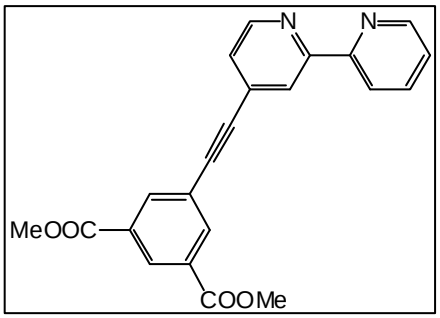

Dimethyl 5-(2,2'-bipyridin-4-ylethynyl) isophthalate 12.[41] A flame-dried round bottom flask was charged with 4-iodo-2,2'-bipyridine (**8**, 200 mg, MW 282, 0.71 mmol), benzene (20 mL), THF (5 mL), diisopropylamine (8 mL), dimethyl 5-ethynyl isophthalate (**11**, 186 mg, MW 218, 0.85 mmol), and $Pd(PPh_3)_4$ (41 mg, MW 1156, 0.035 mmol). The reaction mixture was kept stirring at 80°C under nitrogen atmosphere for 24 hours. After it cooled to room temperature, the reaction mixture was filtered, and the filtrate evaporated under vacuum. After standard workup with chloroform, the crude product was purified by silica column chromatography (ethyl acetate:hexane = 4:6, R_f = 0.36) to give product **12** as white powder (210 mg, MW 372). Yield: 80%. ^{1}H NMR ($CDCl_3$): δ 8.69-8.72 (m, 3H), δ 8.57 (s, 1H), δ 8.41-8.43 (m, 3H), δ 7.83-7.87 (ddd, 1H, J = 1.5, 8.0 Hz), δ 7.41-7.42 (dd, 1H, J = 1.5, 5.0 Hz), δ 7.34-7.36 (m, 1H), δ 3.99 (s, 6H) ppm. The spectral data of the product were consistent with those reported in literature.[41]

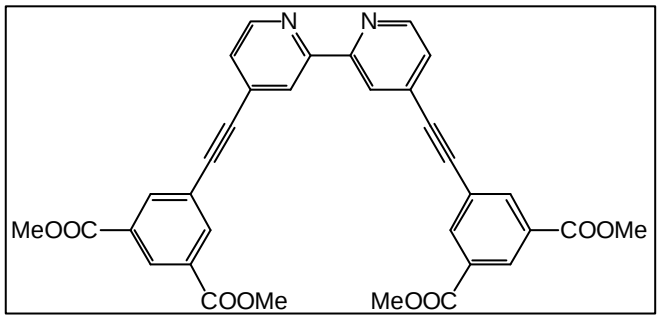

Tetramethyl 5,5'-(2,2'-bipyridine-4,4'-diylbis(ethyne-2,1-diyl))diisophthalate (13). A flame-dried round bottom flask was charged with 4,4'-bromo-2,2'-bipyridine (100 mg, MW 314, 0.32 mmol), benzene (7 mL), diisopropylamine (7 mL), THF (15 mL), dimethyl 5-ethynylisophthalate (**11,** 274 mg, MW 218, 1.28 mmol), and $Pd(PPh_3)_4$ (110 mg, Mw 1156, 0.062 mmol). The reaction mixture was stirred at 80°C under nitrogen atmosphere for 2 days. The progress of the reaction was monitored by

TLC. After cooled to room temperature, the reaction mixture was filtered, and the filtrate was placed under vacuum to remove the solvent. After standard workup with large amount of chloroform, the crude product was purified by silica column chromatography (dichloromethane:methanol = 95:5, R_f = 0.25), followed by precipitation from small amount of chloroform to give product **13** as grey powder (150 mg, Mw 589). Yield: 80%. ^{1}H NMR ($CDCl_3$): δ 8.73-8.74 (d, 2H, J = 5.0 Hz), δ 8.70 (s, 2H), δ 8.59 (s, 2H), δ 8.42 (d, 4H, J = 1.5 Hz), δ 7.46-7.47 (d, 2H, J = 5.0 Hz), δ 4.00 (s, 12H) ppm. MS (ESI) calcd for $C_{34}H_{24}N_2O_8$: 588.15. Found: 589.16. The ^{13}C is not available due to the low solubility.

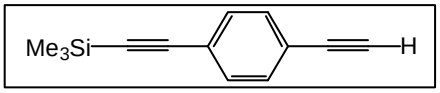

((4-Ethynylphenyl)ethynyl)trimethylsilane (15).[41] A solution of MeLi/LiBr (4.9 mL, 7.4 mmol in hexane) in THF (20 mL) was added dropwise into a solution of 1,4-bis((trimethylsilyl)ethynyl)benzene (**14**, 2 g, MW 270.5, 7.4 mmol) in THF (50 mL) at 0°C. The resulting mixture was stirred for another 15 minutes, and then poured into an ice-cold diluted HCl aqueous solution (10%). Diethyl ether was used for the standard workup. The mixture of compound **14** and **15** was difficult to separate. Thus after a short column (hexane), composition of the purified mixture was checked by GC-MS, Yield: 42%. GC/MS m/z: 198 (M^+), 183 (M -15). The reaction mixture was used in the next reaction. The unreacted starting material **14** was easily isolated and recovered through silica column chromatography in next step. This product was synthesized and reported in literature.[41]

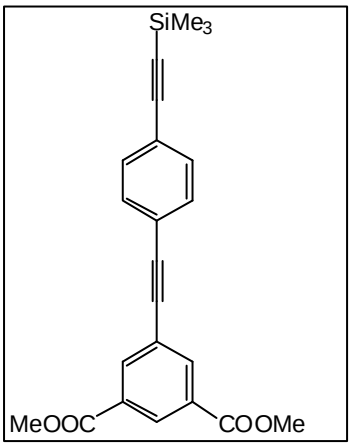

Dimethyl 5-((4-((trimethylsilyl)ethynyl)phenyl) ethynyl)isophthalate (16).[41] A flame-dried round bottom flask was charged with dimethyl 5-bromoisophthalate (**9**, 2.63 g, MW 320, 8.22 mmol), PPh_3 (0.43 g, Mw 262, 1.64 mmol), triethylamine (2.0 mL), THF (200 mL), mixture of 1,4-bis((trimethylsilyl) ethynyl)benzene (**14)** and ((4-ethynyl phenyl)ethynyl)trimethyl silane (**15)** (1.63 g of **14**, MW 198, 8.23 mmol), and $Pd(dba)_2$ (0.24 g, Mw 575, 0.41 mmol). The reaction mixture was stirred for 24 hours at reflux temperature under nitrogen atmosphere. After it cooled to room temperature, the reaction mixture was filtered, and the solvent was removed under vacuum. After standard workup with chloroform, the crude product was purified by silica gel column chromatography (ethyl acetate:hexane = 1:9, R_f = 0.42) to give the product **16** as a pale yellow powder (2.14 g, MW 390). Yield: 67%. Mp: 161-162°C. ^{1}H NMR ($CDCl_3$): δ 8.63 (s, 1H), δ 8.35-8.36 (d, 2H, J = 1.5 Hz), δ 7.47 (m, 4H), δ 3.97 (s, 6H), δ 0.26 (s, 9H) ppm. The spectral data of the product were consistent with those reported in literature.[41]

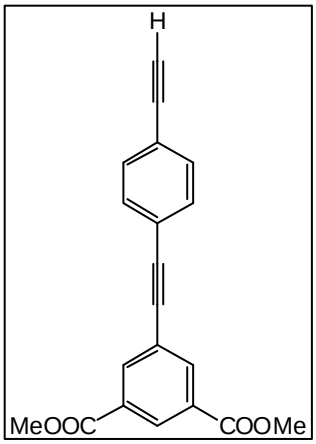

Dimethyl 5-((4-ethynylphenyl)ethynyl)isophthalate (17).[41] Tetrabutylammonium floride trihydrate (in 1 M THF, 0.97 mL, MW 261, 0.97 mmol) in THF (10 mL) was added to a THF (20 mL) solution of dimethyl 5-((4-((trimethylsilyl)ethynyl)phenyl) ethynyl)isophthalate (**16**, 315 mg, MW 390, 0.81 mmol) under stirring at -5°C in an acetone/ice bath. The reaction mixture was stirred at -5°C for 2 hours with TLC monitoring, and quenched by pouring

into sufficient distilled water. Dichloromethane was used to do the standard workup. The crude product was purified by silica gel column chromatography (ethyl acetate:hexane = 1:9, R_f = 0.39) to give the product **17** as white powder (175 mg, MW 318). Yield: 68%. Mp: 161-165°C. ^{1}H NMR ($CDCl_3$): δ 8.63 (s, 1H), δ 8.36 (d, 2H, J = 1.5 Hz), δ 7.50 (s, 4H), δ 3.97 (s, 6H), δ 3.20 (s, 1H) ppm. The spectral data of the product were consistent with those reported in literature.[41]

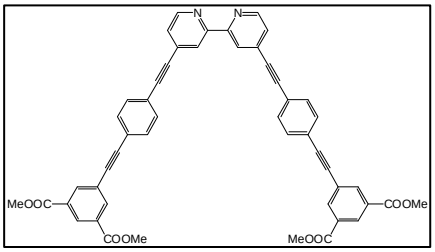

Tetramethyl 5,5'-(4,4'-(2,2'-bipyridine-4,4'-diylbis(ethyne-2,1-diyl))bis(4,1-phenylene)) bis (ethyne-2,1-diyl) diisophthalate (18). A flame-dried round bottom flask was charged with 4,4'-dibromo-2,2'-bipyridine (200 mg, MW 314, 0.64 mmol), benzene (15 mL), diisopropylamine (15 mL), THF (15 mL), dimethyl 5-((4-ethynylphenyl)ethynyl) isophthalate (**17**, 810 mg, MW 318, 2.55 mmol), and $Pd(PPh_3)_4$ (150 mg, MW 1156, 0.13 mmol). The reaction mixture was kept stirring at 80°C under nitrogen atmosphere for at least 3 days. TLC was used to monitor the process. After it cooled to room temperature, the reaction mixture was filtered, and the filtrate was evaporated under vacuum. After standard workup with large amount of chloroform (because of the low solubility of the product), the crude product was purified by silica column chromatography (dichloromethane:methanol = 95:5, R_f = 0.23), followed by precipitation from small amount of chloroform to give product **18** as grey powder (200 mg, MW 788). Yield: 40%. ^{1}H NMR ($CDCl_3$): δ 8.70-8.71 (d, 2H, J = 4.5 Hz), δ 8.65 (s, 2H), δ 8.56 (s, 2H), δ 8.39 (s, 4H), δ 7.58 (s, 8H), δ 7.43-7.44 (d, 2H, J = 4.5 Hz), δ 3.98 (s, 12H) ppm. MS (ESI) calcd for $C_{50}H_{32}N_2O_8$: 788.22. Found: 789.23. The ^{13}C is not available due to the low solubility.

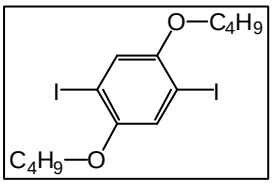

1,4-Dibutoxy-2,5-diiodobenzene (20).[38] The suspension of 1,4-dibutoxybenzene (**19**, 0.89 g, MW 222, 4 mmol), mercury (II) acetate (3.19 g, MW 319, 10 mmol) and iodine (2.54 g, MW 254, 10 mmol) in dichloromethane (70 mL) was kept stirring overnight at room temperature. The mixture was filtered through Celite 521 to remove precipitate. The filtrate was washed with $Na_2S_2O_{3\ aq.}$ (10%), $NaHSO_{3\ aq.}$ (20%), H_2O, and $NaCl_{\ aq.}$ (10%) sequencely. After dried with Na_2SO_4, the solvent was removed under vacuum. The crude product was recrystallized from ethanol to give the product **20** (1.73 g, MW 474). Yield: 77%. ^{1}H NMR ($CDCl_3$): δ 7.18 (s, 2H), δ 3.92-3.95 (t, 4H, J = 6.5 Hz), δ 1.76-1.81 (m, 4H), δ 1.50-1.57 (m, 4H), δ 0.97-1.00 (t, 6H, J = 7.0 Hz) ppm. ^{13}C NMR ($CDCl_3$): δ 152.77, 122.69, 86.27, 69.96, 31.18, 19.25, 13.79.

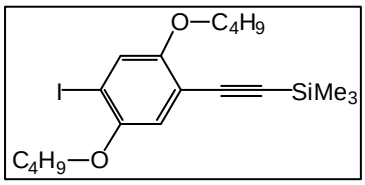

((2,5-Dibutoxy-4-iodophenyl)ethynyl)trimethyl silane (21).[38] A flame-dried round bottom flask was charged with 1,4-dibutoxy-2,5-diiodobenzene (**20**, 6.0 g, MW 474, 12.66 mmol), diisopropylamine (35 mL), THF (85 mL), CuI (120 mg, MW 190, 0.633 mmol), trimethylsilylacetylene (1.75 mL, Mw 98, 12.66 mmol), and $Pd(PPh_3)_2Cl_2$ (0.89 g, Mw 701, 1.266 mmol). Trimethylsilylacetylene was diluted with 15 mL THF and was added into the reaction mixture dropwise. The reaction mixture was kept stirring overnight at room temperature under nitrogen atmosphere. Then the resulting mixture was filtered, and the solvent was removed under vacuum. After standard workup with chloroform, the remaining crude product was purified by silica gel column chromatography (chloroform:hexane = 1:4, R_f = 0.30) to give the yellow oil product **21** (2.3 g, MW 444.42). Yield: 41%. ^{1}H NMR ($CDCl_3$): δ 7.40 (s, 1H), δ 6.92 (s, 1H), δ

3.98-4.03 (ddd, 4H, J = 1.5, 6.5 Hz), δ 1.72-1.80 (m, 4H), δ 1.52-1.60 (m, 4H), δ 0.96-0.99 (t, 6H, J = 7.0 Hz), δ 0.22 (s, 9H) ppm. ^{13}C NMR ($CDCl_3$): δ 154.88, 151.70, 123.92, 116.23, 113.49, 100.76, 99.41, 87.86, 69.76, 69.56, 31.33, 31.25, 19.31, 19.19, 13.84, 13.81, 0.10.

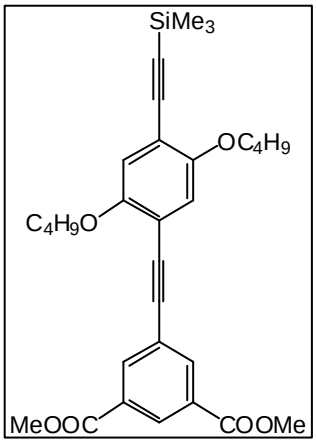

Dimethyl 5-((2,5-dibutoxy-4-((trimethylsilyl)ethynyl) phenyl)ethynyl)isophthalate (22). A flame-dried round bottom flask was charged with ((2,5-dibutoxy-4-iodophenyl)ethynyl) trimethylsilane (**21**, 1.22 g, MW 444, 2.75 mmol), diisopropylamine (10 mL), THF (35 mL), CuI (26 mg, Mw 190, 0.137 mmol), dimethyl 5-ethynylisophthalate (11, 0.72 g, Mw 218, 3.29 mmol), and $Pd(PPh_3)_2Cl_2$ (0.19 g, MW 701, 0.275 mmol). The reaction mixture was kept stirring overnight at 40°C under nitrogen atmosphere. After cooled to room temperature, the resulting mixture was filtered, and the solvent was removed under vacuum. After standard workup with chloroform, the crude product was purified by silica gel column chromatography (ethyl acetate:hexane = 1:9, R_f = 0.41) to give the product **22** as yellow powder (1.24 g, Mw 534). Yield: 84%. Mp: 105-106°C. ^{1}H NMR ($CDCl_3$): δ 8.61 (s, 1H), δ 8.34 (s, 2H), δ 6.96-6.98 (d, 2H, J = 8.0 Hz), δ 3.99-4.03 (m, 4H), δ 3.96 (s, 6H), δ 1.80-1.85 (m, 4H), δ 1.55-1.61 (m, 4H), δ 0.98-1.04 (m, 6H), δ 0.27 (s, 9H) ppm. ^{13}C NMR ($CDCl_3$): δ 165.53, 154.08, 153.62, 136.33, 130.86, 129.92, 124.48, 117.10, 116.85, 114.37, 113.22, 100.90, 100.44, 92.59, 87.83, 69.24, 69.21, 52.45, 31.30, 31.29, 19.28, 19.20, 13.84, 0.14.

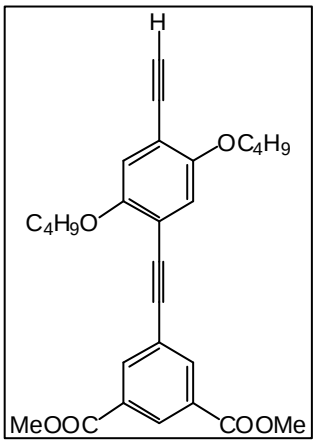

Dimethyl 5-((2,5-dibutoxy-4-ethynylphenyl)ethynyl) isophthalate (23). Tetrabutylammonium fluoride trihydrate (1 M in THF, 1.2 mL, Mw 261, 1.2 mmol) in THF (5 mL) was added to a THF (40 mL) solution of dimethyl 5-((2,5-dibutoxy-4-((trimethylsilyl)ethynyl)phenyl)ethynyl)isophthalate (**22**, 500 mg, MW 534, 0.94 mmol) at -5°C (acetone/ice bath). The reaction mixture was stirred at -5°C for 2 hours with TLC monitoring, and quenched by pouring into distilled water. Dichloromethane was used for the standard workup. The crude product was purified by silica gel column chromatography (ethyl acetate:hexane = 1:9, R_f = 0.23) to give the product **23** as yellow powder (320 mg, MW 462). Yield: 74%. Mp: 128-129°C. ^{1}H NMR ($CDCl_3$): δ 8.63 (s, 1H), δ 8.36-8.37 (d, 2H, J = 1.5 Hz), δ 7.00-7.01 (d, 2H, J = 5.0 Hz), δ 4.02-4.05 (ddd, 4H, J = 2.5, 6.5 Hz), δ 3.97 (s, 6H), δ 3.37 (s, 1H), δ 1.80-1.87 (m, 4H), δ 1.50-1.63 (m, 4H), δ 0.99-1.04 (m, 6H) ppm. ^{13}C NMR ($CDCl_3$): δ 165.53, 154.08, 153.62, 136.33, 130.86, 129.92, 124.48, 117.10, 116.85, 114.37, 113.22, 100.90, 100.44, 92.59, 87.83, 69.24, 69.21, 52.45, 31.30, 31.29, 19.29, 19.20, 13.84.

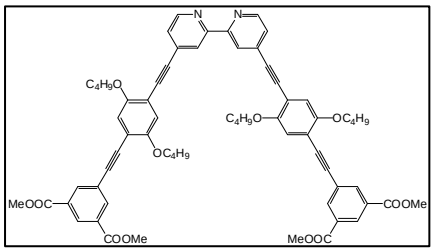

Tetramethyl 5,5'-((([2,2'-bipyridine]-4,4'-diylbis(ethyne-2,1-diyl))bis(2,5-dibutoxy-4,1-phenylene))bis (ethyne-2,1-diyl))diisophthalate (24). A flame-dried round bottom flask was charged with 4,4'-diiodo-2,2'-bipyridine (**4**, 120 mg, MW 408, 0.29 mmol), THF (14 mL), triethylamine (2 mL), PPh_3 (15 mg, MW 262, 0.0588 mmol), dimethyl 5-((2,5-dibutoxy-4-ethynylphenyl)ethynyl)isophthalate (**23**, 300 mg, MW 462, 0.65 mmol), and $Pd(PPh_3)_4$

(34 mg, MW 1155, 0.0294 mmol). The reaction mixture was kept stirring at 50°C under nitrogen atmosphere for 4 days with TLC monitoring. After cooled to room temperature, the reaction mixture was filtered, and the filtrate was placed under vacuum to remove the solvent. After standard workup with chloroform, the crude product was purified by silica column chromatography (dichloromethane:THF = 9:1, R_f = 0.21) to give a yellow powder **24** (220 mg, MW 1077). Yield: 69%. ^{1}H NMR ($CDCl_3$): δ 8.68-8.69 (d, 2H, J = 5.0 Hz), δ 8.63(s, 2H), δ 8.55(s, 2H), δ 8.37-8.38 (d, 4H, J = 1.5 Hz), δ 7.41-7.42 (dd, 2H, J = 1.5, 5.0 Hz), δ 7.05-7.06 (d, 4H, J = 4.0 Hz), δ 4.06-4.09 (t, 8H, J = 6.5 Hz), δ 3.97 (s, 12H), δ 1.85-1.91 (m, 8H), δ 1.59-1.64 (m, 8H), δ 1.03-1.06 (m, 12H) ppm. ^{13}C NMR ($CDCl_3$): δ 165.59, 155.76, 154.00, 153.83, 149.20, 136.43, 132.59, 131.01, 130.08, 125.36, 124.50, 123.17, 117.25, 117.06, 114.29, 113.54, 93.09, 92.50, 90.62, 87.80, 69.48, 69.47, 52.48, 31.35, 19.34, 19.32, 13.89, 13.86. LRMS (ESI) calcd for $C_{66}H_{64}N_2O_{12}$: 1076.45. Found: 1077.46.

Homoleptic ruthenium complex 3SSC.

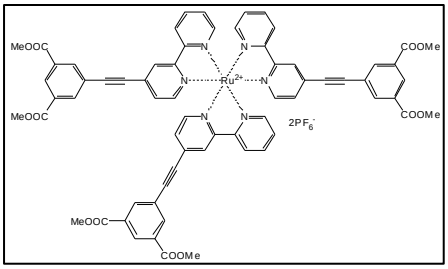

(a) Synthesis of $Ru(DMSO)_4(PF)_6$. A round bottom flask was charged with $Ru(DMSO)_4Cl_2$, $AgPF_6$, and ethanol. The reaction mixture was heated to reflux for 12 hours under nitrogen atmosphere. After it cooled to room temperature, the reaction mixture was filtered through Celite 521. A few drop of ethanol was used to rinse the Celite pad. The orange-yellow filtrate was placed under nitrogen flow overnight to remove solvent. The resulting $Ru(DMSO)_4(PF_6)_2$ (MW 673) was kept under nitrogen atmosphere for next step.

(b) Complexation. $Ru(DMSO)_4(PF_6)_2$ (56 mg, MW 703, 0.08 mmol), dimethyl 5-(2,2'-bipyridin-4-ylethynyl)isophthalate (**12**, 100 mg, MW 372, 0.28 mmol), THF (5 mL), and nitrogen-purged 1-butanol (12 mL) were added into a round bottom flask, and the reaction mixture was heated to reflux under nitrogen atmosphere. Every 24 hours, the reaction mixture was monitored by UV-Vis spectroscopy until the reaction completed (Figure A-2-6.1). The reaction mixture was cooled to room temperature and filtered. The resulting powder was rinsed with acetone. The filtrate was evaporated under vacuum and an orange powder (**3SSC**, 78 mg, MW 1508) formed by adding hexane. Yield: 66%. ^{1}H NMR (acetone)-d_6: δ 8.80(broad, 3H), δ 8.71(broad, 3H), δ 8.65-8.67(m, 3H), δ 8.53(s, 6H), δ 8.24(broad, 3H), δ 7.92-7.93(broad, 3H), δ 7.85-7.86(broad, 3H), δ 7.62-7.63(broad, 3H), δ 7.57-7.58(broad, 3H), δ 4.05(s, 18H). MS (ESI) calcd for $C_{66}H_{48}N_6O_{12}Ru^{2+}$: 1218.24. Found: 1218.24. The ^{13}C was not available due to the low solubility. IR-ATR (cm^{-1}): 2952 (C-H_{Ar}), 2848 (C-H_{CH3}), 2217 ($C{\equiv}C$), 1730 ($C{=}O$), 1610 ($C{=}C_{Ar}$), 1476, 1440, 1352, 1319, 1303, 1247 (C-O), 1198, 1155, 998, 914, 837 (C-H_{Ar}).

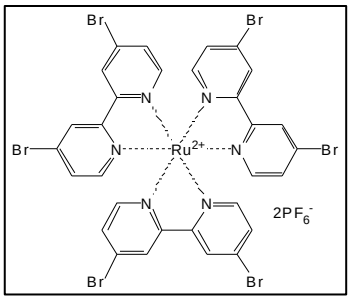

Ruthenium tris(4,4'-dibromo-2,2'-bipyridine) (26). $Ru(DMSO)_4(PF_6)_2$ (440 mg, MW 703, 0.58 mmol), 4,4'-dibromo-2,2'-bipyridine (**25**, 650 mg, Mw 314, 2.03 mmol), THF (5 mL), and nitrogen-purged 1-butanol (30 mL) were added into a round bottom flask, and the reaction mixture was heated to reflux under nitrogen atmosphere. Every 24 hours, the reaction mixture was monitored by UV-Vis spectroscopy until the reaction completed (Figure A-2-6.1). The reaction mixture was cooled to room temperature and filtered. The filtrate was condensed by under vacuum and an orange powder (**26**, 300 mg, Mw 1333) formed by adding hexane. Yield: 48%. ^{1}H

NMR (methanol)-d_4: δ 9.04(d, 3H, J = 1.5 Hz), δ 7.60-7.75(m, 6H). ^{13}C NMR (methanol)-d_4: δ 158.51, 153.66, 136.33, 132.91, 130.13.

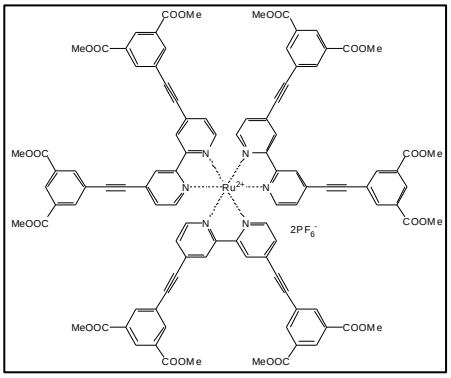

Homoleptic ruthenium complex SSC. A flame-dried round bottom flask was charged with ruthenium tris(4,4'-dibromo-2,2'-bipyridine) (**26**, 50 mg, MW 1333, 0.038 mmol), benzene (2.5 mL), diisopropylamine (2 mL), THF (2 mL), dimethyl 5-ethynylisophthalate (**11**, 106 mg, Mw 218, 0.486 mmol), and $Pd(PPh_3)_4$ (5 mg, Mw 1156, 0.004 mmol). The reaction mixture was stirred at 80°C under nitrogen atmosphere for 3 days and monitored with TLC. After it cooled to room temperature, the reaction mixture was filtered, and the solvent was removed in vaccum. The crude product was purified by silica gel column chromatography (acetonitrile:H_2O = 85:15) to remove any unreacted starting material. The last band of silica gel was saved and rinsed with THF and acetone to give orange-red powder (**SSC**, 40 mg, MW 2157). Yield: 48%. ^{1}H NMR (acetone)-d_6: δ 9.22 (s, 6H), δ 8.64 (s, 6H), δ 8.40 (s, 12H), δ 8.36-8.37 (d, 6H, J = 6.0 Hz), δ 7.81-7.83 (m, 6H), δ 3.98 (s, 36H) ppm. MS (ESI) calcd for $C_{102}H_{72}N_6O_{24}Ru^{2+}$: 1866.36. Found: 1866.37. The ^{13}C was not available due to the low solubility. IR-ATR (cm^{-1}): 2952 (C-H_{Ar}), 2850 (C-H_{CH3}), 2218 ($C{\equiv}C$), 1720 ($C{=}O$), 1610 ($C{=}C_{Ar}$), 1479, 1441, 1311, 1249 (C-O), 1201, 1159, 995, 916, 879, 842 (C-H_{Ar}).

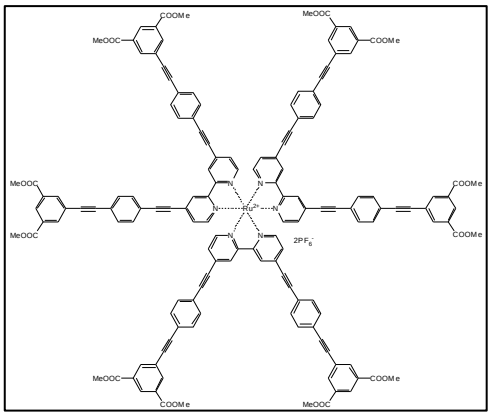

Homoleptic ruthenium complex LSC. A flame-dried round bottom flask was charged with ruthenium tris(4,4'-dibromo-2,2'-bipyridine) (**26**, 50 mg, MW 1333, 0.038 mmol), benzene (2.5 mL), diisopropylamine (2 mL), THF (4 mL), dimethyl 5-((4-ethynylphenyl) ethynyl) isophthalate (**17**, 180 mg, MW 390, 0.460 mmol), and $Pd(PPh_3)_4$ (5 mg, MW 1156, 0.004 mmol). The reaction mixture was stirred at 80°C under nitrogen atmosphere for 4 days and monitored with TLC. After it cooled to room temperature, the reaction mixture was filtered, and the solvent was removed in vaccum. The crude product was purified by silica gel column chromatography (acetonitrile:H_2O = 85:15) to remove any unreacted starting material. The last band of silica gel was saved and rinsed with THF and acetone to give orange-red powder (**LSC**, 30 mg, Mw 2757). Yield: 30%. ^{1}H NMR (THF)-d_8: δ 8.92(s, 6H), δ 8.60 (broad, 6H), δ 8.36 (s, 12H), δ 8.04-8.06 (m, 6H), δ 7.67 (broad, 30H), δ 3.93 (s, 36H) ppm. MS (ESI) calcd for $C_{150}H_{96}N_6O_{24}Ru^{2+}$: 2466.55. Found: 2466.58. The ^{13}C is not available due to the low solubility. IR-ATR (cm^{-1}): 2956 (*C-H$_{Ar}$*), 2858 (*C-H$_{CH3}$*), 2216 (*C≡C*), 1724 (*C=O*), 1600 (*C=C$_{Ar}$*), 1508, 1459, 1438, 1378, 1351, 1247 (*C-O*), 1120, 1070, 1039, 993, 912, 837 (*C-H$_{Ar}$*).

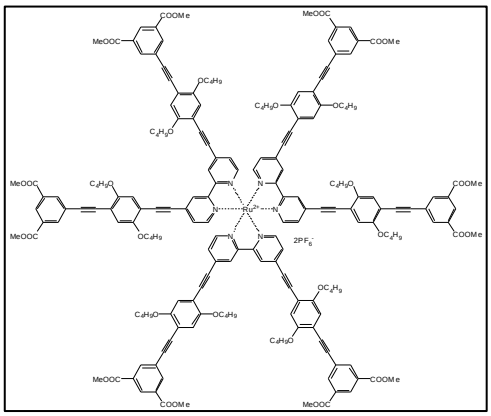

Homoleptic ruthenium complex SLSC. $Ru(DMSO)_4(PF_6)_2$ (12 mg, MW 703, 0.017 mmol), Tetramethyl 5,5'-((([2,2'-bipyridine]-4,4'-diylbis(ethyne-2,1-diyl))bis(2,5-dibutoxy-4,1-

phenylene))bis (ethyne-2,1-diyl))diisophthalate (**24**, 63 mg, Mw 1077, 0.058 mmol), THF (4 mL), and nitrogen-purged 1-butanol (4 mL) were added into a round bottom flask, and the reaction mixture was heated to reflux under nitrogen atmosphere. Every 24 hours, the reaction mixture was monitored by UV-Vis spectroscopy until the reaction completed (Figure A-2-6.1). The reaction mixture was cooled to room temperature and filtered. The crude product, a brown powder, was rinsed with acetone and filtered. The filtrate was condensed by under vacuum and orange-red powder (**SLSC**, 20 mg, MW 3597) formed by adding hexane. Yield: 34%. ^{1}H NMR (acetone)-d_6: δ 8.98-9.02 (broad, 6H), δ 8.56(s, 6H), δ 8.30(broad, 18H), δ 7.65-7.66 (broad, 6H), δ 7.35 (broad, 6H), δ 7.24-7.25 (broad, 6H), δ 4.14-4.18 (broad, 24H), δ 3.97 (s, 36H), δ 1.85-1.86 (m, 24H), δ 1.59-1.66 (m, 24H), δ 1.01-1.07 (m, 36H) ppm. ^{13}C NMR (acetone)-d_6: δ 164.84, 157.02, 154.43, 153.91, 152.13, 135.67, 133.26, 131.57, 129.68, 129.10, 126.19, 124.26, 117.14, 117.02, 115.49, 112.09, 95.45, 93.33, 90.78, 87.61, 69.28, 69.07, 52.09, 31.31, 31.14, 19.19, 19.05, 13.32, 13.28. MS (ESI) calcd for $C_{198}H_{192}N_6O_{36}Ru^{2+}$: 3331.24. Found: 3331.27. IR-ATR (cm^{-1}): 2956 (C-H_{Ar}), 2873 (C-H_{CH3}), 2208 ($C{\equiv}C$), 1728 ($C{=}O$), 1605 ($C{=}C_{Ar}$), 1502, 1438, 1411, 1382, 1355, 1326, 1245 (C-O), 1138, 1120, 1105, 1064, 1024, 1002, 9912, 839 (C-H_{Ar}).

A-2-9. References

1. Sprintschnik, G.; Sprintschnik, H. W.; Kirsch, P. P.; Whitten, D. G. Preparation and Photochemical Reactivity of Surfactant Ruthenium(II) Complexes in Monolayer Assemblies and at Water-Solid Tnterfaces. *J. Am. Chem. Soc.* **1977**, *99*, 4947.

2. Liska, P.; Vlachopoulos, N.; Nazeeruddin, M. K.; Comte, P.; Grätzel, M. cis-Diaquabis(2,2'-bipyridyl-4,4'-dicarboxylate)ruthenium(II) Sensitizes Wide Band Gap

Oxide Semiconductors Very Efficiently over a Broad Spectral Range in the Visible. *J. Am. Chem. Soc.* **1988**, *110*, 3686.

3. Ohkudo, K.; Hamada, T.; Inaoka, T.; Ishida, H. Photoinduced Enantioselective and Catalytic Reduction of Tris(acetylacetonato)cobalt with a Chiral Ruthenium Photosensitizer. *Inorg. Chem.* **1989**, *28*, 2021.

4. Hesek, D.; Inoue, Y.; Everitt, S. R. L.; Ishida, H.; Kunieda, M.; Drew, M. G. B. Novel Synthetic Routes to Several New, Differentially Substituted Ruthenium Tris(4,4'-disubstituted-2,2-bipyridine) Complexes. *Inorg. Chem.* **2000**, *39*, 308.

5. Broomhead, J. A.; Young, C. G. Tris(2,2'-bipyridine)ruthenium(II) Dichloride Hexahydrate. *Inorg. Synth.* **1990**, *28*, 338.

6. Otsuki, J.; Kameda, H.; Tomihira, S.; Sakaguchi, H.; Takido, T. Ruthenium Complexes Containing Fully Conjugated Ligands Terminated with Thiol Groups. *Chem. Lett.* **2002**, *31*, 610.

7. Chun, S.; Moon, S. J.; Na, Y. M.; Lee, Y.-A.; Jung, O.-S. Selective and Sensitive Recognition of Hexafluorophosphate via an Unusual Equilibrium between a Cationic Square Host and a PF_6^- Guest. *Inorg. Chem. Comm.* **2007**, *10*, 967.

8. James, B. R.; Ochiai, E.; Rempel, G. I. Ruthenium (II) Halide Dimethylsulphoxide Complexes from Hydrogenation Reactions. *Inorg. Nucl. Chem. Lett.* **1971**, *7*, 781.

9. Beer, P. D.; Kocian, O.; Mortimer, R. J.; Ridgway, C. Syntheses, Coordination, Spectroscopy and Electropolymerisation Studies of New Alkynyl and Vinyl Linked Benzo- and Aza-crown Ether–Bipyridyl Ruthenium(II) Complexes. Spectrochemical Recognition of Group IA/IIA Metal Cations *Chem. Commun.* **1991**, 1460.

10. Osawa, M.; Hoshino, M.; Horiuchi, S.; Wakatsuki, Y. Palladium-Mediated One-Step Coupling between Polypyridine Metal Complexes: Preparation of Rigid and Dendritic Nano-Sized Ruthenium Complexes. *Organmetallics* **1999**, *18*, 112.

11. Goze, C.; Kozlov, D. V.; Castellano, F. N.; Suffert, J.; Ziessel, R. Synthesis of Bipyridine and Terpyridine Based Ruthenium Metallosynthons for Grafting of Multiple Pyrene Auxiliaries. *Tetrahedron Lett.* **2003**, *44*, 8713.

12. Goze, C.; Kozlov, D. V.; Tyson, D. S.; Ziessel, R.; Castellano, F. N. Synthesis and Photophysics of Ruthenium(II) Complexes with Multiple Pyrenylethynylene Subunits. *New J. Chem.* **2003**, *27*, 1679.

13. Kozlov, D. V.; Tyson, D. S.; Goze, C.; Ziessel, R.; Castellano, F. N. Room Temperature Phosphorescence from Ruthenium(II) Complexes Bearing Conjugated Pyrenylethynylene Subunits. *Inorg. Chem.* **2004**, *43*, 6083.

14. Sonogashira, K.; Tohda, Y.; Hagihara, N. A Convenient Synthesis of Acetylenes: Catalytic Substitutions of Acetylenic Hydrogen with Bromoalkenes, Iodoarenes and Bromopyridines. *Tetrahedron Lett.* **1975**, *16*, 4467.

15. Takahashi, S.; Kuroyama, Y.; Sonogashira, K.; Hagihara, N. A Convenient Synthesis of Ethynylarenes and Diethynylarenes *Synthesis* **1980**, 627.

16. Dieck, H. A.; Heck, R. F. Palladium Catalyzed Synthesis of Aryl, Heterocyclic and Vinylic Acetylene Derivatives. *J. Organomet. Chem.* **1975**, *93*, 259.

17. Cassar, I. Synthesis of Aryl- and Vinyl-substituted Acetylene Derivatives by the Use of Nickel and Palladium Complexes. *J. Organomet. Chem.* **1975**, *93*, 253.

18. Bunz, U. Poly(aryleneethynylene)s: Syntheses, Properties, Structures, and Applications. *Chem. Rev.* **2000**, *100*, 1605.

19. Thorand, S.; Krause, N. Improved Procedures for the Palladium-Catalyzed Coupling of Terminal Alkynes with Aryl Bromides (Sonogashira Coupling). *J. Org. Chem.* **1998**, *63*, 8551.

20. Wang, D.; Schlegel, J. M.; Galoppini, E. Synthesis of Rigid-rod Linkers to Anchor Chromophores to Semiconductor Nanoparticles. *Tetrahedron* **2002**, *58*, 6027.

21. Soheili, A.; Albaneze-Walker, J.; Murry, J. A.; Dormer, P. G.; Hughes, D. L. Efficient and General Protocol for the Copper-Free Sonogashira Coupling of Aryl Bromides at Room Temperature. *Org. Lett.* **2003**, *5*, 4191.

22. Chinchilla, R.; C., N. The Sonogashira Reaction: A Booming Methodology in Synthetic Organic Chemistry. *Chem. Rev.* **2007**, *107*, 874.

23. Blanksby, S. J.; Ellison, G. B. Bond Dissociation Energies of Organic Molecules. *Acc. Chem. Res.* **2003**, *36*, 255.

24. Tischler, A. N.; Lanza, T. J. 6-Substituted Indoles from O-halonitrobenzenes. *Tetrahedron Lett.* **1986**, *27*, 1653.

25. Jones, R. A.; Roney, B. D.; Sasse, W. H. F.; Wade, K. O. The Synthesis and Physical Properties of Some 4-substituted 2,2'-bipyridyls and Their 1-oxides *J. Chem. Soc. B, Phys. Org.* **1967**, *2*, 106.

26. Wenkert, D.; Woodward, R. B. Studies of 2,2'-bipyridyl N,N'-dioxides. *J. Org. Chem.* **1983**, *48*, 283.

27. Kavanagh, P.; Leech, D. Improved Synthesis of 4,4'-diamino-2,2'-bipyridine from 4,4'-dinitro-2,2'-bipyridine-N,N'-dioxide. *Tetrahedron Lett.* **2004**, *45*, 121.

28. Adams, C. J.; Bowen, L. E.; Humphrey, M. G.; Morrall, J. P. L.; Samoc, M.; Yellowless, L. J. Ruthenium Bipyridyl Compounds with Two Terminal Alkynyl Ligands. *Dalton Trans.* **2004**, 4130.

29. Araki, K.; Mutai, T.; Shigemitsu, Y.; Yamada, M.; Nakajima, T.; Kuroda, S.; Shimao, I. 6-Amino-2,2'-bipyridine as a New Fluorescent Organic Compound *J. Chem. Soc., Perkin Trans. 2* **1996**, *4*, 613.

30. Bair, J. S.; Harrison, R. G. Synthesis and Optical Properties of Bifunctional Thiophene Molecules Coordinated to Ruthenium. *J. Org. Chem.* **2007**, *72*, 6653.

31. Galoppini, E.; Guo, W.; Qu, P.; Meyer, G. J. Long-Distance Electron Transfer Across Molecule-Nanocrystalline Semiconductor Interfaces. *J. Am. Chem. Soc.* **2001**, *123*, 4342.

32. Galoppini, E.; Guo, W.; Zhang, W.; Hoertz, P.; Qu, P.; Meyer, G. J. Long-Range Electron Transfer across Molecule-Nanocrystalline Semiconductor Interfaces Using Tripodal Sensitizers. *J. Am. Chem. Soc.* **2002**, *124*, 7801.

33. Boomgaarden, W.; Vögtle, F.; Nieger, M.; Hupfer, H. Broad Molecular Ribbons of Nanometer Size Composed of Biphenyl Units *Chem. Eur. J.* **1999**, *5*, 345.

34. Ziessel, R.; Suffert, J.; Youinou, M. T. General Method for the Preparation of Alkyne-Functionalized Oligopyridine Building Blocks. *J. Org. Chem.* **1996**, *61*, 6535.

35. Grosshenny, V.; Romero, F. M.; Ziessel, R. Construction of Preorganized Polytopic Ligands via Palladium-Promoted Cross-Coupling Reactions. *J. Org. Chem.* **1997**, *62*, 1491.

36. Eaton, P. E.; Galoppini, E.; Gilardi, R. Alkynylcubanes as Precursors of Rigid-Rod Molecules and Alkynylcyclooctatetraenes. *J. Am. Chem. Soc.* **1994**, *116*, 7588.

37. Miller, J. A.; Zweifel, G. A Convenient Synthesis of 1-Trimethylsilyl-1,3-diynes and their Conversion into Terminal 1,3-Diynes *Synthesis* **1983**, 128.

38. Shirai, Y.; Zhao, Y.; Cheng, L.; Tour, J. M. Facile Synthesis of Multifullerene-OPE Hybrids via in Situ Ethynylation. *Org. Lett.* **2004**, *6*, 2129.

39. Chun, I. S.; Moon, S. J.; Na, Y. M.; Lee, Y.-A.; Yoo, K. H.; Jung, O.-S. Selective and sensitive Recognition of Hexafluorophosphate via an Unusual Equilibrium between a Cationic Square Host and a PF_6 Guest. *Inorg. Chem. Comm.* **2007**, *10*, 967.

40. Abrahamsson, M.; Taratula, O.; Persson, P.; Galoppini, E.; Meyer, G. J. Meta-substituted Ru^{II} rigid rods for sensitization of TiO_2. *J. Photochem. Photobiol. A: Chem* **2009**, *206*, 155.

41. Wang, D. Ph. D. dissertation, Rutgers-Newark, 2004.

CHAPTER A-3:

ELECTROCHEMICAL AND PHOTOPHYSICAL PROPERTIES

OF RUTHENIUM STAR COMPLEXES

IN SOLUTION AND ON FILMS

A-3-1. Introduction

Ruthenium polypyridine complexes are classical photosensitizing dyes for DSSCs application due to their intense MLCT (metal-to-ligand charge transfer) absorption band in the visible region and their long-lived excited state.[1-3] Their high visible light harvesting efficiency, and long-term stability make the ruthenium (II) complex derivatives excellent DSSC sensitizers. By far the most successful sensitizers employed in the DSSCs are still N3 derivatives and closely related analogues with overall conversion efficiency ~10%.[4]

Ruthenium polypyridine complexes anchored to the semiconductor surface through rigid linkers are useful models for fundamental studies of interfacial electron injection[5-11]. The rigid-rod Ru-bpy complexes were made of OPE spacers with the Ru comples in one end and the anchoring group ipa in the other end. Rigid-rod ruthenium polypyridine sensitizers with a rigid linker in one of the bipyridine ligand were synthesized and studied[6]. The length of the rigid-rod was controlled by involving different number of OPE units. The OPE linker acted as a π acceptor group resulting in delocalization of the MLCT state on the linkers. The rigid-rods decreased the charge injection rate from the LUMO of the sensitizers to the conduction band of the semiconductor. A very weak distance dependence (attenuation factor $\beta \approx 0.19$ Å^{-1}) of interfacial injection process was observed[11]. However, the charge recombination rate constants were found to be independent on the structure and linker length of the rigid-rod.[8]

The weak distance dependence was explained from the distance control and orientation control aspects. The homoleptic star complexes (Figure A-3-1.1.): Short Star

Complex (**1**, **SSC**), 3 Short Star Complex (**2**, **3SSC**), Long Star Complex (**3**, **LSC**), and Soluble Long Star Complex (**4**, **SLSC**), were designed and synthesized. They had identical bipyridine ligands with conjugated rigid linkers and anchor groups chelated with ruthenium metal center to insure better separation of the chromophore and the semiconductor nanopaticles compared to the rigid-rods. In this chapter, we describe the study of the novel homoleptic star complexes in solution and on metal oxide semiconductor films.

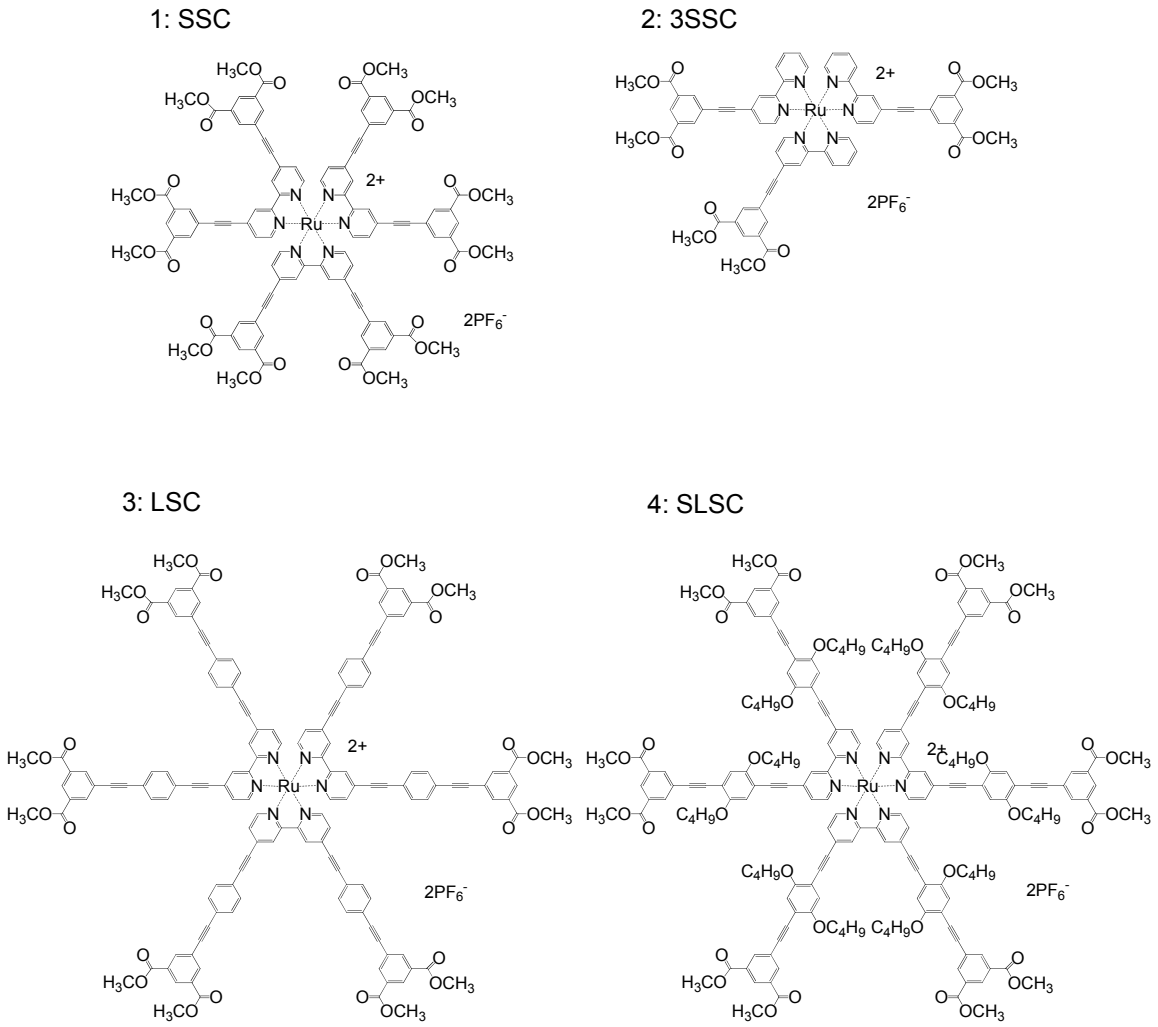

Figure A-3-1.1. Chemical structures with abbreviation names of homoleptic ruthenium star complexes

$Ru(bpy)_3^{2+}$, $Ru(deeb)_3^{2+}$ (deeb is 4,4'-diethylester-2,2'-bipyridine), and rigid-rods were chosen for comparison with the star complexes. Their chemical structures are shown in Figure A-3-1.2.

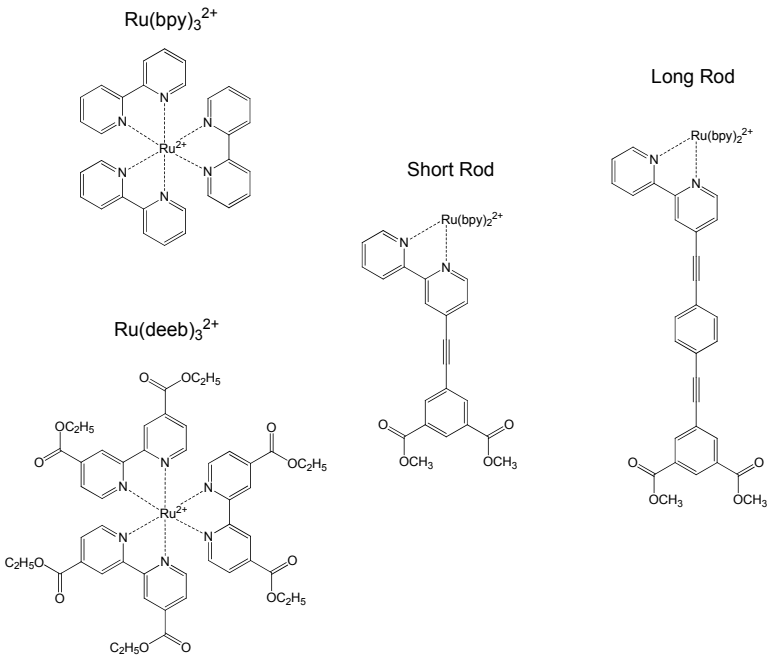

Figure A-3-1.2. Chemical structures of reference compounds $Ru(bpy)_3^{2+}$, $Ru(deeb)_3^{2+}$, and rigid-rods. The counter ion is PF_6^-.

A-3-2. Results and Discussions

A-3-2-1. Metal Oxide Films

Two types of metal oxides thin films were used for photophysical studies: titanium dioxide (TiO_2) and zirconium dioxide (ZrO_2). Both of them are well-known n-type semiconductors that can generate photocurrent under ultraviolet light irradiation.[12-16] The reason for using the metal oxide semiconductors instead of silicon or indium phosphide is that the metal oxide semiconductors have excellent stability against photo-corrosion on

optical excitation due to their wide band gaps and weak absorption in solar spectrum.[17] Anatase TiO_2 is a commonly used semiconductor because of its low-cost, and nontoxicity.[1,18] The excited state kinetics like electron injection, intermolecular charge transfer, charge separation, and charge recombination of dyes bound to TiO_2 surfaces have been investigated by a number of research groups worldwide. ZrO_2 is a semiconducting material often used to study the properties of excited states. ZrO_2 band gap is 5.0 eV.[19-21] Thus the ZrO_2 film behaves as an insulator precluding possible electron injection (TiO_2 anatase band gap is about 3.2 eV[22]) from the sensitizers (Figure A-3-2-1.1). Also the morphology of ZrO_2 film is quite similar to the TiO_2 film (Figure A-3-2-1.2[23,24]). Thus ZrO_2 films are an excellent substrate to study the fluorescence emission of sensitizers on metal oxide film (Figure A-3-2-1.1).

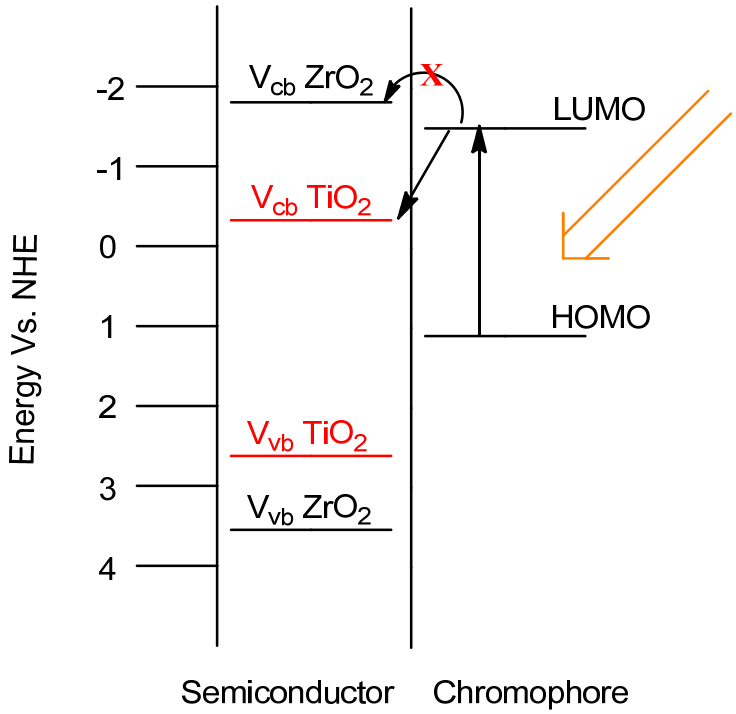

Figure A-3-2-1.1. Schematic illustration of band gaps of TiO_2 and ZrO_2[25]

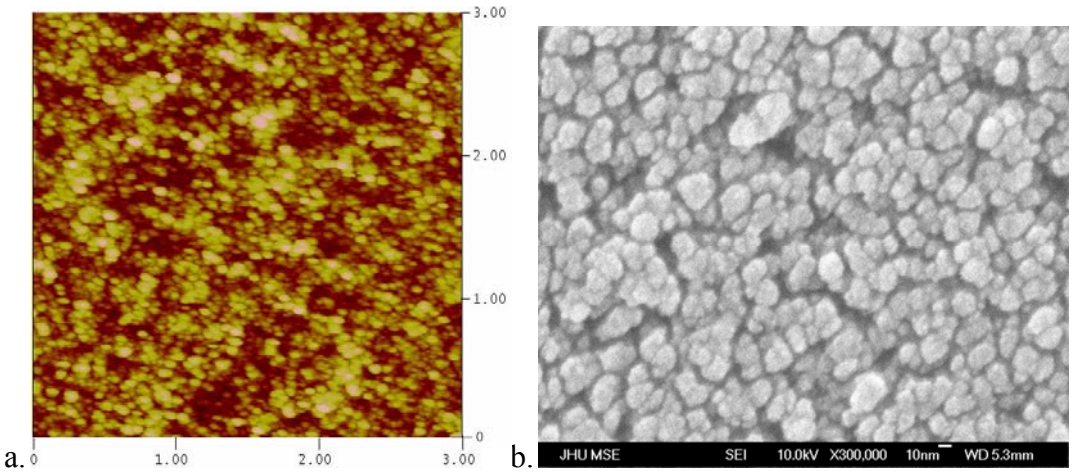

Figure A-3-2-1.2. a. ATM image of TiO_2 thin films. The average diameter of TiO_2 nanoparticles ~ 15 to 20 nm.[24] b. SEM image of ZrO_2 thin film. The average diameter of ZrO_2 nanoparticles ~ 10 nm.[23]

Figure A-3-2-1.3 shows a comparison between the absorption spectra of TiO_2 and ZrO_2, indicating the absorption edges of these two metal oxide semiconductors coated on cover glasses. Any higher energy transition beyond the edge will be obscured by the absorption of the metal oxide semiconductor. Based on the absorption spectra, the fundamental absorption of TiO_2 is ~ 380 nm and ~ 330 nm for ZrO_2.

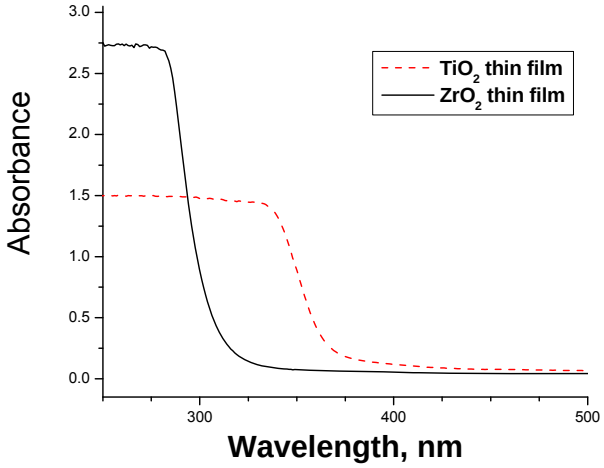

Figure A-3-2-1.3. UV-Vis absorption spectra of TiO_2/glass and ZrO_2/glass

The metal oxide semiconductor films studied in this thesis are mesoporous, nanocrystalline thin films.[26] They provide high surface area for the binding of the sensitizers. High surface area property is critical for solar harvesting.[27] Compared to the planar electrode materials, the actual area for sensitizer binding is about three order of magnitudes larger.[27] Moreover, porous film ensures the efficient penetration of redox electrolyte, allowing fast regeneration of the oxidized dye. The commonly used method to prepare the film is the sol-gel technique,[27-30] which is described in the Experimental Section A-3-3-1. The resulting semiconductor film was typically 10 μm thick, with an average particle size ~ 20 nm.

A-3-2-2. Binding Study

For DSSCs applications, the sensitizers should bind strongly to the semiconductor surfaces via functional groups to avoid desorption of the dyes. Also the binding groups should offer great electron orbital overlap with metal oxide semiconductors and ensure electronic coupling. Functional groups based on the carboxylic acids, phosphonates, alcohols, amides, etc. have all been tested.[28] The ruthenium star complexes were bound onto the metal oxide semiconductors through two -COOR anchoring group on Ipa unit, which is known to provide a strong interfacial link.[31,32]

Previous studies of rigid-rods on TiO_2 surface showed that the binding mode of COOR (R = H, Me) group depends on the surface acidity, which can be controlled after the film preparations by treatment with aqueous acid or basic solutions. On acidic semiconductor surfaces, monodentate ester-type linkage was formed; on basic and untreated semiconductor surfaces, the bidentate-type linkage was dominant.[8,33] Figure A-

3-2-2.1 shows possible binding modes for the attachment of a carboxylic group to the metal oxide semiconductor surface under different binding conditions. The bound rigid-rods were not perpendicular to the nanoparticle surface. Persson reported DFT-optimized geometries of Ipa group bound to a TiO_2 cluster. This work shows that Ipa unit is tilted ca. 45° relative to the surface when both COOH groups bind[34] (Figure A-3-2-2.2).

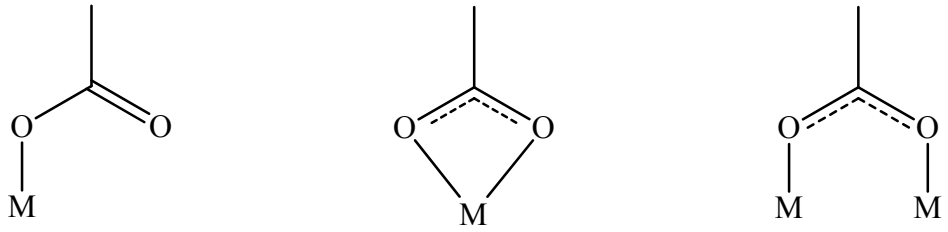

(a) monodentate ester type (b) bidentate chelating (c) bidentate bridging

Figure A-3-2-2.1. Three possible binding modes for the attachment of a carboxylic group to metal oxide semiconductor surface.

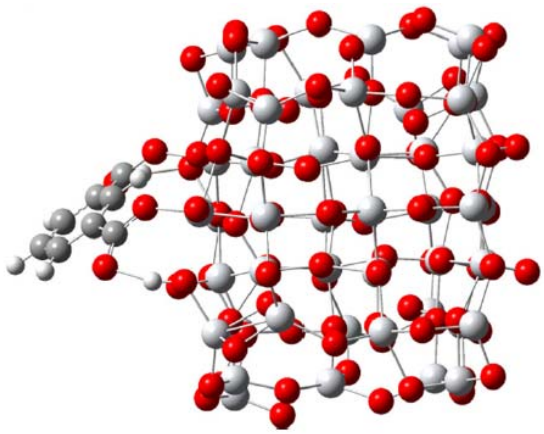

Figure A-3-2-2.2. DFT optimized geometrie for Ipe group binding to a model TiO_2 nanoparticles. The aromatic moiety of the Ipa unit is tilted ca. 45° relative to the surface.[34]

The nature of the binding to TiO_2 for compounds 3SSC, SSC, LSC, and SLSC was studied through ATR-IR spectroscopy. Transmission IR could not be used since

chromophores studied in our lab cannot be casted on IR transparent substrates (glass is not IR transparent). Thus Fourier-transform infrared attenuated total reflectance (FT-TR-ATR) spectrometer was selected instead of normal IR spectrometer. In the case of the star complexes, the more soluble carboxylic ester was used as the anchoring group to attach the ruthenium star complexes onto the anatase TiO_2. However, previous work indicate that the carboxylic ester can be a strong binding group for ruthenium polypyridine complexes, affording large surface coverages (10^{-8} mol/cm^2) and high binding constants (10^{-5} M^{-1}).[35,36] In analyzing the IR spectra of the dyes, the region of particular interest is between 1300 and 1800 cm^{-1}, in particular, the C=O stretching bands at ~ 1700 cm^{-1}. A free ester or carboxylic acid group typically gives a strong band at ~ 1700 cm^{-1} (Figure A-3-2-2.1 a), which is attributed to the C=O stretching mode ($\nu_{C=O}$).[37] The monodentate ester type binding mode also shows this band in similar region. The bidentate linkage (Figure A-3-2-2.1 b and c) exhibits two strong and broad bands, symmetric stretching mode (ν_s, 1600 cm^{-1}) and asymmetric stretching mode (ν_{as}, 1400 cm^{-1}).[37] IR measurements for the star complexes 3SSC, SSC, LSC, and SLSC were performed before and after binding. All of the TiO_2 films were immersed into sensitizer actonitrile solutions without any acid or base pre-treatment. Figure A-3-2-2.3 shows the spectra of all four star complexes. Since the neat star complexes gave much stronger IR signal than the one of sensitized films, the overlaid spectra were normalized at the peak of C=O stretching band.

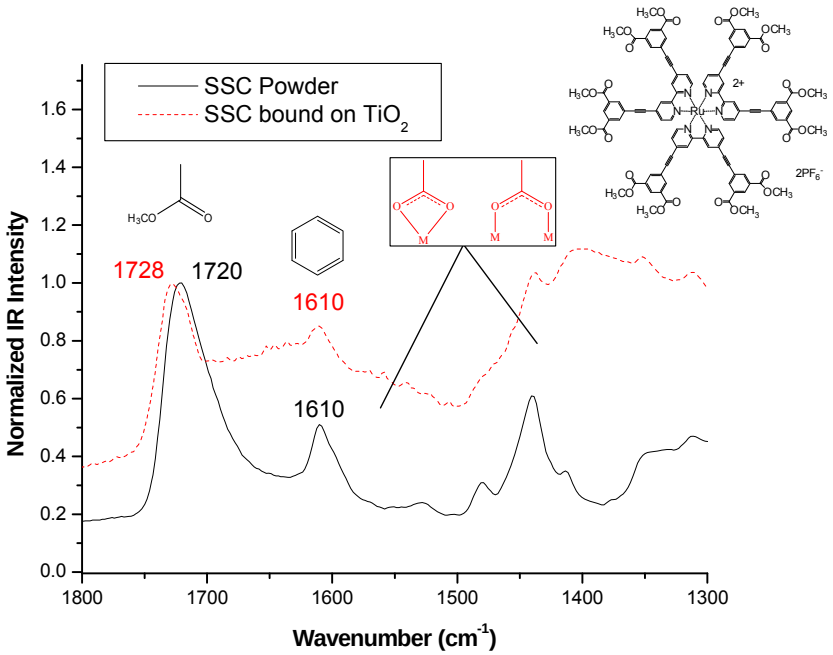
SSC Powder
SSC bound on TiO2
1728
1720
1610
1610
Normalized IR Intensity
Wavenumber (cm-1)
2PF6-

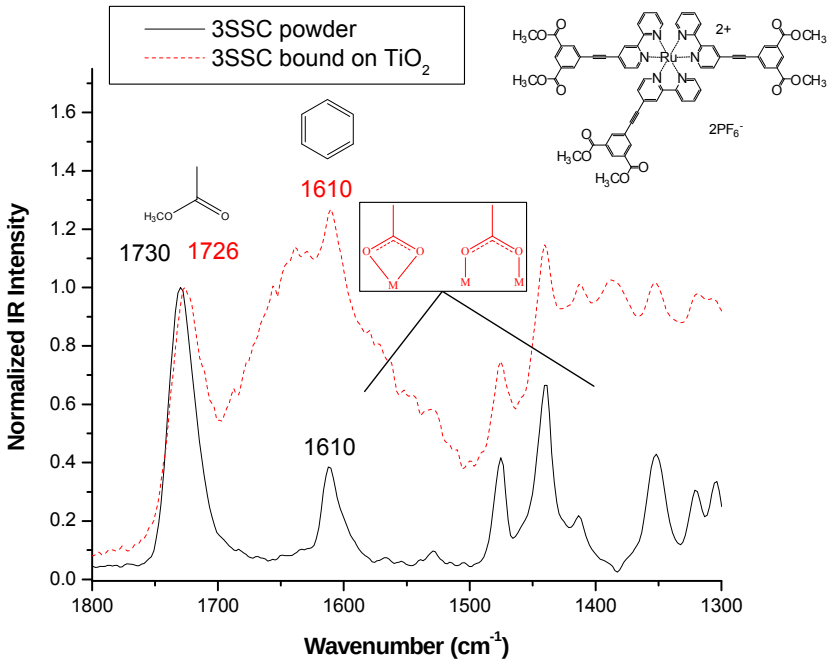
3SSC powder
3SSC bound on TiO2
1730
1726
1610
1610
Normalized IR Intensity
Wavenumber (cm-1)
2PF6-

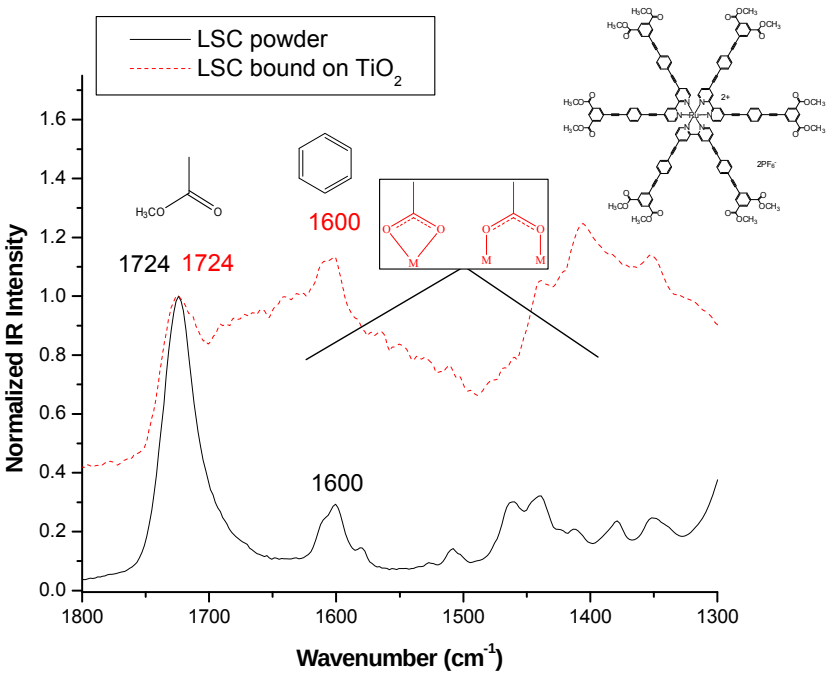

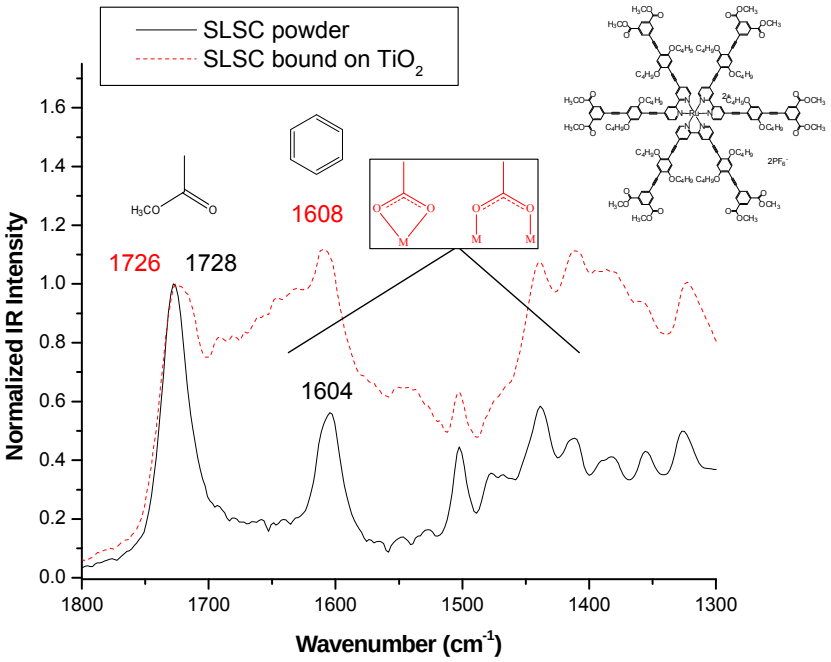

Figure A-3-2-2.3. IR spectra of star complexes before and after binding on TiO_2 films.

All the spectra of the esters powder showed the presence of intense bands at ~ 1720 cm^{-1} ($\nu_{C=O}$) for the carbonyl group and at ~ 1610 cm^{-1} ($\nu_{C=C}$) for the phenylene group. Upon binding to the TiO_2 films, the IR spectra showed a very small (up to 8 cm^{-1}) shift of the carbonyl stretch and no changes for the phenylene group band. The carbonyl bands remained in the spectra showed that not all of the anchoring groups were bound on the TiO_2 films as expected. The new-appeared bands for the films in IR spectra were broad carboxylate bands at ~1640 cm^{-1} (ν_s) and 1400 cm^{-1} (ν_{as}), which was consistent with bidentate coordination modes.

A control of the pH value is important not only affects the binding nature but is also important in the interfacial charge transfer study because pH could shift energy level of the conduction band (E_{cb}) of the semiconductor relative to the sensitizer by as much as 0.059 V/pH[38]. An acidic pre-treatment would lower E_{cb} thus favoring electron injection; a basic pre-treatment increases E_{cb}, thus inhibiting electron injection. Thus potential determining ions, such as Li^+, were normally introduced for basic pre-treated films to shift the conduction band edge to lower level and promote electron injecton.[39-42]

A-3-2-3. Electrochemistry

Figure A-3-2-3.1 and Figure A-3-2-3.2 show the cyclic voltammetry (CV) data of the 3SSC and SLSC for $Ru^{III/II}$ reduction potential at different scan rate in acetonitrile solution with tetrabutylammonium hexafluorophosphate (0.1 g/mL) electrolyte. Both star sensitizers displayed quasi-reversible $Ru^{III/II}$ reductions in acetonitrile solution as expected. Due to their low solubility, the CV spectra of SSC and LSC were not obtained.

Table A-3-2-3.1 gives the electrochemical data for star complexes (*vs.* Fc/Fc+) and three reference compound in acetonitrile solution.

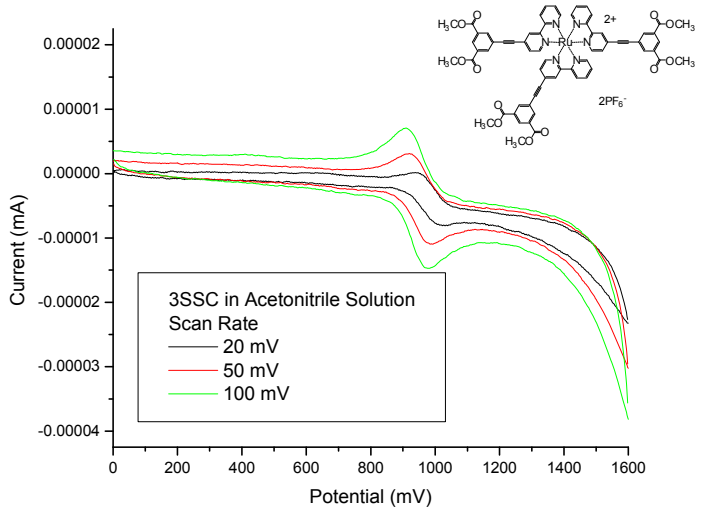

Figure A-3-2-3.1. CV spectrum of 3SSC in CH_3CN vs. Fc/Fc^+ for $Ru^{III/II}$ reduction potential.

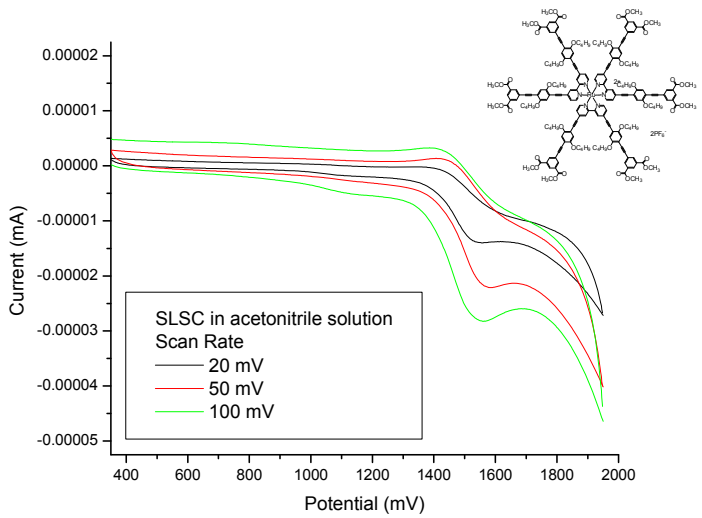

Figure A-3-2-3.2. CV spectrum of SLSC in CH_3CN vs. Fc/Fc^+ for $Ru^{III/II}$ reduction potential.

Table A-3-2-3.1. Electrochemical data for ruthenium star complexes and reference compounds in acetonitrile solution vs. Fc/Fc^+.

Sensitizers	$E_{1/2}(Ru^{III/II})$ mV[a]	ΔG_{es} eV[b]	$E_{1/2}(Ru^{III/II*})$ mV[c]
3SSC	1400	2.16	-760
SSC	-	2.08	-
LSC	-	2.10	-
SLSC	1557	2.08	-523
$Ru(bpy)3^{2+}$ [d]	1260	2.12	-860
Short-rod[e]	1300	2.12	-820
Long-rod[e]	1300	2.13	-830

All measurements were performed in acetonitrile at room temperature under nitrogen atmosphere. a. Half-wave potentials were reported *vs.* Fc/Fc^+ with experimental error ± 20 mV. b. Gibbs free energy stored in the thermally equilibrated excited state, which was calculated based on the photoluminescence spectra, see experimental section.c. Excited state reduction potentials. d. Data from ref. 36. e. Data from ref. 8.

When compared to the ground state reduction potential value of $Ru(bpy)_3$ (1260 mV) and rigid-rods (1300 mV), the $E_{1/2}$ value of 3SSC (1400 mV) and SLSC (1557 mV) were shifted to more positive potential. The excited state reduction potentials of the ruthenium star complexes were less negative than the value of reference sensitizers. Thus, charge injection from the excited state of the ruthenium star complexes sensitizer to the conduction band of the semiconductor is expected to be inhibited. This was consistent with the interfacial charge transfer studies, which showed less injection yield values of ruthenium star complexes compared to the values of rigid-rods.

A-3-2-4. Photophysical Studies

The photophysical study was a collaborative work with Dr. G. J. Meyer's research group at John Hopkins University, Chemistry Department. Measurements were run by Patrik Johansson and Maria Abrahamsson.

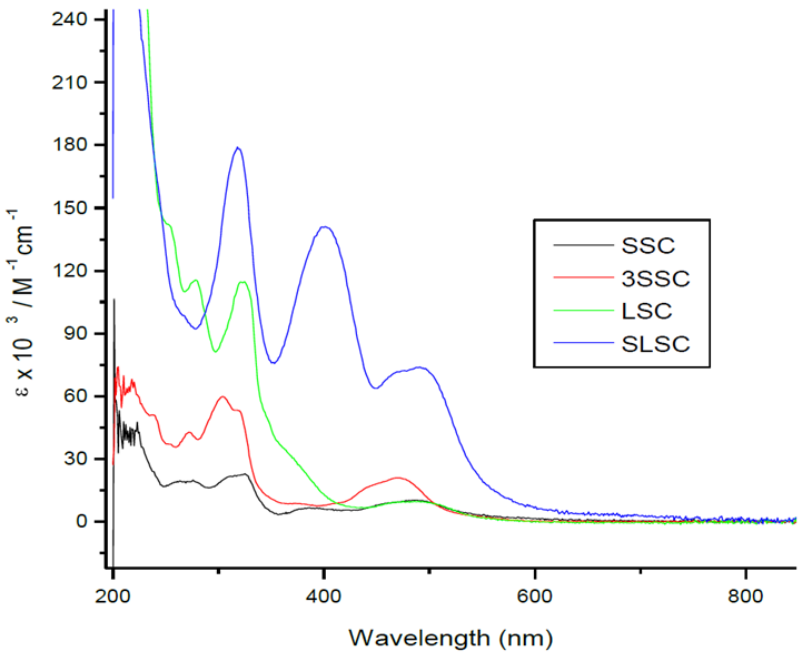

Figure A-3-2-4.1. Ground state absorption spectra of star complexes in acetonitrile.

The UV-Vis absorption spectra of star complexes in acetonitrile solution are shown in an overlay in Figure A-3-2-4.1. The intense bands at higher energy, ~310 nm, were assigned to the π, π* transition of the bpy ligand. And the second band at ~ 370 for complexes SSC, 3SSC and LSC at ~370 nm was assigned as a rod (π, π*) and MLCT mixed state.[43] The SLSC complex gives a second large π, π* transition band at ~ 400 nm assigned to the electron donation of the oxygen on the butoxy side chain group (Figure A-3-2-4.2). This band shifts to longer wavelength from 375 nm to 405 nm for the SLSC star complex compared to the SLSC ligand, due to increased electron delocalization.

Thus the butoxy group not only increases the solubility of the star complex, but also influences the photophysical properties. The MLCT band was red-shift compared to the $Ru(bpy)_3^{2+}$ (~ 450 nm) and the rigid-rods (~ 465 nm).[8] This can be explained by the different number of OPE units in the molecules. The OPE unit is known to be electron withdrawing and is therefore expected to stabilize the MLCT excited states. As the number of OPE unites increases, the MLCT absorption band shifts to the red.[43-49]

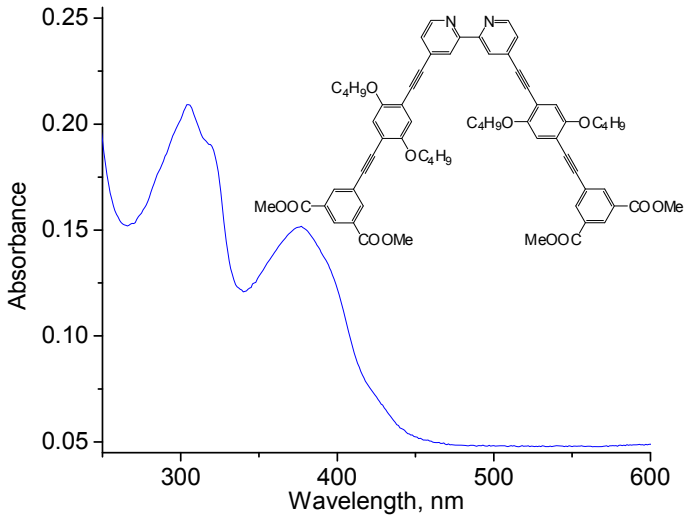

Figure A-3-2-4.2. Absorption spectrum of SLSC ligand in acetonitrile.

The MLCT band in the spectra of SSC, LSC, and SLSC appeared in the same spectra region (SSC ~ 489 nm, LSC ~ 490 nm, and SLSC ~ 492 nm). However, MLCT band for 3SSC, at ~ 470 nm, has a ~ 20 nm red shift compared to the value of the other star complexes.

Another interesting issue is the extinction coefficient values of the star complexes. The rigid-rods were reported with $\varepsilon \sim 2.0 \times 10^4\ M^{-1}cm^{-1}$ at their MLCT band maxima. The ε value didn't change significantly with additional OPE units.[8] 3SSC gave a similar

value, while SSC and LSC gave the ε ~ 1.0 x 10^4 $M^{-1}cm^{-1}$. However, the SLSC showed a largely increased ε value, ~ 7.5 x 10^4 $M^{-1}cm^{-1}$, compared to the values of the rigid-rods and the other three star complexes (Figure A-3-2-4.1 and Table A-3-2-4.1). This enhancement has been reported by Odobel and coworkers with ruthenium tris(bpy) C_{60} dyads linked via OPE units with alkoxy substituents on the phenyl groups, and was assigned to the electron donation from the alkoxy groups on the rigid linker.[50]

The absorption spectra of the star complexes bound on the TiO_2 and ZrO_2 films shows the characteristically broad MLCT band at 490 nm (Figure A-3-2-4.3). The higher energy absorption was covered by the absorption of the semiconductor.

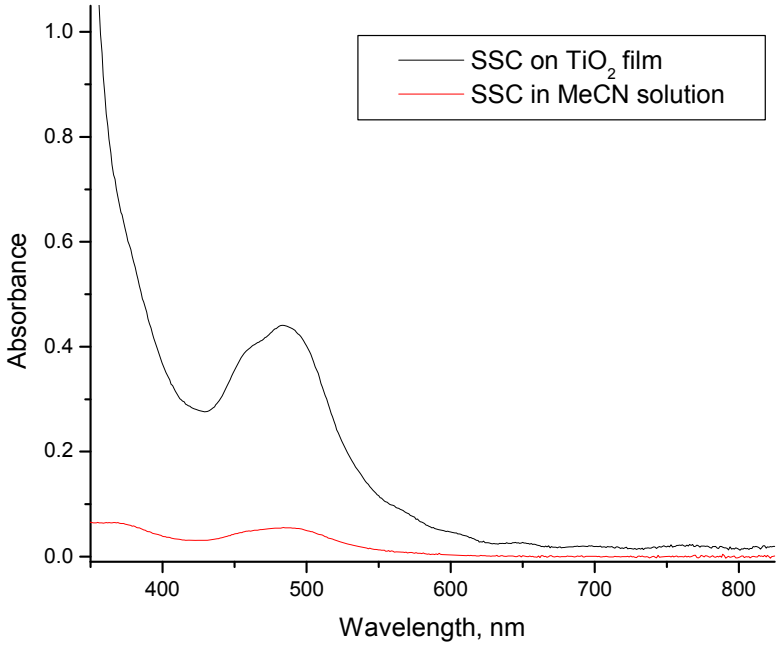

Figure A-3-2-4.3. Absorption spectra of SSC on TiO_2 film and in acetonitrile

Normalized fluorescence emission spectra of star complexes at room temperature are shown in Figure A-3-2-4.4. Table A-3-2-4.1 summarizes key photophysical

properties of the star complexes and reference compounds. The energy band gap of the star complexes were determined by photoluminescence measurements at 77 K, and are shown with their lifetimes at 77 K in Table A-3-2-4.2. Corresponding calculations are described in the experimental section A-3-3-3.

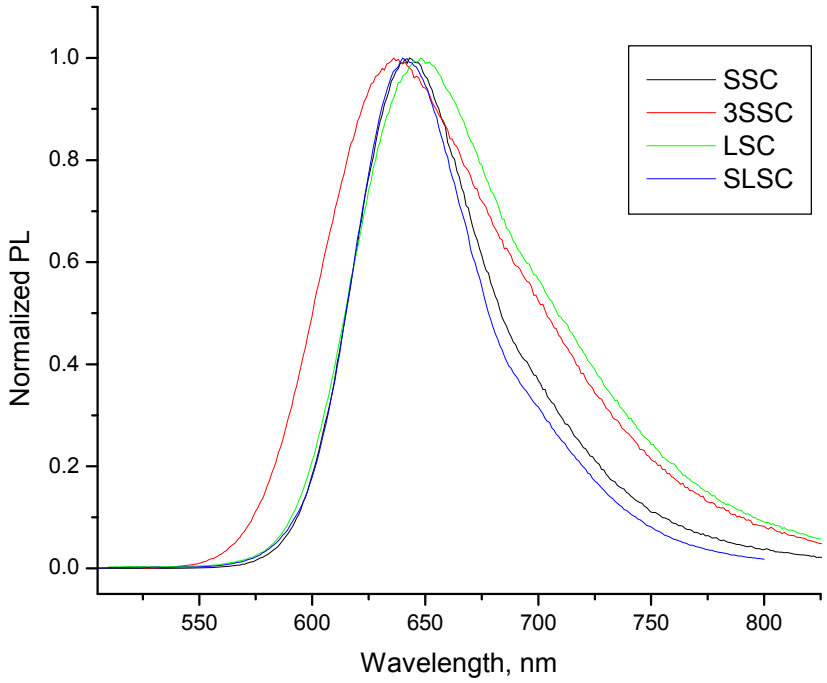

Figure A-3-2-4.4. Normalized fluorescence emission spectra of star complexes at room temperature in MeCN. λ_{exc} = 420 nm.

Compared to the rigid-rods (1.9 and 2.3 μs), star complexes gave slightly shorter excited state lifetime τ (1.6 to 1.8 μs). $Ru(bpy)_3$ exhibited the shortest lifetime (0.8 μs). The 77 K lifetimes, as expected, were higher than the values at room temperature in all cases.

Table A-3-2-4.1.Photophysical properties of star complexes and reference compounds.

Sensitizer	λ_{abs}, nm (ε, $M^{-1}cm^{-1}$)	λ_{PL} (nm)	τ (μs)	ΔG_{es}[a] (eV)	Φ_{PL} ($x10^{-2}$)	k_r[b] (10^4 s^{-1})	k_{nr}[c] ($x10^5$ s^{-1})
SSC	489 (1.0 x 10^4)	643	1.7	2.08	7.2	4.2	5.5
3SSC	470 (2.1 x 10^4)	636	1.8	2.16	6.4	3.7	5.4
LSC	490 (1.0 x 10^4)	648	1.6	2.10	3.8	2.5	6.0
SLSC	492 (7.5 x 10^4)	642	1.6	2.08	11.5	7.2	5.5
$Ru(bpy)_3^{2+}$ [d]	450	610	0.8	2.24	6.2	7.8	12
short rod[d]	462 (1.6 x 10^4)	640	1.9	2.12	11	5.8	4.7
long rod[d]	465 (2.0 x 10^4)	640	2.3	2.13	13	5.7	3.8

All measurements were performed in acetonitrile at room temperature. a. Gibbs free energy stored in the thermally equilibrated excited state. b. Radiative constant. c. Non-radiative constant. d. Data from ref. 8.

Table A-3-2-4.2. Band gaps and lifetimes of star complexes at 77K.

Sensitizer	OPE units	band gap (eV)	lifetime (μs)
SSC	6	1.99	4.3
3SSC	3	2.02	6.1
LSC	12	1.98	3.2
SLSC	12	1.98	4.1

All measurements were performed in acetonitrile at 77K. The solvent was degassed under nitrogen before measurement.

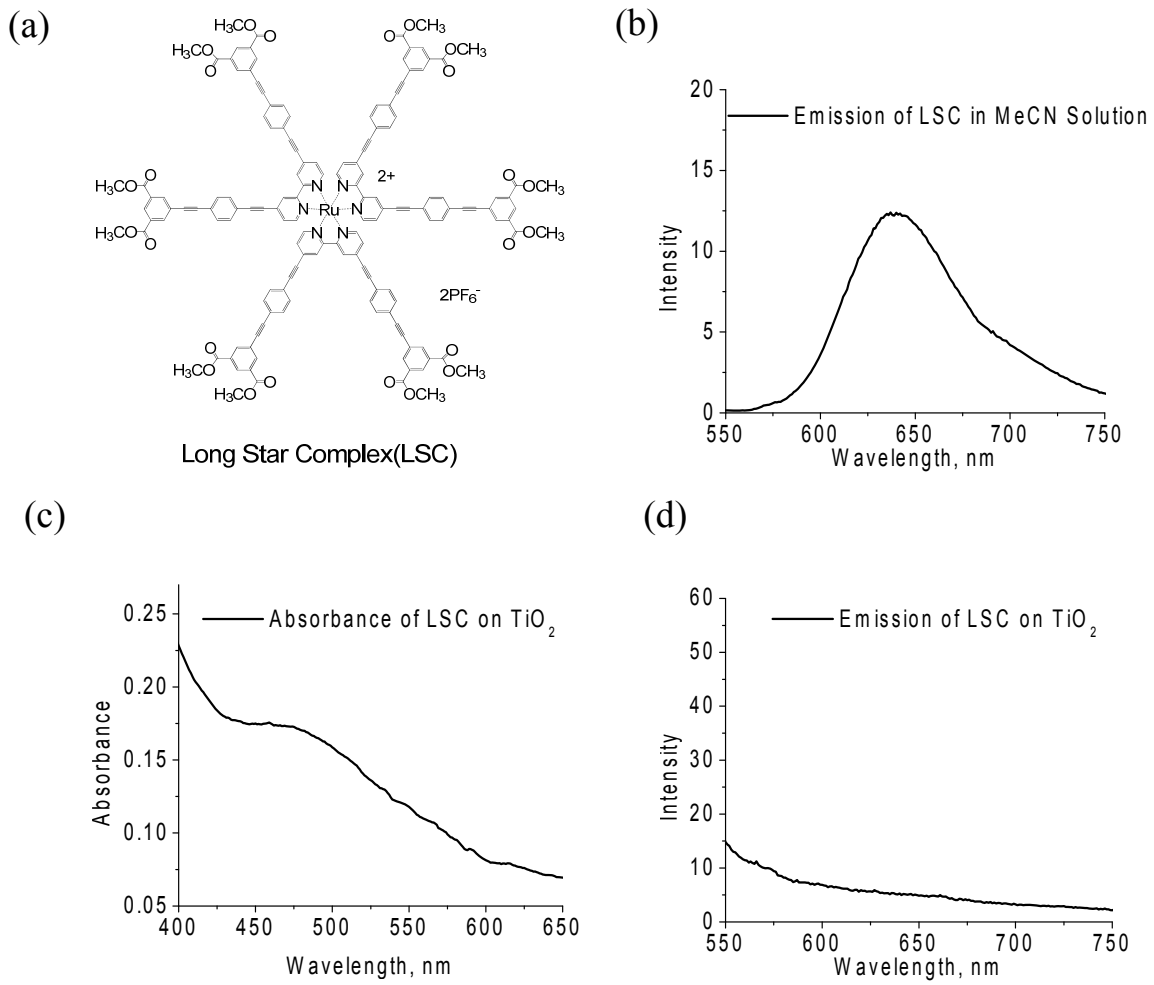

Figure A-3-2-4.5. (a) Chemical structure of LSC. (b) Emission spectra of LSC in CH_3CN solution. λ_{exc} = 485 nm. (c) Absorption spectra of LSC bound onto TiO_2. (d) Emission spectra of LSC bound onto TiO_2. λ_{exc} = 485 nm.

The excited state lifetimes of star complexes decrease as the number of OPE units in the linker increases. This trend obeys the energy gap law for 3SSC, SSC, and LSC: an increase in the lifetime is generally accompanied by a blue shift in the fluorescence emission spectra and it has been observed in Ru and Os complexes.[51,52] The photoluminescence emission maxima value for SLSC was similar to that of SSC, but the excited state lifetime was shorter suggesting that, in this case, the energy law is not followed.[8] The photoluminescence quantum yield Φ_{PL} of 3SSC, SSC and LSC decreased as the OPE linker increased. This trend is opposite to the one of rigid-rods. Also the

photoluminescence quantum yield values were lower than the one observed for the rigid-rods. SLSC photoluminescence quantum yield (Φ_{PL} 11.5%) was higher than that of other star complexes. This value was close to the one of rigid-rods (Φ_{PL} 11% and 13%).

When bound onto the TiO_2 films, the fluorescence emission of all the star complexes was quenched. Figure A-3-2-4.5 shows the chemical structure of LSC, the absorption spectra of LSC bound onto TiO_2 thin films and a comparison of the fluorescence emission of LSC in acetonitrile solution and bound onto TiO_2 thin films.

Transient absorption spectra of four star complexes bound onto the TiO_2 and in acetonitrile solution are shown in Figure A-3-2-4.6 and Figure A-3-2-4.7, respectively.

Transient absorption spectra were used to quantify interfacial electron transfer dynamics and yields. The interfacial electron transfer processes were influenced by the pH, since the conduction band edge shifts by about 0.059 V/pH unit,[25,53] as mentioned before. On acid pre-treated TiO_2, the injection is typical ultrafast (femtoseconds to picoseconds timescale). However, since this was beyond Dr. Meyer's nanosecond instrument time resolution (~ 10 ns), the films used for the measurements were pre-treated with base. Thus, the injection yield was low. This is due to the shift of the conduction band edge shifts to higher E, resulting in poor orbital overlap with the excited sensitizer.[54,55] Therefore, $LiClO_4$ was added into the acetonitrile solution to shift the conduction band edge and promote electron injection,[39-42,56] thus increasing the injection yield. In summary, the TiO_2 surface pre-treatment with acid, base, or potential determining ions has a profound influence dynamics and quantum yields. These factors

will need to be evaluated carefully in future work. Future work will involve the use of femtosecond laser spectroscopy, thus eliminating the need for any surface pre-treatment.

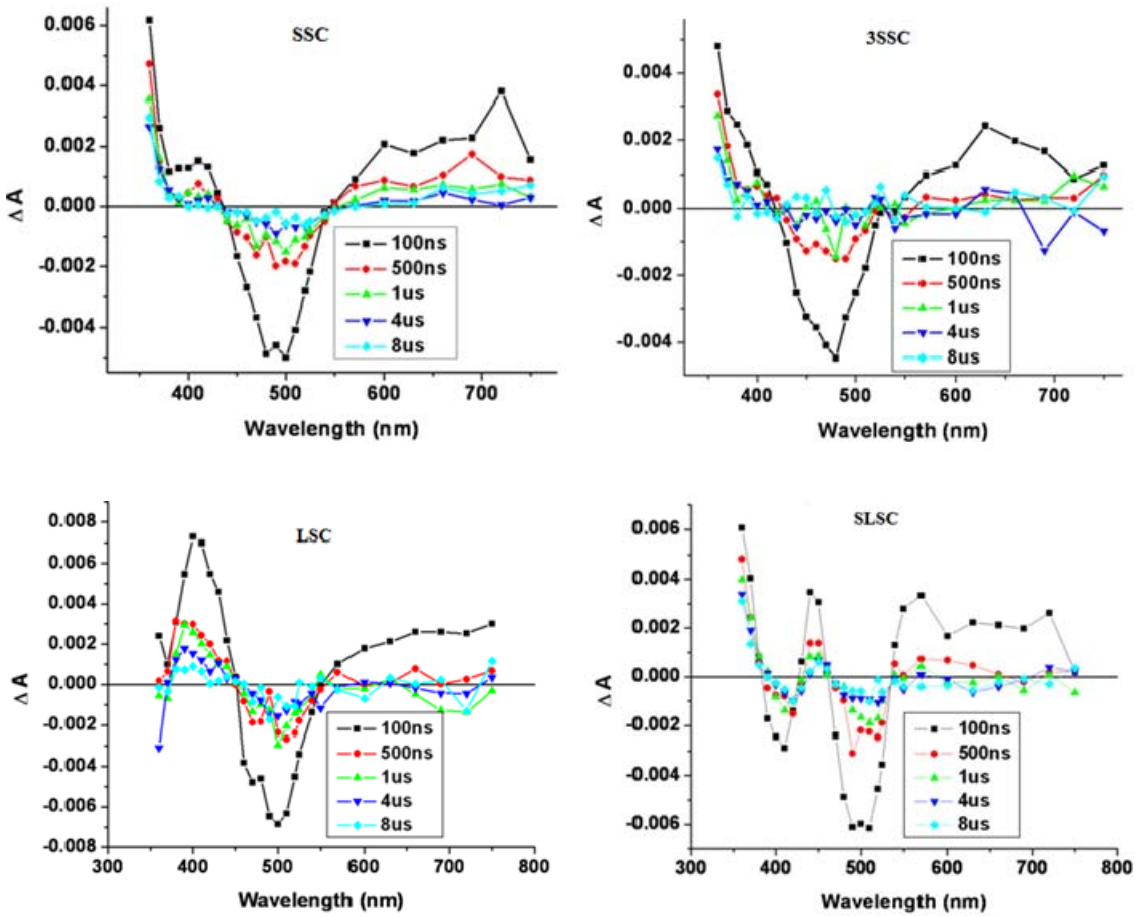

Figure A-3-2-4.6. Transient absorption spectra of ruthenium star complex bound onto TiO_2. λ_{exc} = 532 nm. Data were recorded at 100 ns (–■–), 500 ns (–●–), 1 µs (–▲–), 4 µs (–▼–), and 8 µs (–♦–) delays after the laser pulse.

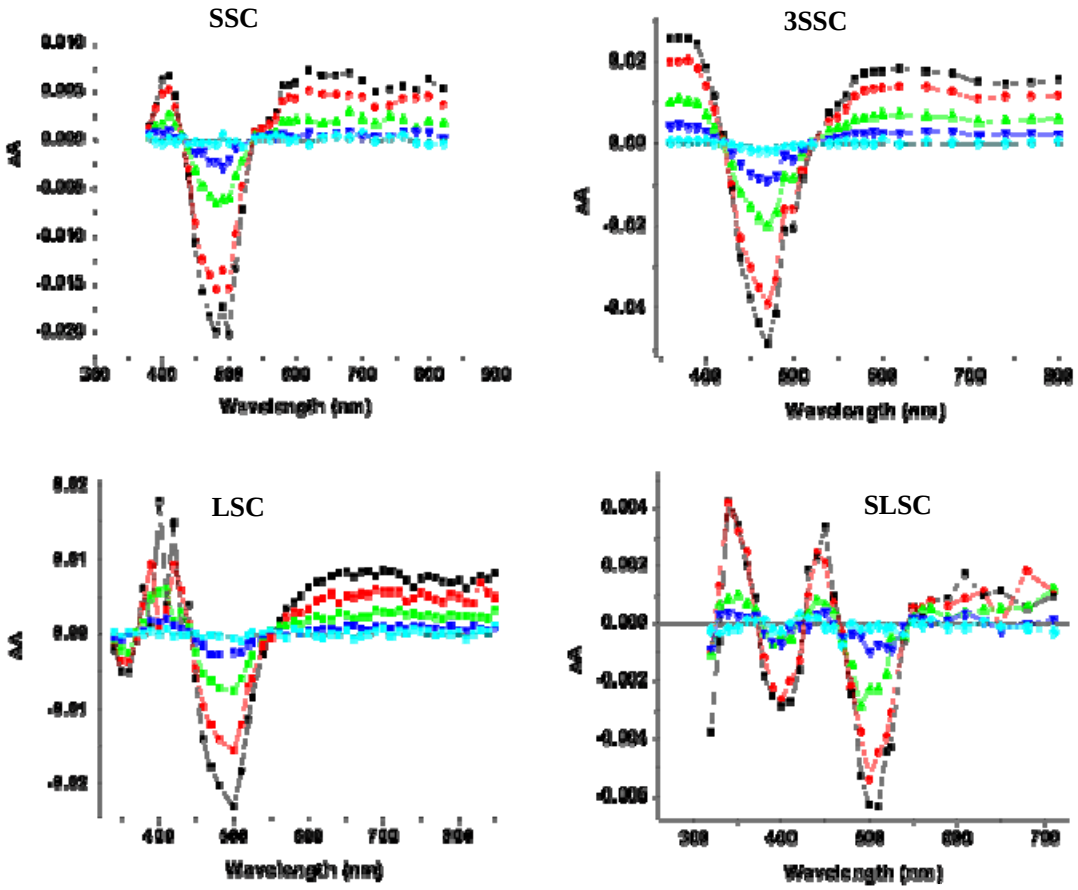

Figure A-3-2-4.7. Transient absorption spectra of ruthenium star complex in acetonitrile solution. λ_{exc} = 532 nm. Data were recorded at 100 ns (–■–), 500 ns (–●–), 1 μs (–▲–), 4 μs (–▼–), and 8 μs (–♦–) delays after the laser pulse.

To eliminate possible contributions from the excited state, the measurements were performed at the wavelengths corresponding to the excited/ground state isosbestic point. Thus the formation and loss of the interfacial injection and recombination processes could be clearly observed. At the isosbestic point, the transient absorption signal of excited state and ground state are the same. The isosbestic points were determined on ZrO_2 films, where only the ground and MLCT excited states were observed: 433 nm for SSC and 442 nm for LSC. The injection yields for excited state electron injection into empty states of nanocrystalline TiO_2 were quantified by comparative actinometry[39,42,56] (Table A-3-2-4.3). As the distances between the ruthenium metal center and

semiconductor surface increase for the star complexes, the injection yields decrease for SSC, 3SSC, and LSC as expected. This trend has been observed also for the rigid-rods.[8] Although SLSC gave a high photoluminescence quantum yield in solution, the electron injection yield was lower under experimental condition compared to other star complexes, including the LSC, which had similar rigid linker length.

The excited state $Ru^{III/II*}$ reduction potentials determined by CV measurements provide a possible explanation to the observed behavior. The relatively low reduction potential reduces the electron injection of SLSC LUMO to the conduction band of TiO_2.

Table A-3-2-4.3. Injection yields of star complexes.

Sensitizer	SSC	3SSC	LSC	SLSC
Φ_{inj}	0.073	0.14	0.034	0.0040

Nanosecond scale charge injections were observed for the SSC and LSC when bound onto TiO_2 (Figure A-3-2-4.8). The absorption spectra decreased bwtween 100 - 150 ns for SSC, and 50- 100 ns for LSC. As a comparison, the absorption change signals of star complexes when bound onto ZrO_2 were collected which showed no charge injection happened. The absorption signal stayed the same within experimental error in this case.

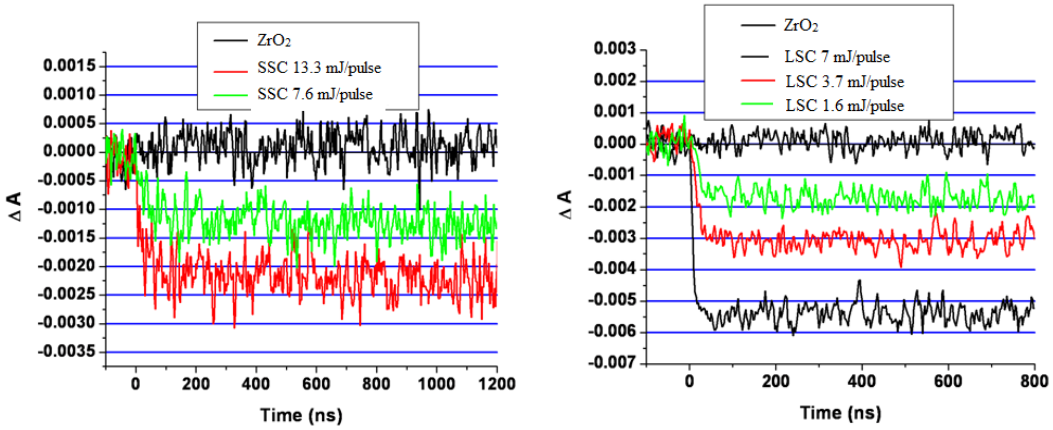

Figure A-3-2-4.8. Absorption changes recorded at isosbestic points for SSC (433 nm) and LSC (442 nm) on TiO_2. λ_{exc} = 532 nm.

To reduce the charge recombination rate is a main goal to involve the rigid linkers in the ruthenium polypyridine complexes. The charge recombination of the star complexes to the ground state molecule followed non exponential pathways and required more than 8 ms for completion (Figure A-3-2-4.9), with a recombination rate at 10^5 s^{-1} order (Table A-3-2-4.4). For SLSC, this data is not available due to the high signal-to-noise.

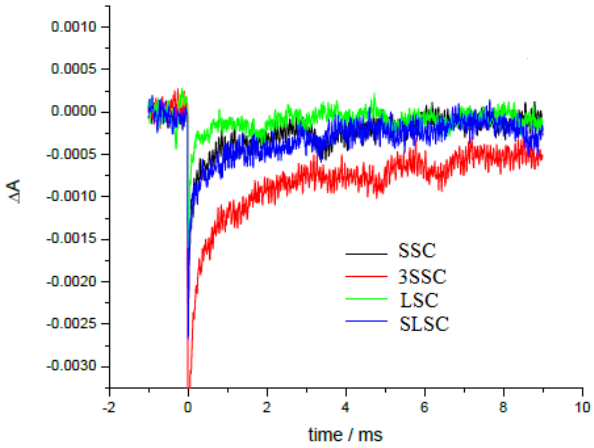

Figure A-3-2-4.9. Excited state decay of star complexes.

Table A-3-2-4.4. Recombination kinetics of star complexes.

Sensitizer	SSC	3SSC	LSC	rigid-rods
k_{obs} 10^5 s^{-1}	1.4	3.7	2.5	~ 250

The recombination rates did not show strong relation to the rigid linkers' length of these star complexes. However, the recombination rate was largely reduced compared to the value of rigid-rods. For rigid-rods, the recombination was independent of the length of the rigid-rods, with an average rate constant ~ 250 x 10^5 s^{-1}. *Thus the star complexes show much slower charge recombination dynamics (about two orders of magnitudes) than the one of rigid-rods.* This behavior was ascribed to the separation of the ruthenium metal center from metal oxide semiconductor surface, the result of the sensitizers' homoleptic structure.

A-3-2-5. Conclusions

New homoleptic ruthenium polypyridine star complexes were synthesized following two different synthetic approaches. All the star complexes were bound onto anatase TiO_2 nanoparticle thin film through carboxylic ester anchoring group with bidentate binding modes. Upon binding to TiO_2 film, the emissions of the star complexes were quenched. The injection yield decreases in the order of 3SSC, SSC, LSC, and SLSC as the length of the rigid linkers increased. SLSC gave high extinction coefficient and quantum yield due to the presence of butoxy groups on the linkers. However, the charge injection from SLSC to a base pre-treated TiO_2 film was inhibited (with injection yield 0.0040). This was due to the low LUMO level for SLSC relative to the conduction band

of TiO_2. Nanosecond scale charge injections were observed for SSC and LSC on base pre-treated TiO_2 films.

The main goal of this study was to reduce charge recombination by fixing the distance between ruthenium metal center and metal oxide surface. Homoleptic star complexes gave recombination rate at 10^5 s^{-1} order. Thus the interfacial recombination kinetics was significantly reduced compared to the one of rigid-rods (with recombination rate at 10^7 s^{-1} order). Future work will focus on ultrafast spectroscopic measurements and on solar cell performance.

A-3-3. Experimental Section

A-3-3-1. Metal Oxide Film Preparation

TiO_2 and ZrO_2 nanoparticle films were prepared in our lab with sol-gel techniques. Scheme A-3-3-1.1 shows the general procedure to make the metal oxide films.

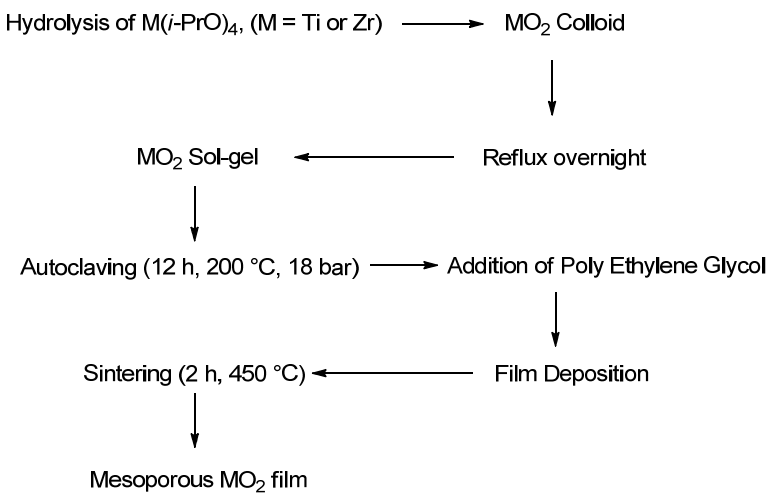

Scheme A-3-3-1.1. General procedure to prepare MO_2 nanoparticle films

Materials: isopropanol (Pharmco HPLC grade), nitric acid (Fisher ACS grade), deionized ultra filtered (DIUF) water (Fisher), poly(ethyleneglycol) (PEG, av. Mol. Wt. 2000, Aldrich) titanium (IV) isopropoxide (Aldrich), zirconium (IV) isopropoxide (70% in 1-propanol, Aldrich).

TiO_2 Film Preparation. TiO_2 nanoparticles was prepared via hydrolysis of titanium (IV) isopropoxide in an aqueous nitric acid solution under nitrogen atmosphere using previously reported procedures.[28,57] A three-neck round bottom flask was equipped with a thermometer, a dropping funnel and a Dean-Stark apparatus. The dropping funnel was placed in the central position of the flask. This is important to avoid formation of deposit on the walls of the flask during the hydrolysis. A solution of water (100 mL) containing HNO_3 (0.69 mL, 68 – 70 %) was placed in the round bottom flask and allowed to stir vigorously at room temperature. Titanium (IV) isopropoxide (20 mL) was added to the dropping funnel, and diluted with isopropanol (80 mL). This solution was purged with nitrogen for 15 minutes and kept under nitrogen to prevent hydrolysis prior to the addition to the acidic solution. This mixture was then added dropwise to the acidic solution at a rate of about one drop per second. A white solid immediately formed once the titanium (IV) isopropoxide / isopropanol mixture was added into the acidic solution, indicating rapid hydrolysis of the titanium (IV) isopropoxide. The reaction mixture was stirred vigorously during the addition to prevent the formation of large particles of TiO_2.

After completion of the addition, the dropping funnel was replaced with a glass stopper and the reaction mixture was heated to reflux. Aluminum foil was used to cover the flask to help the distillation. Isopropanol was distilled out (T = 84°C) from the reaction mixture via the Dean-Stark apparatus. During the first 3 hours of reflux, a

volume of *ca.* 160 mL isopropanol was collected (Figure A-3-3-1.1).[58] When the reflux temperature reached 100 ºC, all isopropanol was distilled, and the Dean-Stark apparatus was replaced with a condenser. The reaction mixture was refluxed overnight with stirring. Then the condenser and thermometer were removed and the flask was left open. The heat was sustained and the water was allowed to evaporate from the flask until a final volume of 33 mL was reached (the flask had been previously labeled for the 33 mL value). It was important to maintain vigorous stirring throughout the whole procedure to ensure homogeneity of the sol-gel. After cooling down, the resulting white colloid was sonicated for 2 minutes to remove any particles from the wall of the flask. Then the reaction mixture was transferred to a glass beaker with a stirring bar, and placed in a sealed custom-made titanium autoclave (Model 4760, Parr). The sol was allowed to stir in the autoclave at 200 ^{o}C for 12 h. A typical pressure of 17 – 18 bar was observed (Figure A-3-3-1.2).[58]

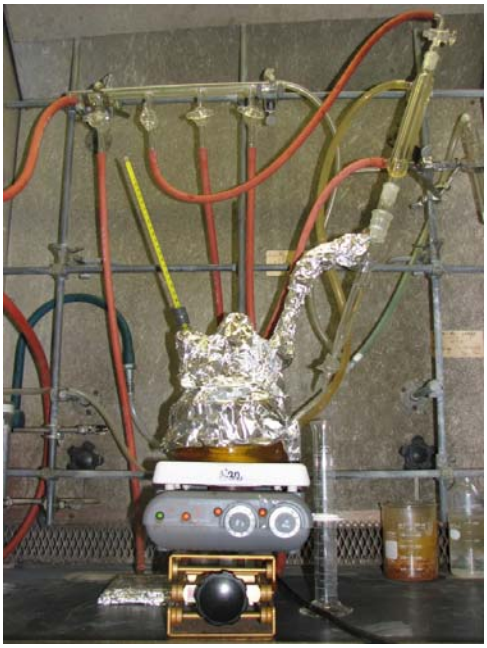

Figure A-3-3-1.1. Picture of the reaction set-up for colloidal TiO_2 preparation[58]

Figure A-3-3-1.2. Picture of the autoclave for colloidal TiO_2 preparation[58]

The white sol was allowed to cool, and then transferred to a 50 mL Erlenmeyer flask with a small stirring bar. PEG was added into the white sol to separate the TiO_2 nanoparticles. The amount of PEG added was 40 % wt. of the TiO_2 (*ca.* 1.5 g PEG per 25 cm^3 TiO_2 sol-gel). The mixture was stirred until a uniform sol gel formed. Then the gel was applied to cover glass slides by the doctor-blade technique over an area of 1 x 2 cm^2 via a glass dropper. Scotch tape was used to control the thickness of the TiO_2 film formed. The film was allowed to air dry and was sintered in the oven at 450 ºC for 2 h. The PEG was burned out in this step. The TiO_2 films prepared should be transparent (Figure A-3-3-1.3). If the films were opaque, the white sol was kept stirring for additional 2-3 days prior to use. The sol was cast either onto cover glass slides or onto the FTO conductive substrates. All films were stored under ambient conditions, and were heated at 120 ºC for 30 minutes before the binding step to remove physisorbed water and other impurities. The white sols were kept stirring in the Erlenmeyer flask protected from light for further use until the sols became slightly yellow or big particles were observed in the sols. Typically the sols were discarded after 4 weeks.

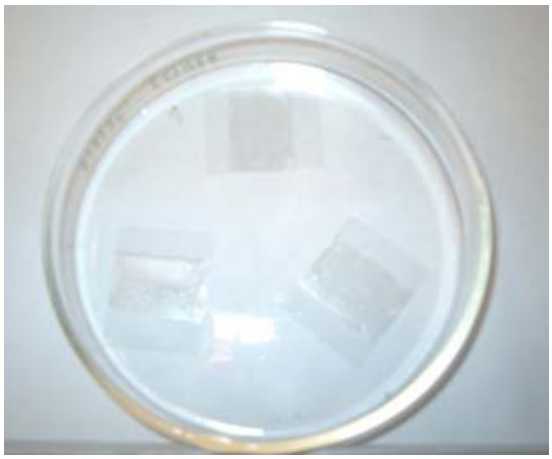

Figure A-3-3-1.3. Picture of transparent TiO_2 films on glass slides.

The crystal structure of the TiO_2 was determined by Raman (Figure A-3-3-1.4) and was proved to be mostly anatase type according to the reported data.[59] The diameter of TiO_2 nanoparticles in the mesoporous film was ~20 nm determined by AFM.[60]

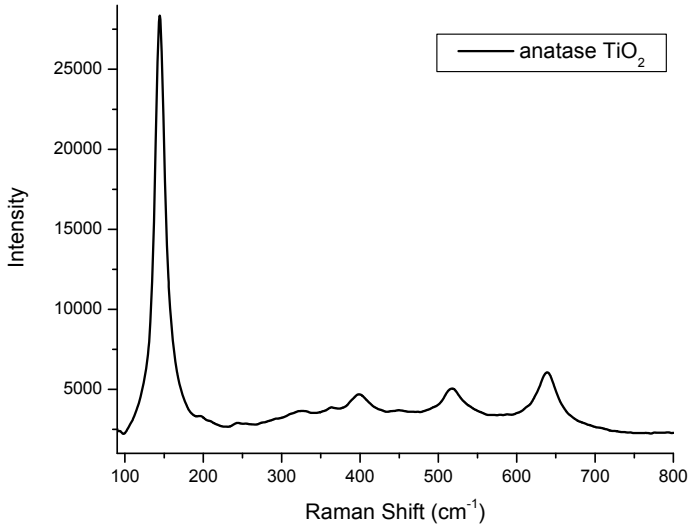

Figure A-3-3-1.4. Raman spectra of anatase TiO_2.

ZrO_2 Film Preparation. The procedure for the ZrO_2 preparation is very similar to the one for the TiO_2. A three-neck round bottom flask was equipped with a thermometer,

a dropping funnel and a Dean-Stark apparatus. The dropping funnel was placed in the central position of the flask. A solution of water (100 mL) containing conc. HNO_3 (0.69 mL, 68 – 70 %) was placed in the round bottom flask and allowed to stir vigorously at room temperature. Zirconium (IV) isopropoxide (20 mL) was added to the dropping funnel and diluted with isopropanol (80 mL). This solution was purged with nitrogen for 15 minutes and kept under nitrogen to prevent hydrolysis occurring before addition to the acidic solution. This mixture was then added dropwise to the acidic solution at a rate of about one drop per second. The reaction mixture should be kept stirring vigorously during the addition to prevent the formation of any large particles of ZrO_2.

After completion of the addition, the dropping funnel was replaced with a glass stopper and the reaction mixture was heated to reflux. Aluminum foil was used to cover the flask to help the distillation. Isopropanol was distilled out (T = 84°C) from the reaction mixture via the Dean-Stark apparatus. During the first 3 hours of reflux, a volume of *ca.* 160 mL isopropanol was collected. When the reflux temperature reached 100 ºC, all isopropanol was distilled, and the Dean-Stark apparatus was replaced with a condenser. The reaction mixture was refluxed overnight. Then the condenser and thermometer were removed and the flask was left open. The heat was sustained and the water was allowed to evaporate from the flask until a final volume of ~ 20 mL was reached. After cooling down, the resulting white colloid was sonicated for 2 minutes and the reaction mixture was transferred to a glass beaker with a stirring bar and placed in a sealed titanium autoclave. The sol was allowed to stir in the autoclave at 200 ^{o}C for 12 h. A typical pressure of 17 – 18 bar was observed.[58]

The white sol was allowed to cool, and then transferred to a 50 mL Erlenmeyer flask with a small stirring bar. PEG was added into the white sol to separate the TiO_2 nanoparticles. The amount of PEG added was 40 % wt. of the TiO_2 (*ca.* 1.5 g PEG per 25 cm^3 ZrO_2 sol-gel). The mixture was stirred until a uniform sol gel formed. The gel was applied to cover glass slides by the doctor-blade technique over an area of 1 x 2 cm^2 via a glass dropper. Scotch tape was used to control the thickness of the ZrO_2 film formed. The film was allowed to air dry and was sintered in the oven at 450 ºC for 2 h. The PEG was burned out in this step. The ZrO_2 films prepared should be transparent. If the films were opaque, the white sol was kept under stirring for additional 2-3 days prior to use. The sol was cast onto cover glass slides for spectroscopic measurements. All films were stored under ambient conditions, and were heated to 120 ºC for 30 min before absorbing any dyes. The white sol was stored with stirring in an Erlenmeyer flask protected from light for further use until the sol became slightly yellow or big particles were observed. The morphology of the ZrO_2 films was similar to the TiO_2 films with an average diameter of ZrO_2 nanoparticles about 10 nm (Figure A-3-2-1.2).[23]

A-3-3-2. General Binding Procedure

All films were dried by heating to 120°C for 30 minutes and cooled to 80°C prior to immersion in the dye solution. The binding of the dyes onto the films was carried out by immersing the films in dye solutions at room temperature for 2 h or overnight depending on the concentration or the type of dye. Acid (pH 1) or base (pH 11) pre-treatment in this thesis was not done. The sensitized films were washed thoroughly with neat solvent and then immersed into neat solvent until UV-Vis spectra showed the absence of dye

desorption. The sensitized films were then used for spectroscopic measurement. For ground state absorption, transient absorption, and photoluminescence studies, the films were cast onto cover glass slides.

A-3-3-3. Spectroscopy

Fourier-transform infrared attenuated total reflectance (FT-IR-ATR) spectra of dye molecules (powder) and the sensitizers bound to the metal oxide films were collected on a Thermo Electron Corporation Nicolet 6700 FT-IR using ZnSe crystal. Before every measurements the spectrometer were purged with nitrogen for at least 30 minutes. For neat dye molecules powder, atmosphere was selected as the background. For sensitized films, an blank film was used as the background. Between each measurement, the ZnSe crystal was cleaned with methanol or acetone to eliminate residues of dye molecules.

Raman spectra were collected on a HoloLab 5000/Raman Rxn1 Confocal Raman Spectrometer (Kaiser Optical Systems, Inc.) with an Invictus 785 nm laser diode.

Ground state UV-Vis absorption spectra were collected on a VARIAN Cary-500 instrument using a Hewlett-Packard 8453 diode array spectrometer. Acetonitrile solutions were measured in a 1 cm square cuvette at ambient condition. Sensitized film measurements were made in the same cuvette with the films placed diagonally while collecting spectra.

Transient absorption spectra were collected at John Hopkins University using a Surelite II Nd:YAG, Q-switched laser pulsing at 532 nm (8 ns fwhm, 1-5 mJ/pulse) as the excitation source. The sample was then probed at a right angle using a 150 W pulsed Xe

lamp from Applied Photophysics. Each kinetic track was acquired by averaging 30-60 laser shoots at 1 Hz.

Fluorescence spectra were collected on a VARIAN Cary-Eclipse instrument with a Spex Fluorolog that had been calibrated by a standard NIST tungsten-halogen lamp. Dye solutions were measured in a 1 cm square cuvette at ambient condition. Sensitized film measurements were made in the same cuvette with the films placed diagonally while collecting spectra. The excitation beam was directed 45º to the film surface, and the emitted light was monitored from the front face of the surface-bound sample and from a 90º angle in the case of dye solutions.

Photoluminescence quantum yields Φ_{PL} of the ruthenium star complexes were calculated using the optically dilute technique with $Ru(bpy)_3(PF_6)_2$ in acetonitrile as the reference based on the equation (1):[61]

$$\Phi_s = (A_{ref}/A_s)\ (I_s/I_{ref})\ (\eta_s/\eta_{ref})^2\ \Phi_{ref} \quad (1)$$

The subscript 's' refers to the sample, the subscript 'ref' refers to the reference, A is the absorbance at the excitation wavelength, I is the integrated emission area, and η is the solvent refraction index used for the sample and reference. Φ_{ref} was the quantum yield for $Ru(bpy)_3(PF_6)_2$ in acetonitrile based on the literature ($\Phi_{ref} = 0.062$).[62]

Time-resolved fluorescence decays were acquired with a nitrogen-pumped dye laser according to the published literature.[63] For solution studies, excited state lifetime τ was obtained by fitting the traces to a first-order kinetic model. Values for radiative and nonradiative constants, k_r and k_{nr} respectively, were calculated from equations (2) and (3):

$$\Phi_{PL} = k_r/(k_r + k_{nr}) \quad (2)$$

$$\Phi_{PL} = k_r\tau \quad (3)$$

For recombination kinetics measurements, the transient data was fitted to a Kohlrausch-Williams-Watts (KWW) kinetic model[64] with the equation (4). I_0 is the initial amplitude and I_f is final amplitudes of the signal. β is inversely related to the width of a stretched Levy distribution of the rate constant, and is between 0 and 1.

$$I = (I_0 - I_f)\, exp\, [-\, (k_{obs}\, t)^{\beta}] + I_f \quad (4)$$

A-3-3-4. Solution Electrochemistry

<u>*Cyclic Voltammetry (CV)*</u> for solution studies was performed in tetrabutylammonium hexafluorophosphate/acetonitrile (0.1 g/mL) electrolyte. Standard three-electrode arrangement was used. A glassy carbon electrode (2 mm diameter) was used as the working electrode along with a platinum wire auxiliary electrode and an Ag^+/AgCl reference electrode. The solution had a sensitizer concentration of ~0.5 mM. A BAS model CV-50W potentiostat was used and the CV measurements were carried out at room temperature under nitrogen atmosphere. Ferrocene was used as the internal reference. The half-wave potential ($E_{1/2}$) represented E_{HOMO} of the sensitizer, and was calculated from the equation (5). Cathodic peak potential (E_{pc}) and anodic peak potential (E_{pc}) were collected according to the CV spectra.

$$E_{1/2} = (E_{pa} + E_{pc})/2 \quad (5)$$

The excited state reduction potential ($E_{1/2}^{*}$) represented E_{LUMO} of the sensitizer, and was calculated from the equation (6).

$$E_{1/2}(Ru^{III/II*}) = E_{1/2}(Ru^{III/II}) - \Delta G_{es} \quad (6)$$

The ΔG_{es} is the free energy stored in the thermally equilibrated excited states, and was estimated from a tangent to the high energy side of the photoluminescence spectra of the sensitizer in neat acetonitrile[65] as shown in Figure A-3-3-4.1.

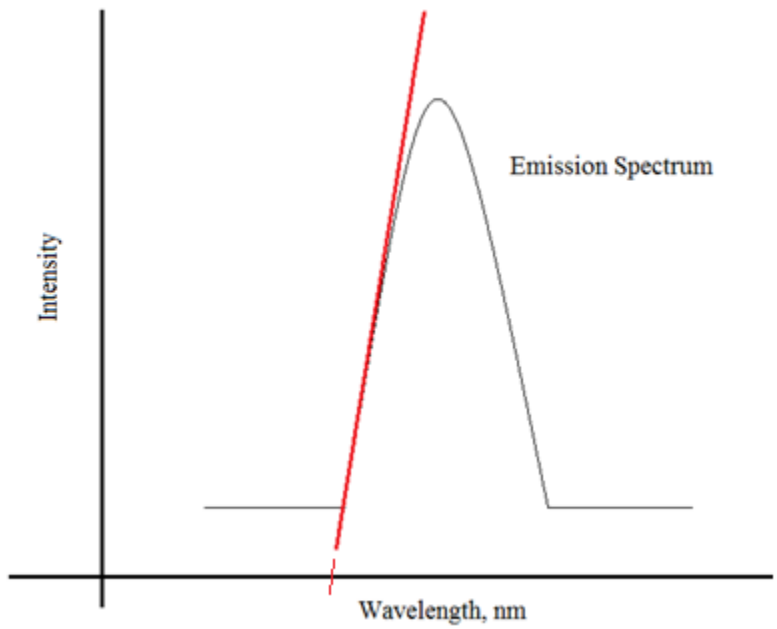

Figure A-3-3-4.1. Determination of ΔG_{es} based on photoluminescence spectrum.

A-3-4. References

1. Kamat, P. V. Photochemistry on Nonreactive and Reactive (semiconductor) Surfaces. *Chem. Rev.* **1993**, *93*, 267.

2. Juris, A.; Balzani, V.; Barigelletti, F.; Campagna, S.; Belser, P.; Von Zelewsky, A. Ru(II) Polypyridine Complexes: Photophysics, Photochemistry, Eletrochemistry, and Chemiluminescence. *Coord. Chem. Rev.* **1988**, *84*, 85.

3. Grätzel, M. Photoelectrochemical Cells. *Nature* **2001**, *414*, 338.

4. Nazeeruddin, M. K.; Kay, A.; Rodicio, I.; Humphry-Baker, R.; Mueller, E.; Liska, P.; Vlachopoulos, N.; Grätzel, M. Conversion of Light to Electricity by cis-X_2bis(2,2'-bipyridyl-4,4'-dicarboxylate) Ruthenium(II) Charge-transfer Sensitizers (X = Cl^-, Br^-, I^-, CN^-, and SCN^-) on Nanocrystalline Titanium Dioxide Electrodes. *J. Am. Chem. Soc.* **1993**, *115*, 6382.

5. Galoppini, E. Linkers for Anchoring Sensitizers to Semiconductor Nanoparticles. *Coord. Chem. Rev.* **2004**, *248*, 1283.

6. Wang, D.; Schlegel, J. M.; Galoppini, E. Synthesis of Rigid-rod Linkers to Anchor Chromophores to Semiconductor Nanoparticles. *Tetrahedron* **2002**, *58*, 6027.

7. Hoertz, P. G.; Carlisle, R. A.; Meyer, G. J.; Wang, D.; Piotrowiak, P.; Galoppini, E. Organic Rigid-Rod Linkers for Coupling Chromophores to Metal Oxide Nanoparticles. *Nano Lett.* **2003**, *3*, 325.

8. Wang, D.; Mendelsohn, R.; Galoppini, E.; Hoertz, P. G.; Carlisle, R. A.; J., M. G. Excited State Electron Transfer from Ru(II) Polypyridyl Complexes Anchored to Nanocrystalline TiO_2 through Rigid-Rod Linkers. *J. Phys. Chem. B* **2004**, *108*, 16642.

9. Lamberto, M.; Pagba, C.; Piotrowiak, P.; Galoppini, E. Synthesis of Novel Rigid-rod and Tripodal Azulene Chromophores. *Tetrahedron Lett.* **2005**, *46*, 4895.

10. Kilså, K.; Mayo, E. I.; Kuciauskas, D.; Villahermosa, R.; Lewis, N. S.; Winkler, J. R.; Gray, H. B. Effects of Bridging Ligands on the Current-Potential Behavior and Interfacial Kinetics of Ruthenium-Sensitized Nanocrystalline TiO_2 Photoelectrodes. *J. Phys. Chem. A* **2003**, *107*, 3379.

11. Myahkostupov, M.; Piotrowiak, P.; Wang, D.; Galoppini, E. Ru(II)-Bpy Complexes Bound to Nanocrystalline TiO_2 Films through Phenyleneethynylene (OPE) Linkers: Effect of the Linkers Length on Electron Injection Rates. *J. Phys. Chem. C* **2007**, *111*, 2827.

12. Fujishima, A.; Honda, K. Electrochemical Photolysis of Water at a Semiconductor Electrode. *Nature* **1972**, *238*, 37.

13. Bard, A. J. Photoelectrochemistry. *Science* **1980**, *207*, 139.

14. Bard, A. J. Design of Semiconductor Photoelectrochemical Systems for Solar Energy Conversion. *J. Phys. Chem.* **1982**, *86*, 172.

15. Gerischer, H. The Impact of Semiconductors on the Concepts of Electrochemistry. *Electrochim. Acta* **1990**, *35*, 1677.

16. Tryk, D. A.; Fujishima, A.; Honda, K. Recent Topics in Photoelectrochemistry: Achievements and Future Prospects. *Electrochim. Acta* **2000**, *45*, 2363.

17. Heben, M. J.; Kumar, A.; Zheng, C.; Lewis, N. S. Efficient Photovoltaic Devices for InP Semiconductor/liqud Junctions. *Nature* **1989**, *340*, 621.

18. Meyer, G. J.; Searson, P. C. Photoelectrochemical Solar Energy Conversion at Nanostructured Materials. *Interface* **1993**, *2*, 23.

19. Kay, A.; Humphry-Baker, R.; Grätzel, M. Artificial Photosynthesis. 2. Investigations on the Mechanism of Photosensitization of Nanocrystalline TiO_2 Solar Cells by Chlorophyll Derivatives. *J. Phys. Chem.* **1994**, *98*, 952.

20. Connor, P. A.; Dobson, K. D.; McQuillan, A. J. New Sol-Gel Attenuated Total Reflection Infrared Spectroscopic Method for Analysis of Adsorption at Metal Oxide Surfaces in Aqueous Solutions. Chelation of TiO_2, ZrO_2, and Al_2O_3 Surfaces by Catechol, 8-Quinolinol, and Acetylacetone. *Langmuir* **1995**, *11*, 4193.

21. Dobson, K. D.; McQuillan, A. J. An Infrared Spectroscopic Study of Carbonate Adsorption to Zirconium Dioxide Sol-Gel Films from Aqueous Solutions. *Langmuir* **1997**, *13*, 3392.

22. Kay, A.; Grätzel, M. Low Cost Photovoltaic Modules Based on Dye Sensitized Nanocrystalline Titanium Dioxide and Carbon Powder. *Sol. Energy Mat. Sol. Cells* **1996**, *44*, 99.

23. Thyagarajan, S.; Galoppini, E.; Persson, P.; Giaimuccio, J. M.; Meyer, G. J. Large Footprint Pyrene Chromophores Anchored to Planar and Colloidal Metal Oxide Thin Films. *Langmuir* **2009**, *25*, 9219.

24. Taratula, O. Ph. D. dissertation, Rutgers-Newark, 2008.

25. Kalyanasundaram, K.; Grätzel, M. Applications of Functionalized Transition Metal Complexes in Photonic and Optoelectronic Devices. *Coord. Chem. Rev.* **1998**, *177*, 347.

26. Meyer, G. J. Efficient Light-to-Electrical Energy Conversion: Nanocrystalline TiO_2 Films Modified with Inorganic Sensitizers. *J. Chem. Edu.* **1997**, *74*, 652.

27. Hagfeldt, A.; Grätzel, M. Light-Induced Redox Reactions in Nanocrystalline Systems. *Chem. Rev.* **1995**, *95*, 49.

28. Heimer, T. A.; D'Arcangelis, S. T.; Farzad, F.; Stipkala, J. M.; Meyer, G. J. An Acetylacetonate-Based Semiconductor-Sensitizer Linkage. *Inorg. Chem.* **1996**, *35*, 5319.

29. Grätzel, M. Sol-Gel Processed TiO_2 Films for Photovoltaic Applications. *Sol-Gel Sci. Technol.* **2001**, *22*, 7.

30. Matijevic, E. Uniform Inorganic Colloid Dispersions. Achievements and Challenges. *Langmuir* **1994**, *10*, 8.

31. Asbury, J. B.; Hao, E.; Wang, Y.; Ghosh, H. N.; Lian, T. Ultrafast Electron Transfer Dynamics from Molecular Adsorbates to Semiconductor Nanocrystalline Thin Films. *J. Phys. Chem. B* **2001**, *105*, 4545.

32. Li, J.; Nilsing, M.; Kondov, I.; Wang, H.; Persson, P.; Lunell, S.; Thoss, M. Dynamical Simulation of Photoinduced Electron Transfer Reactions in Dye-Semiconductor Systems with Different Anchor Groups. *J. Phys. Chem. C* **2008**, *112*, 12326.

33. Qu, P.; Meyer, G. J. Proton-Controlled Electron Injection from Molecular Excited States to the Empty States in Nanocrystalline TiO_2. *Langmuir* **2001**, *17*, 6720.

34. Abrahamsson, M.; Taratula, O.; Persson, P.; Galoppini, E.; Meyer, G. J. Meta-substituted Ru^{II} rigid rods for sensitization of TiO_2. *J. Photochem. Photobio. A: Chemistry* **2009**, *206*, 155.

35. Galoppini, E.; Guo, W.; Qu, P.; Meyer, G. J. Long-Distance Electron Transfer Across Molecule-Nanocrystalline Semiconductor Interfaces. *J. Am. Chem. Soc.* **2001**, *123*, 4342.

36. Galoppini, E.; Guo, W.; Zhang, W.; Hoertz, P.; Qu, P.; Meyer, G. J. Long-Range Electron Transfer across Molecule-Nanocrystalline Semiconductor Interfaces Using Tripodal Sensitizers. *J. Am. Chem. Soc.* **2002**, *124*, 7801.

37. Deacon, G. B.; Phillips, R. J. Relationships between the Carbon-oxygen Stretching Frequencies of Carboxylato Complexes and the Type of Carboxylate Coordination. *Coord. Chem. Rev.* **1980**, *33*, 227.

38. Ardo, S.; Meyer, G. J. Photodriven Heterogeneous Charge Transfer with Transition-metal Compounds Anchored to TiO_2 Semiconductor Surfaces. *Chem. Soc. Rev.* **2009**, *38*, 115.

39. Kelly, C. A.; Thompson, D. W.; Farzad, F.; Meyer, G. J. Excited-State Deactivation of Ruthenium(II) Polypyridyl Chromophores Bound to Nanocrystalline TiO_2 Mesoporous Thin Films. *Langmuir* **1999**, *15*, 731.

40. Redmond, G.; Fitzmaurice, D. Spectroscopic Determination of Flatband Potentials for Polycrystalline Titania Electrodes in Nonaqueous Solvents. *J. Phys. Chem.* **1993**, *97*, 1426.

41. Enright, B.; Redmond, G.; Fitzmaurice, D. Spectroscopic Determination of Flatband Potentials for Polycrystalline TiO_2 Electrodes in Mixed Solvent Systems. *J. Phys. Chem.* **1994**, *98*, 6195.

42. Bergeron, B. V.; Kelly, C. A.; Meyer, G. J. Thin Film Actinometers for Transient Absorption Spectroscopy: Applications to Dye-Sensitized Solar Cells. *Langmuir* **2003**, *19*, 8389.

43. Lundqvist, M. J.; Galoppini, E.; Meyer, G. J.; Persson, P. Calculated Optoelectronic Properties of Ruthenium Tris-bipyridine Dyes Containing Oligophenyleneethynylene Rigid Rod Linkers in Different Chemical Environments. *J. Phys. Chem. A* **2007**, *111*, 1487.

44. Walters, K. A.; Dattelbaum, D. M.; Ley, K. D.; Schoonover, J. R.; Meyer, T. J.; Schanze, K. S. Photophysics of Phenyleneethynylene Metal–Organic Oligomers. Probing the Lowest Excited State by Time-Resolved IR Spectroscopy *Chem. Commun.* **2001**, 1834.

45. Walters, K. A.; Ley, K. D.; Cavalheiro, C. S. P.; Miller, S. E.; Gosztola, D.; Wasielewski, M. R.; Bussandri, A. P.; Van Willigen, H.; Scanhze, K. S. Photophysics of

π-Conjugated Metal-Organic Oligomers: Aryleneethynylenes that Contain the (bpy)Re(CO)$_3$Cl Chromophore. *J. Am. Chem. Soc.* **2001**, *123*, 8329.

46. Wang, Y.; Liu, S.; Pinto, M. R.; Dattelbaum, D. M.; Schoonover, J. R.; Schanze, K. S. Excited-State Structure and Delocalization in Ruthenium(II)-Bipyridine Complexes That Contain Phenyleneethynylene Substituents. *J. Phys. Chem. A* **2001**, *105*, 11118.

47. Liu, Y.; Li, Y.; Schanze, K. S. Photophysics of π-conjugated Oligomers and Polymers that Contain Transition Metal Complexes. *J. Photochem. Photobiol. C: Photochem. Rev.* **2002**, *3*, 1.

48. Albano, G.; Belser, P.; De Cola, L.; Gandolfi, M. T. New Luminescent Ruthenium Complexes with Extended π Systems *Chem. Commun.* **1999**, 1171.

49. Schlicke, B.; De Cola, L.; Belser, P.; Balzani, V. Rigid Rod-like Molecular Wires of Nanometric Dimension. Electronic Energy Transfer from a Naphthyl to an Anthracenyl Unit Connected by a 1,4-pentaphenylene Spacer. *Coord. Chem. Rev.* **2000**, *208*, 267.

50. Chaignon, F.; Torroba, J.; Blart, E.; Borgström, M.; Hammarström, L.; Odobel, F. Distance-independent Photoinduced Energy Transfer over 1.1 to 2.3 nm in Ruthenium Trisbipyridine–Fullerene Assemblies. *New J. Chem.* **2005**, *29*, 1272.

51. Meyer, T. J. Photochemistry of Metal Coordination Complexes: Metal to Ligand Charge Transfer Excited States. *Pure and Appl. Chem.* **1986**, *58*, 1193.

52. Kober, E. M.; Caspar, J. V.; Lumpkin, R. S.; Meyer, T. J. Application of the Energy Gap Law to Excited-state Decay of Osmium(II)-polypyridine Complexes: Calculation of Relative Nonradiative Decay Rates from Emission Spectral Profiles. *J. Phys. Chem.* **1986**, *90*, 3722.

53. Strouse, G. F.; Schoonover, J. R.; Duesing, R.; Boyde, S.; Jones, W. E.; Meyer, T. J. Influence of Electronic Delocalization in Metal-to-Ligand Charge Transfer Excited States. *Inorg. Chem.* **1995**, *34*, 473.

54. Clark, W. D. K.; Sutin, N. Spectral Sensitization of n-type Titanium Dioxide Electrodes by Polypyridineruthenium(II) Complexes. *J. Am. Chem. Soc.* **1977**, *99*, 4676.

55. Watson, D. F.; Marton, A.; Stux, A. M.; Meyer, G. J. Insights into Dye-Sensitization of Planar TiO_2: Evidence for Involvement of a Protonated Surface State. *J. Phys. Chem. B* **2003**, *107*, 10971.

56. Kelly, C. A.; Thompson, D. W.; Farzad, F.; Stipkala, J. M.; Meyer, G. J. Cation-Controlled Interfacial Charge Injection in Sensitized Nanocrystalline TiO_2. *Langmuir* **1999**, *15*, 7047.

57. Taratula, O.; Wang, D.; Chu, D.; Galoppini, E.; Zhang, Z.; Chen, H.; Saraf, G.; Lu, Y. Binding Studies of Molecular Linkers to ZnO and MgZnO Nanotip Films. *J. Phys. Chem. B.* **2006**, *110*, 6506.

58. Thyagarajan, S. Ph. D. dissertation, Rutgers - Newark, 2008.

59. Zhang, W. F.; He, Y. L.; Zhang, M. S.; Yin, Z.; Chen, Q. Raman Scattering Study on Anatase TiO_2 Nanocrystals *J. Phys. D: Appl. Phys.* **2000**, *33*, 912.

60. Wang, D. Ph. D. dissertation, Rutgers - Newark, 2004.

61. Demas, J. N.; Crosby, G. A. Measurement of Photoluminescence Quantum Yields. A Review. *J. Phys. Chem.* **1971**, *75*, 991.

62. Casper, J. V.; Meyer, T. J. Photochemistry of Tris(2,2'-bipyridine)ruthenium(2+) ion ($Ru(bpy)_3^{2+}$). Solvent effects. *J. Am. Chem. Soc.* **1983**, *105*, 5583.

63. Castellano, F. N.; Heimer, T. A.; Tandhasetti, T.; Meyer, G. J. Photophysical Properties of Ruthenium Polypyridyl Photonic SiO_2 Gels. *Chem. Mater.* **1994**, *6*, 1041.

64. Lindsey, C. P.; Patterson, G. D. Detailed Comparison of the Williams–Watts and Cole–Davidson Functions. *J. Chem. Phys.* **1980**, *73*, 3348.

65. Qu, P.; Thompson, D. W.; Meyer, G. J. Temperature-Dependent Electron Injection from Ru(II) Polypyridyl Compounds with Low Lying Ligand Field States to Titanium Dioxide. *Langmuir* **2000**, *16*, 4662.

CHAPTER B-1: INTRODUCTION

B-1-1. Aggregation of Organic Dyes

Although inorganic dyes are preferred sensitizers for DSSCs,[1-4] organic dyes, such as perylenes,[5-7] coumarins,[8-10] and other organic dyes have been studied and used in the DSSCs application due to their high extinction coefficient, high quantum yield, low toxicity, and low cost.[5-21] Furthermore, it is possible through unlimited structural modifications to tune the position of excited state energy level relative to the conduction band edge of the metal oxide semiconductor, widen the range of spectral absorption, and increase the extinction coefficient.[22,23] Also organic dyes provide excellent testing systems for elucidating fundamental photophysics of charge injection and recombination processes at the dye/TiO_2 interface.[24-28] Careful molecular design of organic dyes has led to solar cell efficiencies that are competitive with those inorganic sensitizers.[10,20,21,29] The main limitations of organic dyes include low photostability, shorter excited state lifetimes and tendency to form aggregates.

Organic dyes containing π-conjugated systems, such as aromatic hydrocarbons, tend to form aggregates through face-to-face π-π interactions on the surface of the metal oxide semiconductor. This is less likely to occur with ruthenium (II) polypyridine sensitizers, which are reported to form a monolayer on the metal oxide nanoparticles surfaces.[30] A typical example is the formation of pyrene excimer, which produces a broad red-shifted emission band in the fluorescence spectrum compared to the pyrene monomer (Figure B-1-1.1[31]). The formation of a pyrene excimer requires the encounter of an excited pyrene molecule with a second pyrene in the ground state.

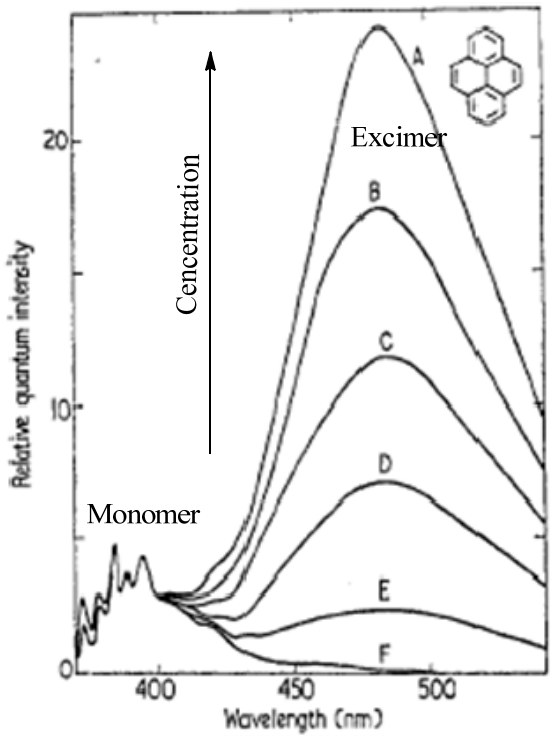

Figure B-1-1.1. Fluorescence spectra of pyrene excimer and monomer in cyclohexane[31]

Aggregation is not always a disadvantage for sensitization purposes. In some limited cases, a controlled aggregation has been proved to enhance the photocurrent generation as a result of wider absorption window, which combined with an efficient charge transfer from the aggregate excited state to the semiconductor.[32-36] For instance, closely packed pyrene-substituted rigid-rods have been reported in our group to be effective sensitizers.[12] However, in most cases, aggregation results in decreased photocurrents and photovoltages through a variety of processes that compete with the photosensitization process, including, for instance energy transfer within π-stacks. Also excess of dye molecules stacked together may act as an optical filter.[32,34,37,38] Thus the separation of the organic dyes on semiconductor surface is an important issue and it has been proven to benefit the DSSCs performance. For example, Sundström and coworkers

showed that with deoxycholic acid (DCA) as the coadsorbate to prevent aggregation, the solar cell efficiency significantly increased for phthalocyanine derivative sensitizers (Figure B-1-1.2).[39]

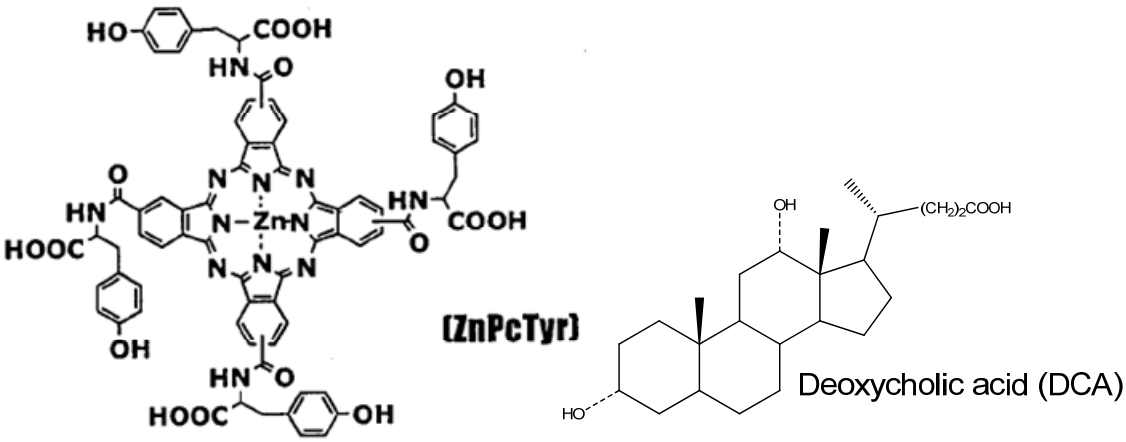

	A_g/A_m	η %
ZnPcTyr	0.80	0.29
ZnPcTyr/DCA	0.59	0.54

Figure B-1-1.2. Solar cell performance improved by avoiding aggregation of zinc phthalocyanines with tyrosine subsitutents (ZnPcTyr).

B-1-2. Strategies to Avoid Aggregation

Several strategies have been developed in the past decade to avoid the aggregation of organic dyes on metal oxide semiconductor surfaces. These strategies include use of coadsorbates, such as DCA, substitution with bulky groups directly on the dyes, modification of sensitizer with large footprints to space out the dye units, and encapsulation of the dye in a host molecule. Each stratergy is described in the following sections.

1) Coadsorbates Fatty acid or carboxylic acids with lipidic substitutents, such as hexadecylmalonic acid (HDMA) and deoxycholic acid (DCA), have been used as coadsorbates to separate dye molecules on the semiconductor surface. The use of coadsorbates often resulted in higher photocurrents and photovoltages thus enhancing the solar cell performance.[40,41] The improvement in photocurrent has been attributed to the inhibition of quenching processes due to energy transfer,[39] as well as to a positive shift (lower energy) of the conduction band edge due to the binding of an acidic adsorbate.[42] Furthermore, the coadsorbate coats the surface and acts as a shield for the electrolyte, inhibiting the recombination processes, thereby suppressing dark currents and increasing photovoltage.[43] Figure B-1-2.1 shows an example reported by Arakawa and coworkers.[9]

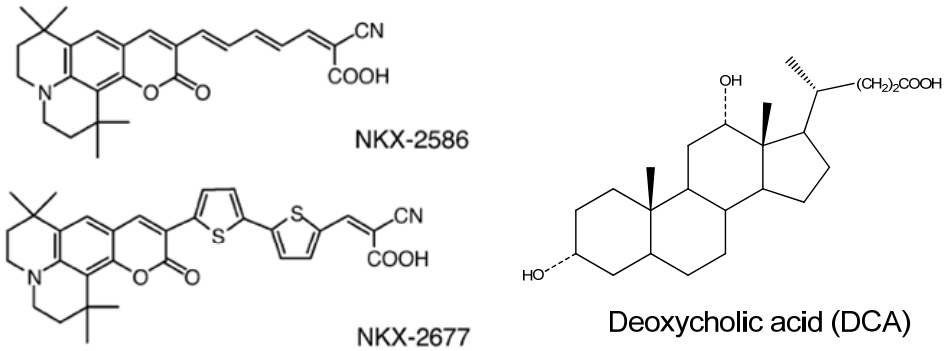

dye	DCA/mM	η/%
NKX-2586	0	3.1
	5	3.3
	20	3.8
	40	3.9
NKX-2677	0	2.8
	20	3.3
	50	3.9
	70	4.0

Figure B-1-2.1. Coadsorbate DCA improves performance of coumarine-based DSSCs[9]

2) Structure modification One of the organic sensitizers' advantages is that they are relatively easy to modify synthetically. This classic method has been used to reduce aggregation by adding directly bulky substituents on the chromophore. The formation of the excimers is avoided without significantly changing the photophysical properties of the dye units. For instance, Willig and coworkers developed the t-butyl-modified perylenes to avoid aggregation for charge injection studies (Figure B-1-2.2).[44] Another example is phthalocyanine dyes substituted with glycine or tyrosine groups. The glycine and tyrosine substituents improved solubility and decreased aggregation.[39,45] The drawback of this strategy is that more synthetic effort may be involved.

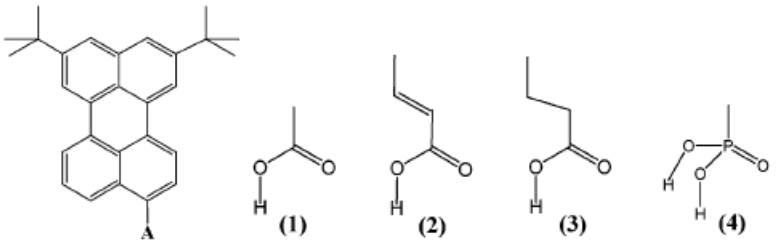

Figure B-1-2.2. Example of t-butyl-modified perylene for sensitization study.[44]

3) Large footprints As mentioned in the previous chapter, tripodal linkers with three carboxylic acid anchoring groups have been developed and used for both inorganic and organic dyes in our group.[46-49] Recently, pyrene-subsitituted tripodal dyes with different footprint sizes were selected for studying aggregation effects.[50,51] Upon binding on a planar sapphire surface, the tripod linker shows monomer band in fluorescence emission spectrum. As a comparison, a short rigid-rod with pyrene dye unit gives red-shifted, broad excimer band in the fluorescence emission spectrum (Figure B-1-2.3[51]). This result

demonstrates that on a planar surface the larger footprints are effective in spacing the dye units.

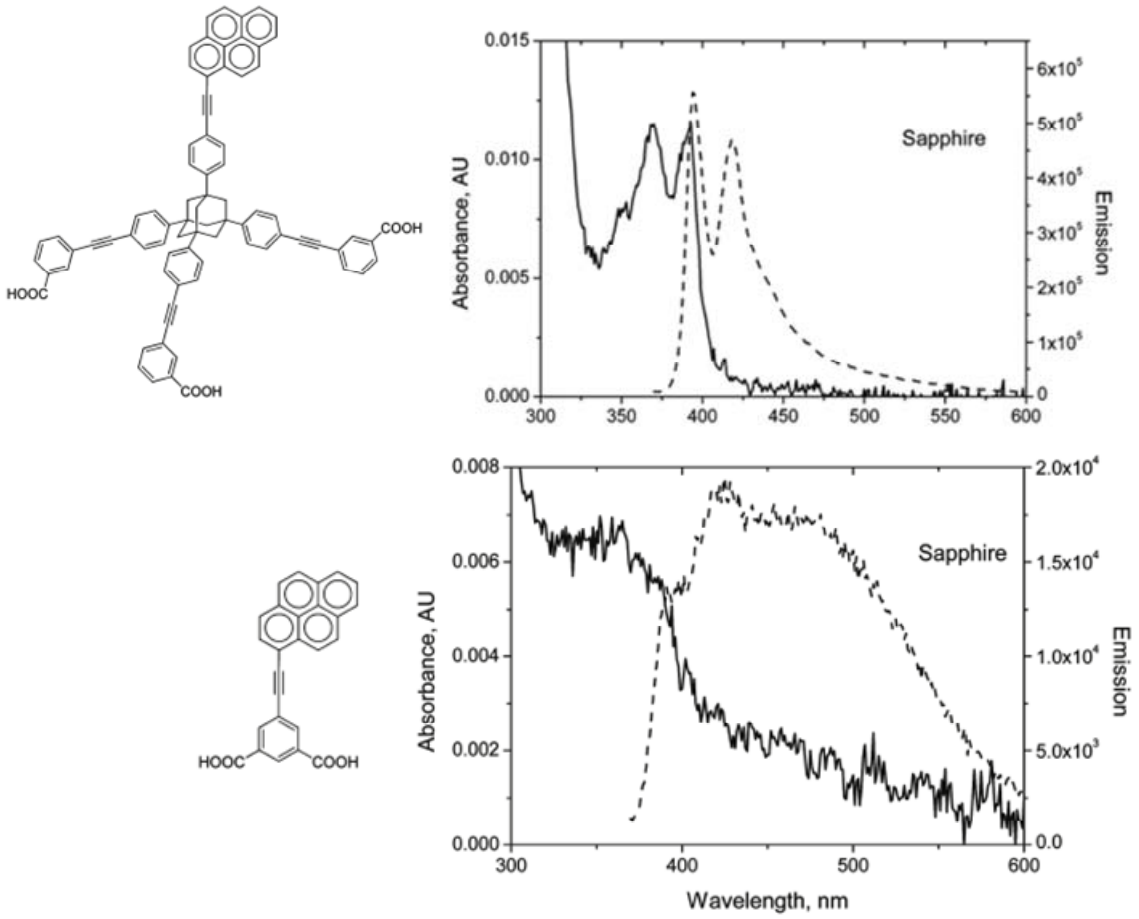

Figure B-1-2.3. Comparison of emission spectra of tripod and rigid-rod on planar surface.[51]

4) Dye@host Molecular encapsulation of dyes in a host molecule, and anchoring of a guest@host complex on the surface is reported as an efficient and yet little explored strategy to avoid aggregation. Piotrowiak and coworkers used azulene complexed in a hemicarcerand host. The modified hemicarcerand uses carboxylic acid functional group as the anchor group and has ~ 200Å^3 internal volume (Figure B-1-2.4). Encapsulation

within the hemicarcerand slowed down the charge recombination process by three orders of magnitude, and the recombination kinetics was fit by a single exponential.[52]

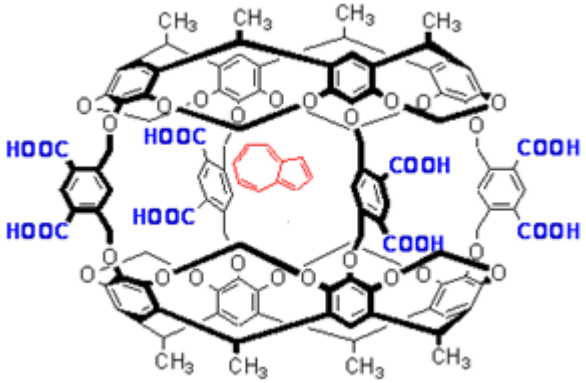

Figure B-1-2.4. Encapsulation of azulene with in a hemicarcerand.[52]

Cucurbituril (CB) has been used recently in our group as an effective host molecule to contain viologen and bind it to TiO_2 films through the cucurbituril itself (Figure B-1-2.5).[53] The redox-active compound viologen formed guest-host complexes with CB(7) and showed reversibility and stability in an electrochemical study, as dimerization and aggregation processes were prevented. Moreover, this approach was useful to avoid the need for synthetic modifications of the viologen with binding groups.

To reduce the organic dyes' aggregation and to improve the solar cell's performance, our group has been synthesis the tripod linkers with a large foot print to separate the pyrene dye and to prevent excimer formation successfully on planar surface.[51] However, upon bound onto porous metal oxide semiconductor surface, red-shift broad emission band which belong to the pyrene excimer was observed in the fluorescence emission spectra (Figure B-1-2.6).

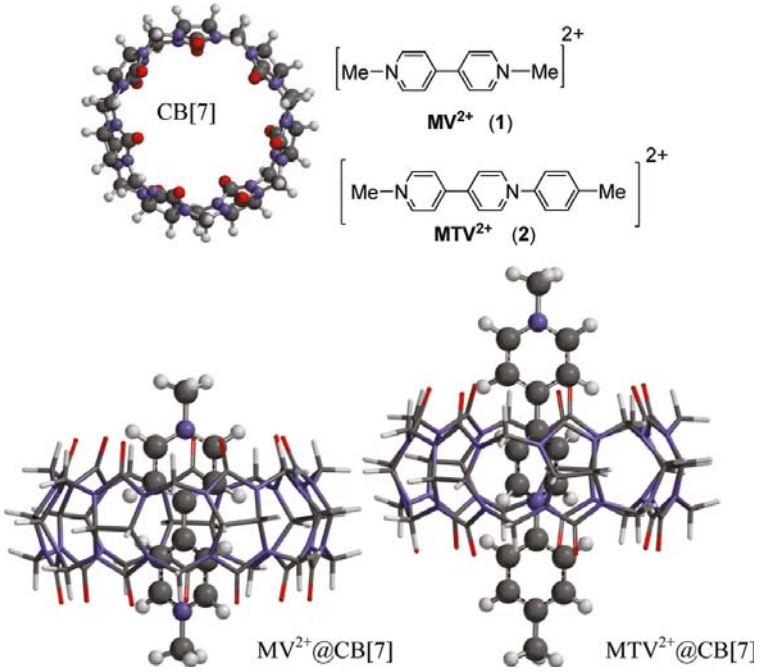

Figure B-1-2.5. Encapsulation of viologen with cucurbituril.[53]

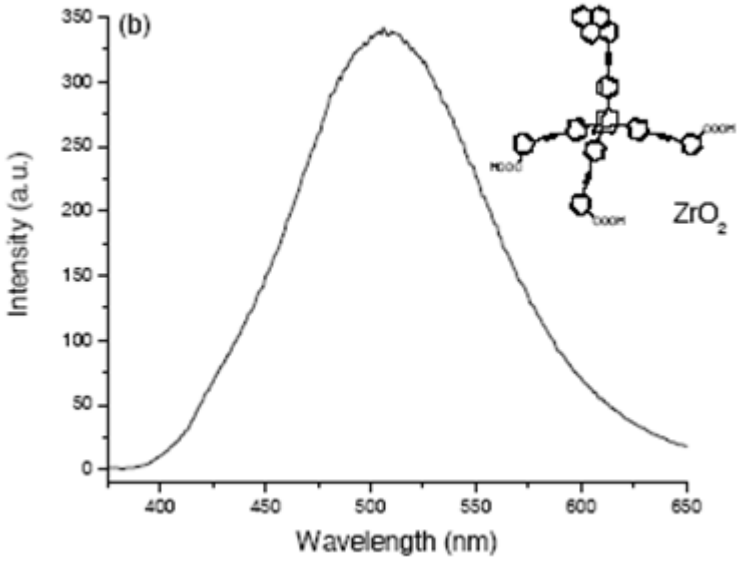

Figure B-1-2.6. Fluorescence emission spectra of tripod bound onto ZrO_2 film.[51]

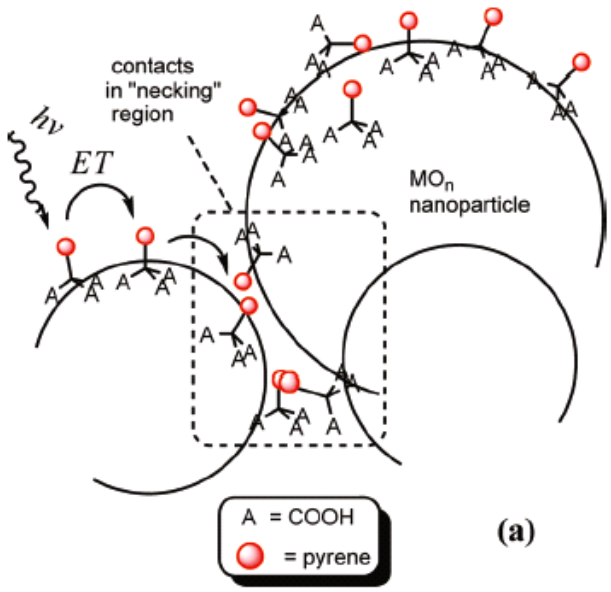

Figure B-1-2.7. Schematic representation of possible binding orientations and positions of Ad-acid(*m*) tripod on nanoparticles film surfaces (not in scale). Excimer could form in the necking regions and between dyes trapped in pores.[51]

This is attributed to the dye contact in 'necking' region as shown in Figure B-1-2.7. Similar observation was observed for rigid-rod pyrene sensitizers.[12] Thus to physical separate the pyrene dye by involving a host molecule, such as cyclodextrin, will be an interesting improvement for sensitization study of organic dye on metal oxide semiconductor surface.

In the Part B of this thesis, cyclodextrin was selected as the host molecule to separate the pyrene derivative on the metal oxide semiconductor surfaces as a comparison with the previously reported pyrene tripods and rods. The next section describes examples of dyes@CDs/TiO_2.

B-1-3. Cyclodextrins (CDs) as Hosts in DSSC Application

Cyclodextrins (CDs) are composed of 5 or more α-D-glucopyranoside units. Commercially available cyclodextrins contain 6, 7, and 8 glucose units (α-, β-, and γ-CDs, respectively). The inner cavity of CDs is hydrophobic, while the outer cavity has OH functional groups which can anchor onto metal oxide nanocrystalline. Obviously, depending on the sizes of the cyclodextrins, different organic compounds can be encapsulated. The chemical structures of cyclodextrins are shown in Figure B-1-3.1 and Table B-1-3.1.[54]

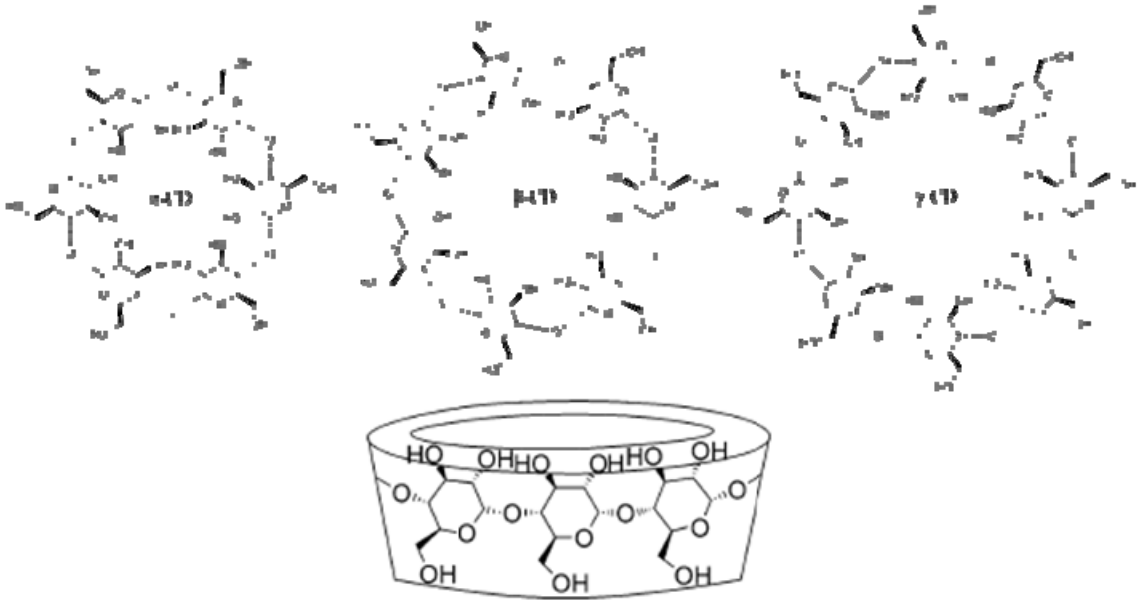

Figure B-1-3.1. Chemical structures of α-, β-, and γ-cyclodextrins

Table B-1-3.1. Structural parameters of α, β, and γ – cyclodextrins.[54]

	α-CD	β-CD	γ-CD
glucose residues	6	7	8
molecular weight	973	1135	1297
cavity diameter (Å)	4.7−5.3	6−6.6	7.5−8.3
cavity height (Å)	7.9	7.9	7.9
cavity volume (mL/mol)	174	262	472

Cyclodextrins' carbohydrate frameworks are colorless and do not contain chromophoric group. Thus, they have been used as host macrocycles to encapsulate chromophores.[54-58] However, the attachment of such complexes to the semiconductor surfaces for charge transfer study remains little explored. Durrant and coworkers studied the encapsulation of azobenzene dyes with cyclodextrins bound to TiO_2 (Figure B-1-3.2).[59] The dye@CD complex binds to TiO_2 through the OH groups from CD. It was observed that for the dye bound through a CD the recombination dynamics were slower than that of the directly bound dye (300 and 4 μs, respectively). This was attributed to the larger physical separation between the dye and the TiO_2 surface.[59] Recently Ko and coworkers reported increased solar cell efficiency by using CD instead of coadsorbates to separate organic dye on the TiO_2 surface (Figure B-1-3.3).[60] Encapsulation inside CDs retarded charge recombination and resulted in improved stability of the dyes under light.[60]

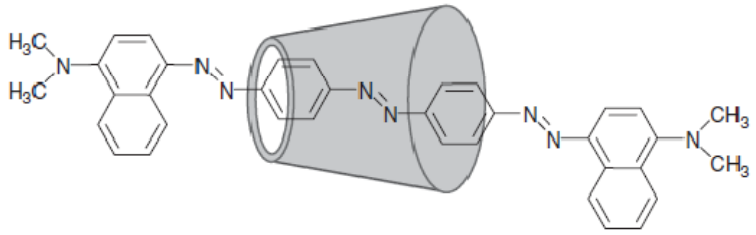

Figure B-1-3.2. Encapsulation of azobenzene dye with cyclodextrin.[59]

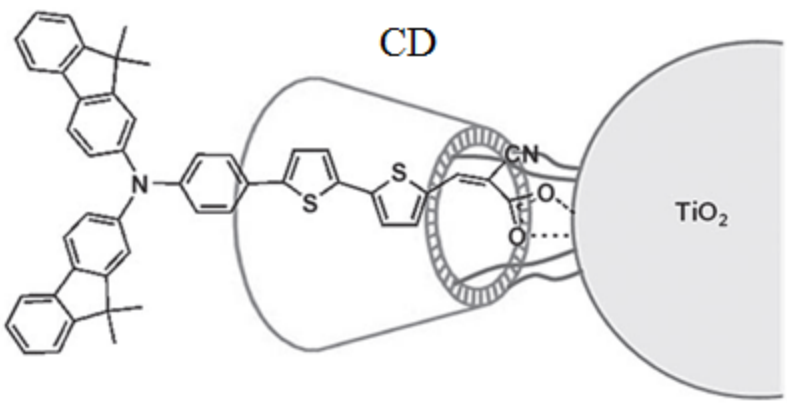

Figure B-1-3.3. JK-2 sensitizer encapsulated in a cyclodextrin anchored to TiO_2.[60]

B-1-4. References

1. Meyer, T. J. Chemical Approaches to Artificial Photosynthesis. *Accts. Chem. Res.* **1989**, *22*, 163.

2. Meyer, T. J. Photochemistry of Metal Coordination Complexes: Metal to Ligand Charge Transfer Excited States. *Pure Appl. Chem.* **1986**, *58*, 1193.

3. Constable, E. C. Novel Oligopyridines for Metallosupramolecular Chemistry. *Pure Appl. Chem.* **1996**, *68*, 253.

4. Hagfeldt, A.; Grätzel, M. Molecular Photovoltaics. *Accts. Chem. Res.* **2000**, *33*, 269.

5. Ferrere, S.; Zaban, A.; Gregg, B. A. Dye Sensitization of Nanocrystalline Tin Oxide by Perylene Derivatives. *J. Phys. Chem. B* **1997**, *101*, 4490.

6. Tian, H.; Liu, P. H.; Meng, F. S.; Gao, E.; Cai, S. Wide Spectral Photosensitization for SnO_2 Nanoporous Electrode with Soluble Perylene Derivatives and Cyanine Dyes. *Synth. Met.* **2001**, *121*, 1557.

7. Zimmermann, C.; Willig, F.; Ramakrishna, S.; Burfeindt, B.; Pettinger, B.; Eichberger, R.; W. Storck, W. Experimental Fingerprints of Vibrational Wave-Packet Motion during Ultrafast Heterogeneous Electron Transfer. *J. Phys. Chem. B* **2001**, *105*, 9245.

8. Hara, K.; Sayama, K.; Ohga, Y.; Shinpo, A.; Suga, S.; Arakawa, H. A Coumarin-derivative Dye Sensitized Nanocrystalline TiO_2 Solar Cell Having a High Solar-energy Conversion Efficiency up to 5.6% *Chem. Commun.* **2001**, *6*.

9. Hara, K.; Dan-oh, Y.; Kasada, C.; Ohga, Y.; Shinpo, A.; Suga, S.; Sayama, K.; Arakawa, H. Effect of Additives on the Photovoltaic Performance of Coumarin-Dye-Sensitized Nanocrystalline TiO_2 Solar Cells. *Langmuir* **2004**, *20*, 4205.

10. Wang, Z. S.; Hara, K.; Dan-oh, Y.; Kasada, C.; Shinpo, A.; Suga, S.; Arakawa, H.; Sugihara, H. Photophysical and (Photo)electrochemical Properties of a Coumarin Dye. *J. Phys. Chem. B* **2005**, *109*, 3907.

11. Galoppini, E.; Thyagarajan, S. Organic Dyes Aggregation on TiO_2 Surfaces. *The Spectrum* **2005**, *18*, 22.

12. Taratula, O.; Rochford, J.; Piotrowiak, P.; Galoppini, E.; Carlisle, R. A.; Meyer, G. J. Pyrene-Terminated Phenylenethynylene Rigid Linkers Anchored to Metal Oxide Nanoparticles. *J. Phys. Chem. B* **2006**, *110*, 15734.

13. Ramakrishna, G.; Ghosh, H. N. Emission from the Charge Transfer State of Xanthene Dye-Sensitized TiO_2 Nanoparticles: A New Approach to Determining Back Electron Transfer Rate and Verifying the Marcus Inverted Regime. *J. Phys. Chem. B* **2001**, *105*, 7000.

14. Sayama, K.; Sugino, M.; Sugihara, H.; Abe, Y.; Arakawa, H. Photosensitization of Porous TiO_2 Semiconductor Electrode with Xanthene Dyes. *Chem. Lett.* **1998**, *8*, 753.

15. Guo, M.; Diao, P.; Ren, Y. J.; Meng, F.; Tian, H.; Cai, S. M. Photoelectrochemical Studies of Nanocrystalline TiO_2 Co-sensitized by Novel Cyanine Dyes. *Sol. Energy Mater. Sol. Cells* **2005**, *88*, 23.

16. Wang, Z. S.; Li, F. Y.; Huang, C. H.; Wang, L.; Wei, M.; Jin, L. P.; Li, N. Q. Photoelectric Conversion Properties of Nanocrystalline TiO_2 Electrodes Sensitized with Hemicyanine Derivatives. *J. Phys. Chem. B* **2000**, *104*, 9676.

17. Martini, I.; Hodak, J. H.; Hartland, G. V. Effect of Structure on Electron Transfer Reactions between Anthracene Dyes and TiO_2 Nanoparticles. *J. Phys. Chem. B* **1998**, *102*, 9508.

18. Kamat, P. V.; Fox, M. A. Photosensitization of TiO_2 Colloids by Erythrosin B in Acetonitrile. *Chem. Phys. Lett.* **1983**, *102*, 379.

19. Rossetti, R.; Brus, L. E. Time-resolved Raman Scattering Study of Adsorbed, Semioxidized Eosin Y Formed by Excited-state Electron Transfer into Colloidal Titanium(IV) Oxide Particles. *J. Am. Chem. Soc.* **1984**, *106*, 4336.

20. Yum, J.-H.; Hagberg, D. P.; Moon, S.-J.; Karlsson, K. M.; Marinado, T.; Sun, L.; Hagfeldt, A.; Nazeeruddin, M. K.; Grätzel, M. A Light-Resistant Organic Sensitizer for Solar-Cell Applications. *Angew. Chem. Int. Ed.* **2009**, *48*, 1576.

21. Hara, K. S., T.; Katoh, R.; Furube, A.; Ohga, Y.; Shinpo, A.; Suga, S.; Sayama, K.; Sugihara, H.; Arakawa, H. Molecular Design of Coumarin Dyes for Efficient Dye-Sensitized Solar Cells. *J. Phys. Chem. B* **2003**, *107*, 597.

22. Hagberg, D.; Yum, J.-H.; Lee, H.-J.; De Angelis, F.; Marinado, T.; Karlsson, K. M.; Humphry-Baker, R.; Sun, L.; Hagfeldt, A.; Grätzel, M.; Nazeeruddin, M. K. Molecular Engineering of Organic Sensitizers for Dye-sensitized Solar Cell Applications. *J. Am. Chem. Soc.* **2008**, *130*, 6259.

23. Qin, P.; Yang, X.; Chen, R.; Sun, L.; Marinado, T.; Edvinsson, T.; Boschloo, G.; Hagfeldt, A. Influence of π-Conjugation Units in Organic Dyes for Dye-Sensitized Solar Cells. *J. Phys. Chem. C.* **2007**, *111*, 1853.

24. Ramakrishna, S.; Willig, F. Pump-Probe Spectroscopy of Ultrafast Electron Injection from the Excited State of an Anchored Chromophore to a Semiconductor Surface in UHV: A Theoretical Model. *J. Phys. Chem. B* **2000**, *104*, 68.

25. Ramakrishna, S.; Willig, F.; May, V.; Knorr, A. Femtosecond Spectroscopy of Heterogeneous Electron Transfer: Extraction of Excited-State Population Dynamics from Pump-Probe Signals. *J. Phys. Chem. B* **2003**, *107*, 607.

26. Giaimuccio, J. M.; Rowley, J. G.; Meyer, G. J.; Wang, D.; Galoppini, E. Heavy Atom Effects on Anthracene-rigid-rod Excited States Anchored to Metal Oxide Nanoparticles. *Chem. Phys.* **2007**, *339*, 146.

27. Ernstorfer, R.; Gundlach, L.; Felber, S.; Storck, W.; Eichberger, R.; Willig, F. Role of Molecular Anchor Groups in Molecule-to-Semiconductor Electron Transfer. *J. Phys. Chem. B* **2006**, *110*, 25383.

28. Persson, P.; Lundqvist, M. J.; Ernstorfer, R.; Goddard, W. A. I.; F., W. Quantum Chemical Calculations of the Influence of Anchor-Cum-Spacer Groups on Femtosecond Electron Transfer Times in Dye-Sensitized Semiconductor Nanocrystals. *J. Chem. Theory and Comput.* **2006**, *2*, 441.

29. Ito, S.; M. Zakeeruddin, S. M.; Humphry-Baker, R.; Liska, P.; Charvet, R.; Comte, P.; Nazeeruddin, M. K.; Péchy, P.; Takata, M.; Miura, H.; Uchida, S.; Grätzel, M. High-Efficiency Organic-Dye-Sensitized Solar Cells Controlled by Nanocrystalline-TiO_2 Electrode Thickness. *Adv. Mater.* **2006**, *18*, 1202.

30. Kalyanasundaram, K.; Grätzel, M. Applications of Functionalized Transition Metal Complexes in Photonic and Optoelectronic Devices. *Coord. Chem. Rev.* **1998**, *177*, 347.

31. Birks, J. B. Excimers. *Rep. Prog. Phys.* **1975**, *38*, 903.

32. Pastore, M.; De Angelis, F. Aggregation of Organic Dyes on TiO_2 in Dye-Sensitized Solar Cells Models: An *ab Initio* Investigation. *ACS Nano* **2009**, *4*, 556.

33. Sayama, K.; Tsukagoshi, S.; Hara, K.; Ohga, Y.; Shinpou, A.; Abe, Y.; Suga, S.; Arakawa, H. Photoelectrochemical Properties of J Aggregates of Benzothiazole Merocyanine Dyes on a Nanostructured TiO_2 Film. *J. Phys. Chem. B* **2002**, *106*, 1363.

34. Ehret, A.; Stuhl, L.; Spitler, M. T. Spectral Sensitization of TiO_2 Nanocrystalline Electrodes with Aggregated Cyanine Dyes. *J. Phys. Chem. B* **2001**, *105*, 9960.

35. Kawasaki, M.; Aoyama, S. High Efficiency Photocurrent Generation by Two-Dimensional Mixed J-Aggregates of Cyanine Dyes. *Chem. Commun.* **2004**, 988.

36. Khazraji, A. C.; Hotchandani, S.; Das, S.; Kamat, P. V. Controlling Dye (Merocyanine-540) Aggregation on Nanostructured TiO_2 Films. An Organized Assembly Approach for Enhancing the Efficiency of Photosensitization. *J. Phys. Chem. B* **1999**, *103*, 4693.

37. Tatay, S.; Haque, S. A.; O'Regan, B.; Durrant, J. R.; Verhees, W. J. H.; Kroon, J. M.; Vidal-Ferran, A.; Gavina, P.; Palomares, E. Kinetic Competition in Liquid Electrolyte and Solid-State Cyanine Dye Sensitized Solar Sells. *J. Mater. Chem.* **2007**, *17*, 3037.

38. Wang, Z.-S.; Cui, Y.; Dan-oh, Y.; Kasada, C.; Shinpo, A.; Hara, K. Thiophene-Functionalized Coumarin Dye for Efficient Dye-Sensitized Solar Cells: Electron Lifetime Improved by Coadsorption of Deoxycholic Acid. *J. Phys. Chem. C* **2007**, *111*, 7224.

39. He, J.; Benkö, G.; Korodi, F.; Polivka, T.; Lomoth, R.; Åkermark, B.; Sun, L.; Hagfeldt, A.; Sundström, V. Modified Phthalocyanines for Efficient Near-IR Sensitization of Nanostructured TiO_2 Electrode. *J. Am. Chem. Soc.* **2002**, *124*, 4922.

40. Kay, A.; Grätzel, M. Artificial Photosynthesis. 1. Photosensitization of Titania Solar Cells with Chlorophyll Derivatives and Related Natural Porphyrins. *J. Phys. Chem.* **2002**, *97*, 6272.

41. Horiuchi, T.; Miura, H.; Sumioka, K.; Uchida, S. High Efficiency of Dye-Sensitized Solar Cells Based on Metal-Free Indoline Dyes. *J. Am. Chem. Soc.* **2004**, *126*, 12218.

42. Kay, A.; Grätzel, M. Artificial Photosynthesis. 1. Photosensitization of Titania Solar Cells with Chlorophyll Derivatives and Related Natural Porphyrins. *J. Phys. Chem.* **1993**, *97*, 6272.

43. Wang, P.; Zakeeruddin, S. M.; Comte, P.; Charvet, R.; Humphry-Baker, R.; Grätzel, M. Enhance the Performance of Dye-Sensitized Solar Cells by Co-grafting Amphiphilic Sensitizer and Hexadecylmalonic Acid on TiO_2 Nanocrystals. *J. Phys. Chem. B* **2003**, *107*, 14336.

44. Burfeindt, B.; Hannappel, T.; Storck, W.; Willig, F. Measurement of Temperature-Independent Femtosecond Interfacial Electron Transfer from an Anchored Molecular Electron Donor to a Semiconductor as Acceptor. *J. Phys. Chem.* **1996**, *100*, 16463.

45. Palomares, E.; Martínez-Díaz, M. V.; Haque, S. A.; Torres, T.; Durrant, J. R. State Selective Electron Injection in Non-aggregated Titanium Phthalocyanine Sensitised Nanocrystalline TiO_2 Films *Chem. Commun.* **2004**, 2112.

46. Galoppini, E.; Guo, W.; Qu, P.; Meyer, G. J. Long-Distance Electron Transfer Across Molecule-Nanocrystalline Semiconductor Interfaces. *J. Am. Chem. Soc.* **2001**, *123*, 4342.

47. Galoppini, E.; Guo, W.; Zhang, W.; Hoertz, P. G.; Qu, P.; Meyer, G. J. Long-Range Electron Transfer across Molecule-Nanocrystalline Semiconductor Interfaces Using Tripodal Sensitizers. *J. Am. Chem. Soc.* **2002**, *124*, 7801.

48. Piotrowiak, P.; Galoppini, E.; Wei, Q.; Meyer, G. J.; Wiewiór, P. Subpicosecond Photoinduced Charge Injection from 'Molecular Tripods' into Mesoporous TiO_2 Over the Distance of 24 Angstroms. *J. Am. Chem. Soc.* **2003**, *125*, 5278.

49. Lee, C.-H.; Zhang, Y.; Romayanantakit, A.; Galoppini, E. Modular Synthesis of Ruthenium Tripodal System with Variable Anchoring Groups Positions for Semiconductor Sensitization. *Tetrahedron* **2010**, *66*, 3897.

50. Thyagarajan, S.; Liu, A.; Famoyin, O. A.; Lamberto, M.; Galoppini, E. Tripodal Pyrene Chromophores for Semiconductor Sensitization: New Footprint Design. *Tetrahedron* **2007**, *63*, 7550.

51. Thyagarajan, S.; Galoppini, E.; Persson, P.; Giaimuccio, J. M.; Meyer, G. J. Large Footprint Pyrene Chromophores Anchored to Planar and Colloidal Metal Oxide Thin Films. *Langmuir* **2009**, *25*, 9219.

52. Pagba, C.; Zordan, G.; Galoppini, E.; Piatnitski, E. L.; Hore, S.; Deshayes, K.; Piotrowiak, P. Hybrid Photoactive Assemblies: Electron Injection from Host-Guest Complexes into Semiconductor Nanoparticles. *J. Am. Chem. Soc.* **2004**, *126*, 9888.

53. Freitag, M.; Galoppini, E. Cucurbituril Complexes of Viologens Bound to TiO_2 Films. *Langmuir* **2010**, *26*, 8262.

54. Hapiot, F.; Tilloy, S.; Monflier, E. Cyclodextrins as Supramolecular Hosts for Organometallic Complexes. *Chem. Rev.* **2006**, *106*, 767.

55. Kaanumalle, L. S.; Gibb, C. L. D.; Gibb, B. C.; Ramamurthy, V. Controlling Photochemistry with Distinct Hydrophobic Nanoenvironments. *J. Am. Chem. Soc.* **2004**, *126*, 14366.

56. Kaanumalle, L. S.; Pattabiraman, M.; Jayaraman, N.; Ramamurthy, V. Water-Soluble Dendrimers as Photochemical Reaction Media: Chemical Behavior of Singlet and Triplet Radical Pairs Inside Dendritic Reaction Cavities. *J. Am. Chem. Soc.* **2004**, *126*, 8999.

57. Rekharsky, M. V.; Inoue, Y. Complexation Thermodynamics of Cyclodextrins. *Chem. Rev.* **1998**, *98*, 1875.

58. Khan, A. R.; Forgo, P.; Stine, K. J.; D'Souza, V. T. Methods for Selective Modifications of Cyclodextrins. *Chem. Rev.* **1998**, *98*, 1977.

59. Haque, S. A.; Park, J. S.; Srinivasarao, M.; Durrant, J. R. Molecular-Level Insulation: An Approach to Controlling Interfacial Charge Transfer. *Adv. Mater.* **2004**, *16*, 1177.

60. Choi, H.; Kang, S.-O.; Ko, J.; Gao, G.; Kang, H.-S.; Kang, M.-S.; Nazeeruddin, M. K.; Grätzel, M. An Efficient Dye-Sensitized Solar Cell with an Organic Sensitizer Encapsulated in a Cyclodextrin Cavity *Angew. Chem. Int. Ed.* **2009**, *48*, 5938.

CHAPTER B-2:

ORGANIC DYE AGGREGATION STUDY

ON METAL OXIDE SEMICONDUCTOR SURFACES

B-2-1. Introduction

Pyrene substituted rigid-rods[1] and pyrene substituted tripods[2] developed in our group aggregate on mesoporous metal oxide semiconductor surface, resulting in a broad red-shift excimer band in fluorescence emission spectra. Molecular encapsulation of chromophores in host molecule, such as cyclodextrins,[3-7] cucurbiturils,[8-11] and calixarenes,[8-11] is reported as an efficient approach to separate chromophores upon binding to semiconductor surfaces. This approach is limited by the relative guest and host properties (such as size and lipophilicity) and their ability to form stable complexes.

In this chapter, cyclodextrins (CDs) were selected as the host molecules to encapsulate dye molecules and bound onto metal oxide semiconductor surfaces for aggregation study. The reason to use CDs is that their carbohydrate framework is colorless and does not contain chromophoric group. Also CDs with different interior cavity sizes are commercially available. Finally, the encapsulation of organic chromophores, such as pyrene, in CDs has been intensely studied in solution.[12] The binding of dye@CD complex remains little explored.

Binding was characterized by FT-IR-ATR spectra by comparing the TiO_2 films before and after binding of CD. The aggregation was investigated by UV-Vis absorption spectra and fluorescence emission spectra of dye@host complexes on ZrO_2 films. ZrO_2 films were used because the morphology is similar to that of TiO_2, but the wider band gap (~ 5 eV) makes it an insulator, and to prevent the excited state quenching.

The chemical structures of pyrene and perylene derivatives used in the study are shown in Figure B-2-1.1. Pyrene was selected as the chromophore to study the

aggregation as it is well known that it is encapsulated in CDs,[12] and because comparisons can be made with previously reported pyrene substituted rigid-rods[1] and tripods[2] with respect to excimer effects. Perylene was studied as it forms excimer,[13] and the perylene@γ-CD complex was also reported[14]. Py-sL-COOH and Pe 4-COOH were employed as references as they have carboxylic acid anchoring groups on the Py and Pe core.

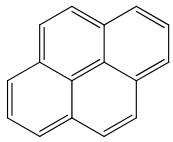

Pyrene (Py)

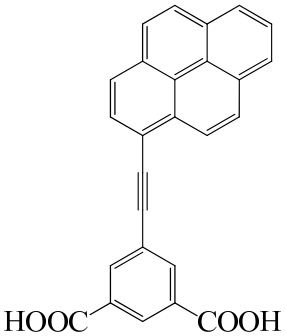

Py-sL-COOH

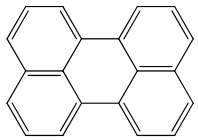

Perylene (Pe)

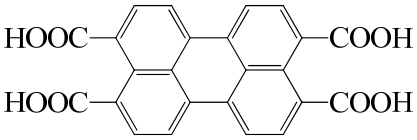

Pe 4-COOH

Figure B-2-1.1. Chemical structures of chromophores used in the study.

Table B-2-1.1 shows the molecular sizes of pyrene,[15] perylene,[15] and parameters of CDs.[3] Based on the relative sizes of CDs and dye molecules, 1:1, 1:2, 2:1, or 2:2 dye@host complexes may formed, and they are shown in Figure B-2-1.2. Due to the larger cavity size of γ–CD (diameter 7.5-8.3 Å), two pyrene molecules can be encapsulated into cavity to form excimer, while β-CD (cavity diameter 6-6.6 Å) can only

contain one pyrene molecule.[3,4,14,16-18] Perylene@β-CD complexes do not form, and α-CD (diameter 4.7-5.3 Å) cannot form guest@host complexes with pyrene and perylene.

Table B-2-1.1. Sizes of the molecules[15] and parameters of α-, β-, and γ-CDs.[3]

molecule	size (Å)		
Pyrene	7.36 x 9.80		
Perylene	7.33-7.37 x 9.82		
	α-CD	β-CD	γ-CD
Glucose Residues	6	7	8
Molecular Weight	973	1135	1297
Cavity Diameter (Å)	4.7-5.3	6-6.6	7.5-8.3
Cavity Height (Å)	7.9	7.9	7.9
Cavity Volume (mL/mol)	174	262	472

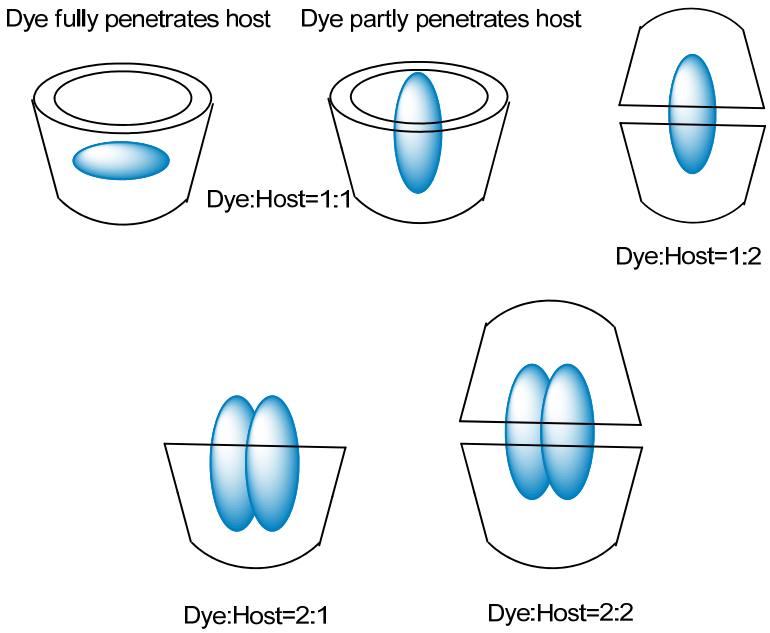

Figure B-2-1.2. Different types of dye@host complexes and possible complexation.

B-2-2. Binding Study

FT-IR-ATR spectroscopy was used as a relatively simple method to determine whether CD adsorbed on TiO_2 films by analyzing the differences of IR spectra before and after binding the CD onto the TiO_2 thin films. In the experiments, β-CD was used as the sample for IR measurements as can it form 1:1 or 1:2 dye@host complex with pyrene. The TiO_2 thin films used in the study were prepared by the previously described sol-gel method[19,20] (Section A-3-3-1), and cast onto a 1 cm^2 cover glass slide. The β-CD/TiO_2 films were prepared by immersing TiO_2 films into β–CD aqueous solutions (5 mM) at room temperature overnight. They were thoroughly rinsed with DIUF water to remove any free β–CD molecules and air dried prior to spectroscopic measurements. Since the FT-IR-ATR signal intensity of the β-CD/TiO_2 films was weak, before every measurement, it was necessary to vigorously purge with nitrogen for at least 60 minutes to reduce the undesired background signals, especially water vapor which appeared in the range of 1700 cm^{-1} and 1400 cm^{-1}. The FT-IR-ATR spectra of β-CD powder, TiO_2 film, β-CD/TiO_2 thin film, and the difference between "β-CD/TiO_2 thin film" and "TiO_2 film" are shown in Figure B-2-2.1. The spectra of β-CD powder and the difference between "β-CD/TiO_2 thin film" and "TiO_2 film" are standardized relative to their highest band and shown in Figure B-2-2.2 as a comparison.

β-CD powder gives a broad band at 3300 cm^{-1} and a band at 2926 cm^{-1} corresponding to the strentching of –OH and $–CH_2$, respectively. The bands at 1080 cm^{-1} and 1024 cm^{-1} were attributed to the formation of H-bonding in the interior of the β-CD molecule structure[21]. TiO_2 film gives a broad band centered at 3300 cm^{-1}. It is a typical

stretching vibration of –OH group at the surface of the nanocrystalline TiO_2 particles. The spectrum of β-CD/TiO_2 film is similar to that of TiO_2. This result was expected since the β-CD molecule bound onto TiO_2 film forms a single layer with weak signal intensity even under FT-IR-ATR measurement condition.

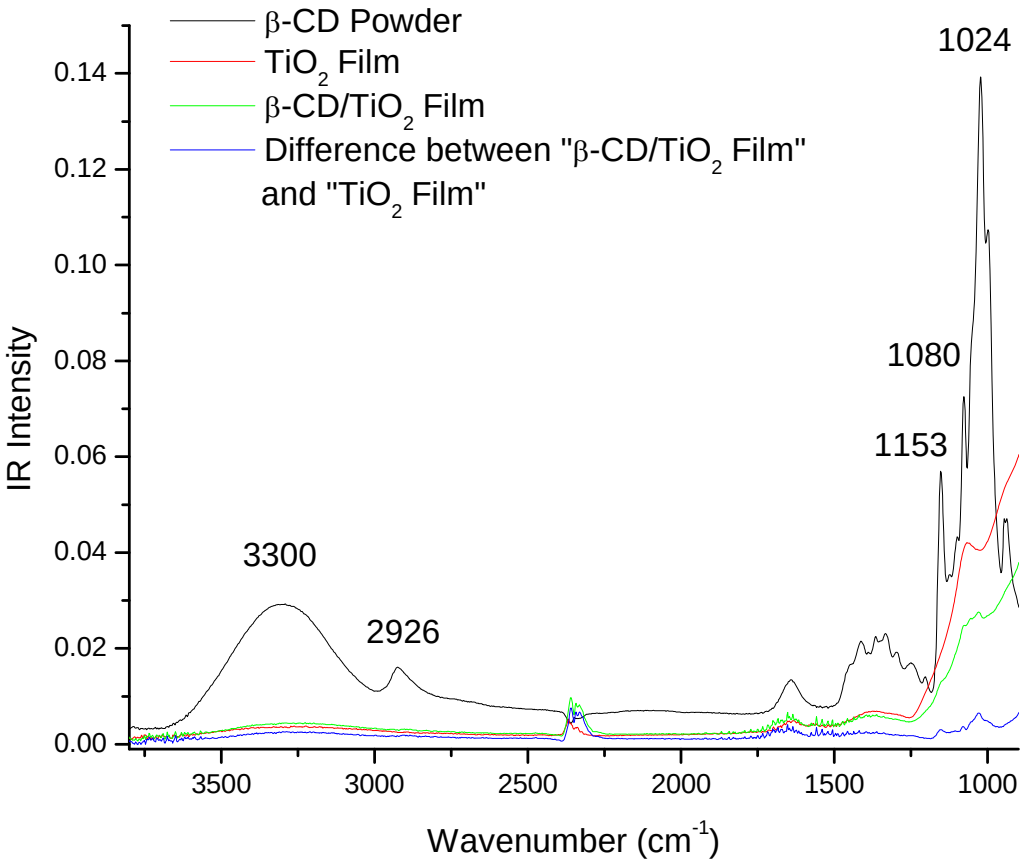

Figure B-2-2.1. FT-IR-ATR spectra of β-CD power, TiO_2 film, β-CD/TiO_2 thin film, and the difference between "β-CD/TiO_2 thin film" and "TiO_2 film".

The difference between "β-CD/TiO_2 thin film" and "TiO_2 film" is standardized relative to their most intense band (1030 cm^{-1} and 1024 cm^{-1}, respectively) and compared with the one of neat β-CD (Figure B-2-2.2). Bands at 1024 cm^{-1}, 1080 cm^{-1}, and 1153 cm^{-}

[1] for the spectrum of neat β-CD powder can be observed in the spectrum of the difference between "β-CD/TiO_2 thin film" and "TiO_2 film". The different spectra indicate β-CD molecules bound to the TiO_2 surface. The band at 2926 cm^{-1} in the spectrum of β–CD powder is not evident in the spectrum of β-CD/TiO_2 (Figure B-2-2.1). This was explained as the stretching vibration of $–CH_2$ for β–CDs absorbed to TiO_2 surface is partially prohibited.[21]

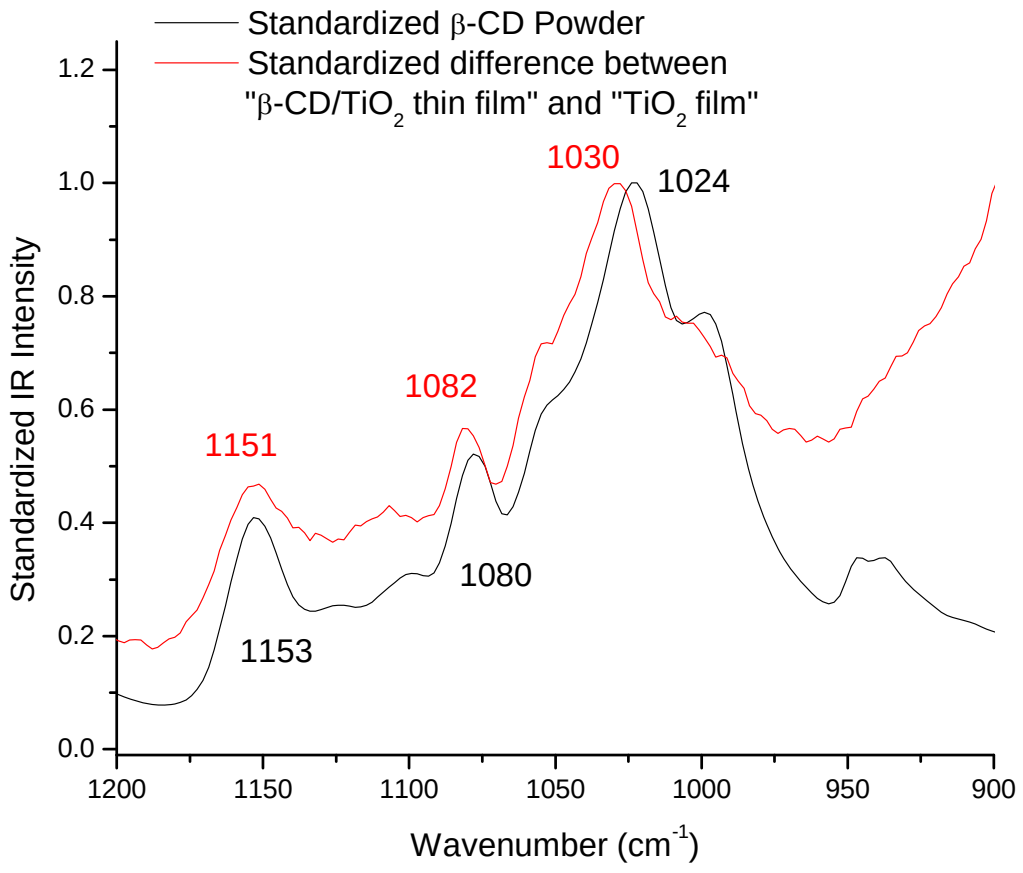

Figure B-2-2.2. Standardized FT-IR-ATR spectra of β-CD powder and the difference between "β-CD/TiO_2 thin film" and "TiO_2 film".

CDs have two types of -OH in each rim, secondary alcohols on the wider rim and primary alcohols on the smaller rim. The binding of all –OH groups to the metal oxide semiconductor surface are presumably. In summary, FT-IR-ATR spectra cannot determine which –OH type is preferred. How the CDs bind to the surface and their orientation has not yet been established.

B-2-3. Aggregation Study

B-2-3-1. Pyrene@CD

CDs' cavities are lipophilic. They readily form guest@host complexes with size-suitable lipophilic organic compounds thus making them water soluble. Pyrene has very low solubility in water (~ 6.7 x 10^{-7} M at 25°C). Upon complexation with β-CD, pyrene has been dissolved in water. First we reproduced complexation studies of pyrene in β- and γ-CDs, as reported in literature.[22] The purpose of the solution study was to find the experimental conditions for encapsulation (Py@CDs) in solutions, and then study the binding of the Py@CDs complexes on MO_n surfaces. The increased water solubility of pyrene chromophore upon adding β-CD was monitored by UV-Vis absorption spectra (Figure B-2-3-1.1) and fluorescence emission spectra (Figure B-2-3-1.2). In both cases, large excess amount of pyrene was added into DIUF water or 10 mM β-CD aqueous solution, respectively. Intensity-enhanced pyrene monomer absorption and emission spectra were observed.

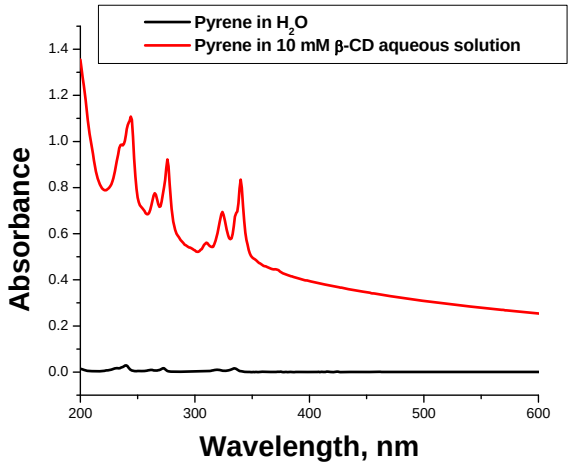

Figure B-2-3-1.1. Absorption spectra of aqueous pyrene solution in the absence and the presence of β-CD.

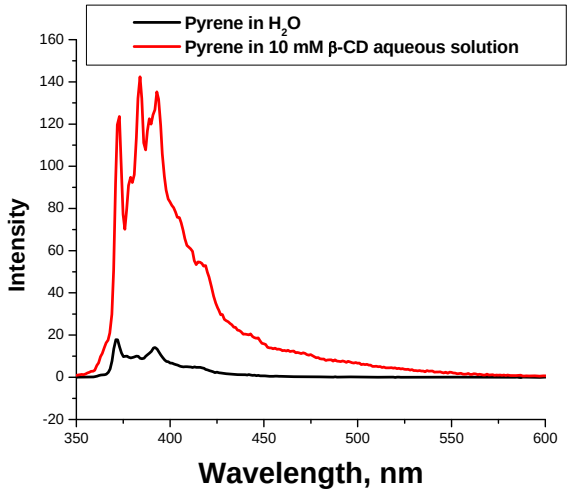

Figure B-2-3-1.2. Emission spectra of aqueous pyrene solution in the absence and the presence of β-CD. λ_{exc} = 335 nm.

By choosing γ-CD as the host molecule instead of β-CD, absorption and emission spectra changed (Figure B-2-3-1.3 and Figure B-2-3-1.4). Pyrene ethanol solution (20 μL, 0.05 M) was added into 5 mL of 10 mM CDs aqueous solution. The spectra show a broader absorption band for Py@γ-CD compared to the one of Py@β-CD (Figure B-2-3-

1.3). In the case of emission spectra, for Py@β-CD mixture, the fluorescence band from 370 nm to 480 nm is attributed to the Py monomer. The broad emission band indicates the presence of pyrene excimer,[23] along with the monomer emission (Figure B-2-3-1.4).

This effect has been reported and it is due to the larger size of the CDs cavity.[16] The large cavity of γ-CD (cavity diameter 7.5-8.3 Å) is capable of including two Py (7.36 x 9.8 Å) molecules, and a 2:1 or 2:2 excimer forms,[3,4,14] and a part of the dimer is placed within the cavity and the substantial part is exposed to an aqueous layer.[17] In summary, β-CD only contain one pyrene molecule to form 1:1 or 1:2 Py@β-CD complexes resulting a monomer band in emission spectra, while γ-CD forms 2:1 or 2:2 complexes leading to excimer formats.

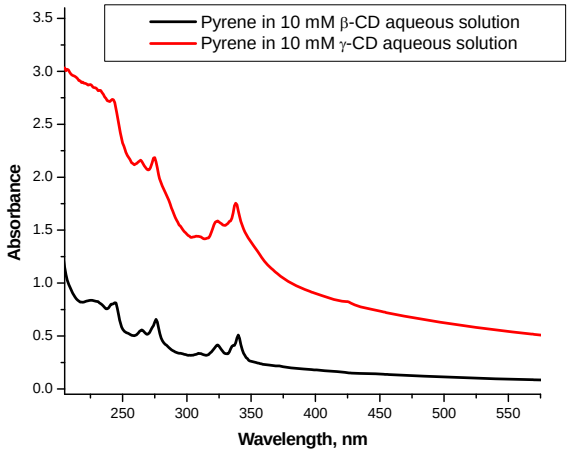

Figure B-2-3-1.3. Absorption spectra of aqueous pyrene solution (10mM) in the presence of β-CD or γ-CD.

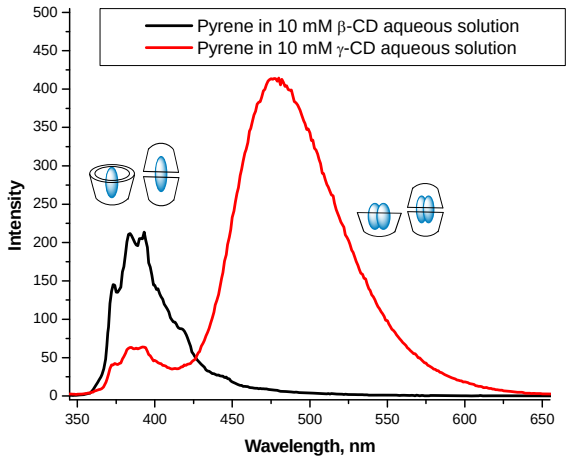

Figure B-2-3-1.4. Emission spectra of aqueous pyrene solution (10 mM) in the presence of β-CD or γ-CD. λ_{exc} = 335 nm.

ZrO_2 films were used as the substrate to study the aggregation effect of Py@CD on the metal oxide semiconductor films. The Py@β-CD solution was filtered to remove any undissolved pyrene. The ZrO_2 thin film was then immersed into the solution overnight and thoroughly rinsed with DIUF water for spectroscopic measurements. However, the absorption and emission spectra showed that no binding occurs. One possible explanation is that the binding of guest molecules within the host CD, is a dynamic equilibrium, and that does not form a stable Py@CD complex upon binding onto the surface.[7]

B-2-3-2. Py-sL-COOH@CD

We then studied encapsulation in CDs and binding of a pyrene derivative with anchoring group, we selected pyrene short rigid-rod (Py-sL-COOH), a compound that has been reported to form excimer on the metal oxide surface.[1] Two different binding procedures were used in this study as a comparison and described as follows:

Method I (binding of complex): Py-sL-COOH was added into CD aqueous solution to form guest@host complexes. ZrO_2 films were immersed into this solution overnight and air-dried. Prior to absorption or emission measurements, the films were thoroughly rinsed with ethanol.

Method II (binding of rod followed by CD): ZrO_2 films were immersed into the Py-sL-COOH ethanol solution to give Py-sL-COOH/ZrO_2 films. After rinsing with ethanol, the resulting films were immersed into the CD aqueous solution overnight and air-dried. Prior to absorption or emission measurements, the films were rinsed with water.

The UV-Vis absorption spectra and fluorescence emission spectra with two binding procedures are shown in Figure B-2-3-2.1 and Figure B-2-3-2.2. The emission spectra were normalized either on the monomer band maxima or excimer band maxima, respectively. In all cases, Py-sL-COOH bound to the ZrO_2 films successfully. The absorption spectra show similar band at ~ 365 nm.

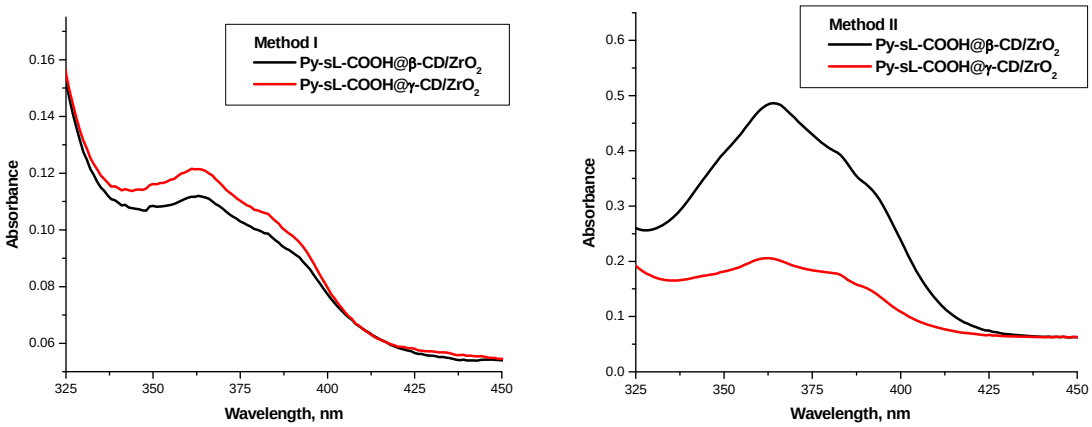

Figure B-2-3-2.1. Absorption spectra of Py-sL-COOH@CDs on ZrO_2 thin films with different binding procedures.

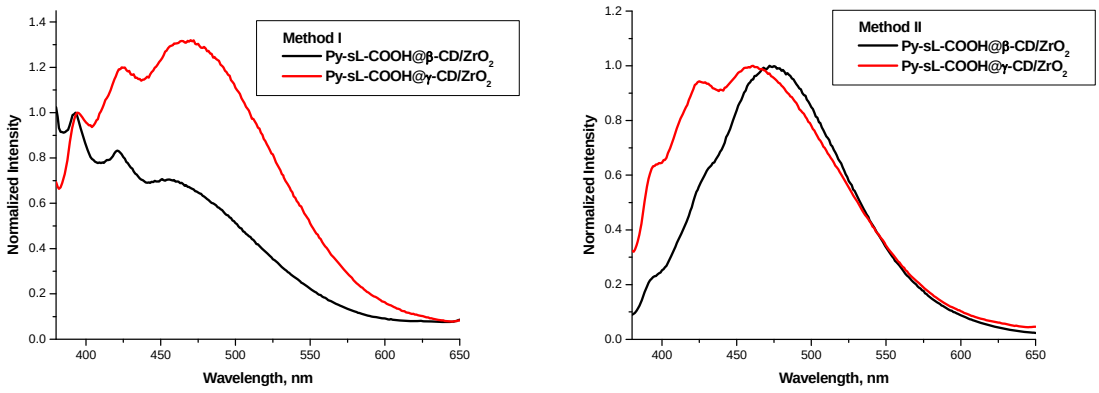

Figure B-2-3-2.2. Emission spectra of Py-sL-COOH@CDs on ZrO_2 thin films with different binding procedures. λ_{exc} = 365 nm.

However, the emission spectra show that different binding procedures result in different aggregation on ZrO_2 films.

In the case of Method I, (the emission spectra are normalized at the monomer band maxima ~ 400 nm), the excimer band of Py-sL-COOH@β-CD/ZrO_2 appears at ~ 475 nm as a shoulder in the spectra. The intensity of Py-sL-COOH monomer band at ~ 400 nm and ~ 430 nm was significant compared to the one of Py-sL-COOH excimer band. As a comparison, the spectra of Py-sL-COOH@γ-CD/ZrO_2 showed strong broad Py-sL-COOH excimer band at ~ 475 nm along with Py-sL-COOH monomer band at ~ 400 nm and ~ 430 nm. *Thus, with method I, Py-sL-COOH@CD complex decreases the excimer formation upon binding to ZrO_2 film.*

In the case of Method II, (spectra were normalized at the excimer band maxima), the excimer band was observed for both Py-sL-COOH@β-CD/ZrO_2 and Py-sL-COOH@γ-CD/ZrO_2. Thus, with method II, Py-sL-COOH was not encapsulated into the cavity of CDs.

In summary, this set of experiments suggests that encapsulation prior to binding is necessary.

B-2-3-3. Perylene derivative@CD

Perylene, which has the advantage of absorption spectrum considerably red-shifted with respect to pyrene, was also used for the aggregation behavior study. Perylene forms excimer with in emission band centered at ~ 650 nm (Figure B-2-3-3.1[13]). Upon binding to semiconductor surfaces, perylene tend to form aggregates through face-to-face π-π interactions. Willig and coworkers developed t-butyl-modified perylenes to avoid aggregation on semiconductor surface in sensitization studies.[24] Perylene has been reported to form guest@host complexes with γ-CD successfully.[14] Thus, we selected γ-CD as the host molecule to study the aggregation of perylene on the metal oxide surface.

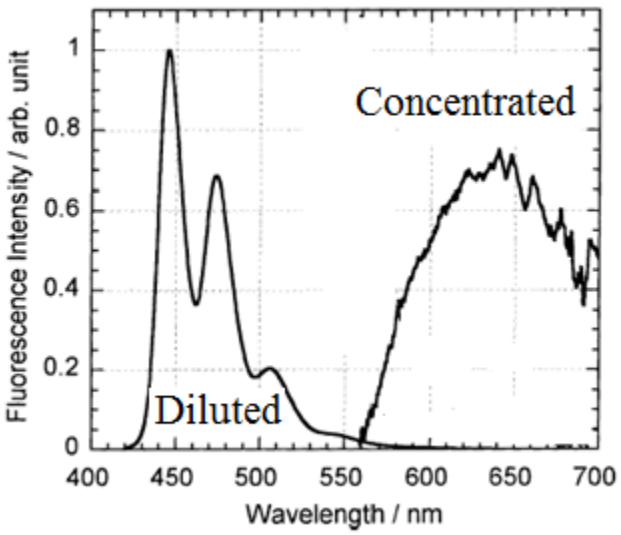

Figure B-2-3-3.1. Emission spectra of perylene monomer and excimer in toluene.[13]

As in the case of Py@CD complexes, however, Pe@CD complexes did not bind onto ZrO_2 films. Pe 4-COOH, with four –COOH anchoring groups on the Pe core, was then synthesized according to a published procedure,[25] by basic hydrolysis of 3,4,9,10-perylene tetracarboxylic dianhydride followed by acidification. The emission band of Pe 4-COOH@γ-CD/ZrO_2 film showed higher intensity ratio of monomer band (~ 490 nm) to excimer band (centered at ~ 575 nm) compared to the one of Pe 4-COOH/ZrO_2 (Figure B-2-3-3.2). Thus γ-CD physical separates Pe 4-COOH on ZrO_2 films. The encapsulation of the Pe 4-COOH in γ-CD is not certain, however, Pe 4-COOH with four carboxylic acid groups attached onto the perylene core is slightly water soluble, and the COOH groups may prevent. In summary, the γ-CD may act as the host molecule to encapsulate the Pe 4-COOH, or as a coadsorbate, to separate Pe 4-COOH on the ZrO_2 surface.

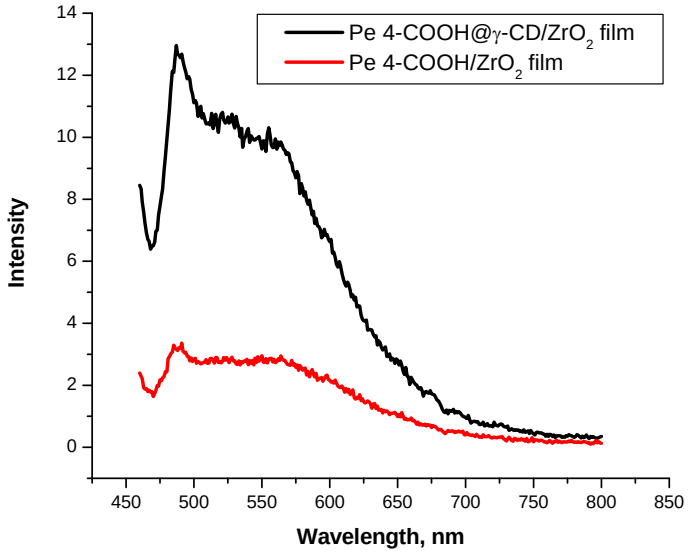

Figure B-2-3-3.2. Fluorescence emission spectra of Pe 4-COOH in the absence and the presence of γ-CD on ZrO_2. λ_{exc} = 440 nm.

B-2-4. Conclusions

In summary, cyclodextrins form water-soluble guest@host complexes with pyrene. β-CD inhibits the excimer formation of pyrene in aqueous solution by formation of a 1:1 complex, while γ-CD leads to pyrene excimer formation in aqueous solution by formation of 2:1 or 2:2 complexation. Cyclodextrins bind to the metal oxide surface by the –OH groups. Cyclodextrins separate a pyrene rigid-rod as a Py-sL-COOH@β-CD complex and perylene derivative as Pe 4-COOH@γ-CD complex on ZrO_2 films, although the latter result needs to be confirmed, reduced excimer band and enhanced monomer band were observed in fluorescence emission spectra on ZrO_2. The encapsulation of the chromophores with cyclodextrins was not sufficiently strong to bind Py or Pe chromophores without any anchor group to the ZrO_2 through cyclodextrins. Thus, anchoring groups were attached to the chromophore molecules in both cases. The sequence of the encapsulation and binding steps was important to ensure physical separation of the dye@CD on the metal oxide surface. Further study of the encapsulation conditions and characterization of the sensitized films is of interest and is in process.

B-2-5. References

1. Taratula, O.; Rochford, J.; Piotrowiak, P.; Galoppini, E.; Carlisle, R. A.; Meyer, G. J. Pyrene-Terminated Phenylenethynylene Rigid Linkers Anchored to Metal Oxide Nanoparticles. . *J. Phys. Chem. B.* **2006**, *110*, 15734.

2. Thyagarajan, S.; Galoppini, E.; Persson, P.; Giaimuccio, J. M.; Meyer, G. J. Large Footprint Pyrene Chromophores Anchored to Planar and Colloidal Metal Oxide Thin Films. *Langmuir* **2009**, *25*, 9219.

3. Hapiot, F.; Tilloy, S.; Monflier, E. Cyclodextrins as Supramolecular Hosts for Organometallic Complexes. *Chem. Rev.* **2006**, *106*, 767.

4. Rekharsky, M. V.; Inoue, Y. Complexation Thermodynamics of Cyclodextrins. *Chem. Rev.* **1998**, *98*, 1875.

5. Khan, A. R.; Forgo, P.; Stine, K. J.; D'Souza, V. T. Methods for Selective Modifications of Cyclodextrins. *Chem. Rev.* **1998**, *98*, 1977.

6. Szeijtli, J.; Osa, T.; Atwood, J. L.; Davis, J. E. D.; Macnicol, D. D.; Vögtle, F. *Comprechensive Supramolecular Chemistry*; Pegamon/Elsevier: Oxford, 1996; Vol. 3.

7. Martin Del Valle, E. M. Cyclodextrins and Their Uses: a Review. *Process Biochemistry* **2004**, *39*, 1033.

8. Danil de Namor, A. F.; Cleverley, R. M.; Zapata-Ormachea, M. L. Thermodynamics of Calixarene Chemistry. *Chem. Rev.* **1998**, *98*, 2495.

9. Ananchenko, G. S.; Udachin, K. A.; Pojarova, M.; Dubes, A.; Ripmeester, J. A.; Jebors, S.; Coleman, A. W. Van der Waals Nanocapsular Complexes of Amphiphilic Calixarenes. *Cryst. Growth Des.* **2006**, *6*, 2141.

10. Hippius, C.; Schlosser, F.; Vysotsky, M. O.; Bohmer, V.; Wurthner, F. Energy Transfer in Calixarene-Based Cofacial-Positioned Perylene Bisimide Arrays. *J. Am. Chem. Soc.* **2006**, *128*, 3870.

11. Asfari, Z.; Böhmer, V.; Harrowfield, J.; Vicens, J. *Calixarenes*; Academic Publisher: Boston, 2001.

12. Patonay, G.; Shapira, A.; Diamond, P.; Warner, I. M. A Systematic Study of Pyrene Inclusion Complexes with α-, β-, γ-Cyclodextrins. *J. Phys. Chem.* **1986**, *90*, 1986.

13. Katoh, R.; Sinha, S.; Murata, S.; Tachiya, M. Origin of the Stabilization Energy of Perylene Excimer as Studied by Fluorescence and Near-IR Transient Absorption Spectroscopy. *J. Photochem. Photobio. A: Chem.* **2001**, *145*, 23.

14. Pistolis, G.; Malliaris, A. Evidence for Highly Selective Supramolecular Formation between Perylene/γ-CD and Pyrene/γ-CD Complexes in Water. *J. Phys. Chem. B.* **2004**, *108*, 2846.

15. Liu, X.; Iu, K.-K.; Thomas, J. K.; He, H.; Klinowski, J. Spectroscopic Studies of Protonated Aromatic Species and Radical Cations in H+-Zeolites. *J. Am. Chem. Soc.* **1994**, *116*, 11811.

16. Kano, K.; Takenoshita, I.; Ogawa, T. γ-Cyclodextrin-enhanced Excimer Fluorescence of Pyrene and Effect of n-Butyl Alcohol. *Chem. Lett.* **1982**, 321.

17. Yorozu, T.; Hoshino, M.; Imamura, M. Fluorescence Studies of Pyrene Inclusion Complexes with .Alpha.-, .Beta.-, and .Gamma.-Cyclodextrins in Aqueous Solutions. Evidence for Formation of Pyrene Dimer in .Gamma.-Cyclodextrin Cavity. *J. Phys. Chem.* **1982**, *26*, 4426.

18. Herkstroeter, W. G.; Martic, P. A.; Evans, T. R.; Farid, S. Cyclodextrin Inclusion Complexes of 1-pyrenebutyrate. The Role of Coinclusion of Amphiphiles. *J. Am. Chem. Soc.* **1986**, *108*, 3275.

19. Heimer, T. A.; D'Arcangelis, S. T.; Farzad, F.; Stipkala, J. M.; Meyer, G. J. An Acetylacetonate-Based Semiconductor-Sensitizer Linkage. *Inorg. Chem.* **1996**, 35.

20. Taratula, O.; Wang, D.; Chu, D.; Galoppini, E.; Zhang, Z.; Chen, H.; Saraf, G.; Lu, Y. Binding Studies of Molecular Linkers to ZnO and MgZnO Nanotip Films. *J. Phys. Chem. B.* **2006**, *110*, 6506.

21. Si, S. H.; Fung, Y. S.; Zhu, D. R. Improvement of Piezoelectric Crystal Sensor for the Detection of Organic Vapors using Nanocrystalline TiO_2 Films. *Sensors and Actuators B* **2005**, *108*, 165.

22. *Hamai, S.* Pyrene Excimer Formation in γ-Cycloddextrin Solutions: Association of 1:1 Pyrene-γ-Cycloextrin Inclusion Compounds. *J. Phys. Chem.* **1989**, *93*, 6527.

23. Birks, J. B. Excimers. *Rep. Prog. Phys.* **1975**, *38*, 903.

24. Burfeindt, B.; Hannappel, T.; Storck, W.; Willig, F. Measurement of Temperature-Independent Femtosecond Interfacial Electron Transfer from an Anchored Molecular Electron Donor to a Semiconductor as Acceptor. *J. Phys. Chem.* **1996**, *100*, 16463.

25. Mo, X.; Shi, M.-M.; Huang, J.-C.; Wang, M.; Chen, H.-Z. Synthesis, Aggregation and Photoconductive Properties of Alkoxycarbonyl Substituted Perylenes. *Dyes and Pigments* **2008**, *76*, 236.

APPENDIX I LIST OF ABBREVIATIONS

DSSC:	dye-sensitized solar cell
ITO:	indium tin oxide
MLCT:	metal to ligand charge transfer
HOMO:	highest occupied molecular orbital
LUMO:	lowest unoccupied molecular orbital
MO_n:	metal oxide nanoparticle
CB:	conduction band
VB:	valence band
IPCE:	incident-photon-to-electron conversion efficiency
IR:	infra-red
FT-IR-ATR:	fourier-transform infrared attenuated total reflectance
NMR:	nuclear magnetic resonance
UV-Vis:	ultraviolet-visible
GC-MS:	gas chromatography-mass spectrometry
STM:	scanning tunneling microscopy

LRMS:	low resolution mass spectrometry
ESI:	electrospray ionization
TLC:	thin layer chromatography
DIUF:	deionized ultra filtered
PEG:	poly(ethyleneglycol)
MeCN/ACN:	acetonitrile
THF:	tetrahydrofuran
3SSC:	3 Short Star Complex
SSC:	Short Star Complex
LSC:	Long Star Complex
SLSC:	Soluble Long Star Complex
TBAF:	tetrabutylammonium fluoride
TMS:	trimethylsilyl
DCA:	deoxycholic acid
HDMA:	hexadecylmalonic acid
CD:	cyclodextrin
dcb:	4,4’-dicarboxylic acid bipyridine

bpy: 2,2’-bipyridine

OPE: oligophenylenethynylene

Ipa: isophthalic acid

Py: pyrene

Pe: perylene

N3:

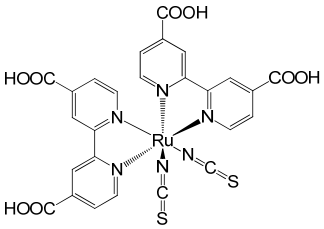

JK-2:

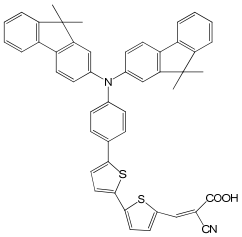

Py-sL-COOH:

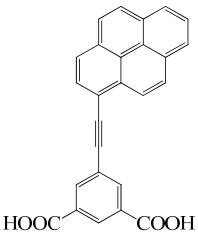

Pe 4-COOH:

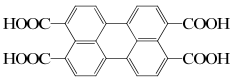

APPENDIX II ^{1}H AND ^{13}C NMR SPECTRA

4-nitro-2-(pyridin-2-yl)pyridine 1-oxide **2**

^{1}H NMR ($CDCl_3$):

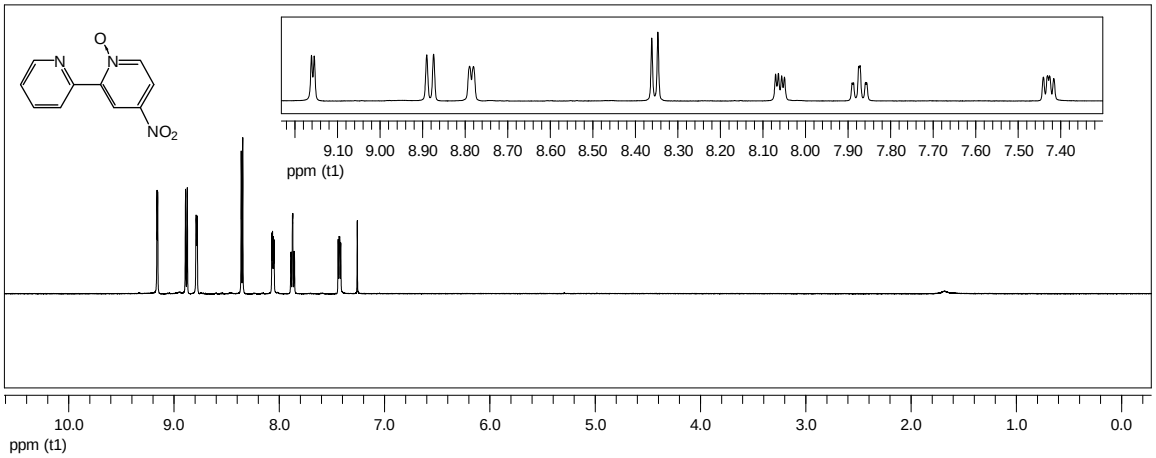

2,2'-bipyridine-4-amine **3**

^{1}H NMR ($CDCl_3$):

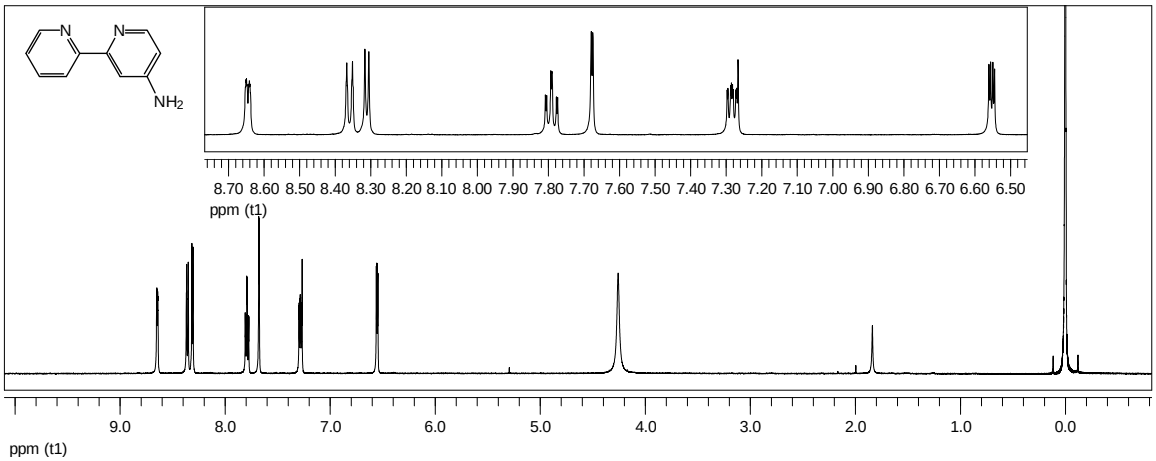

4-iodo-2,2'-bipyridine **4**

^{1}H NMR ($CDCl_3$):

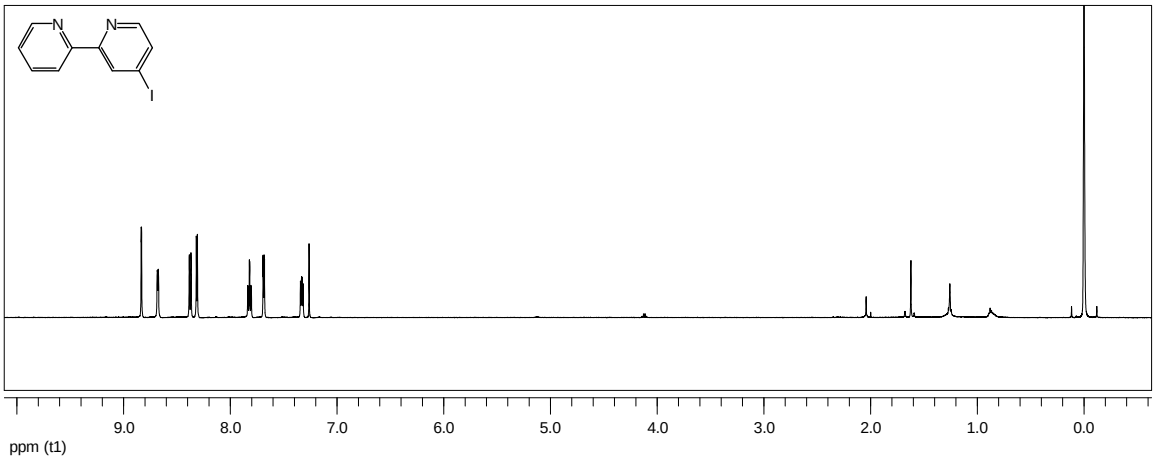

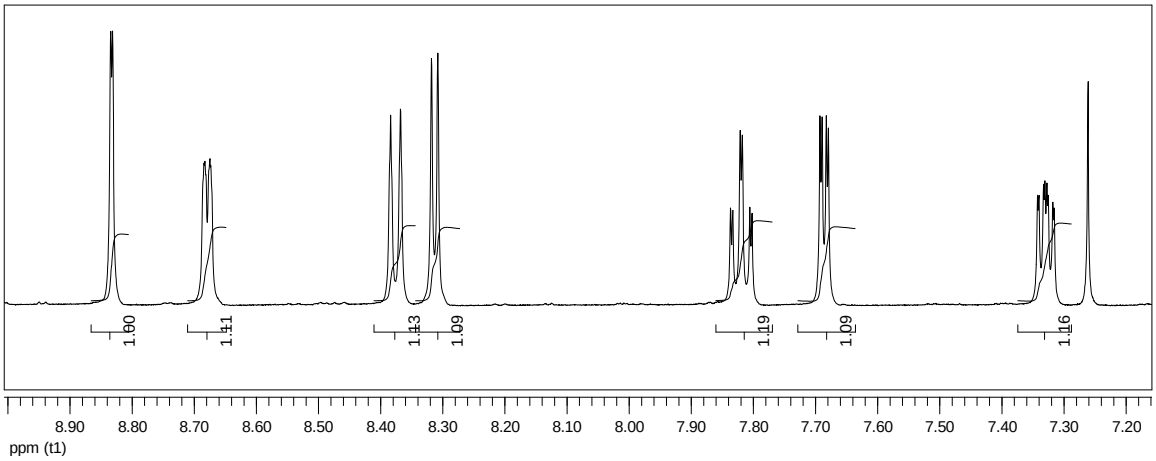

4,4'-dinitro-2,2'-bipyridine 1,1'-dioxide **6**

^{1}H NMR (DMSO)-d_6:

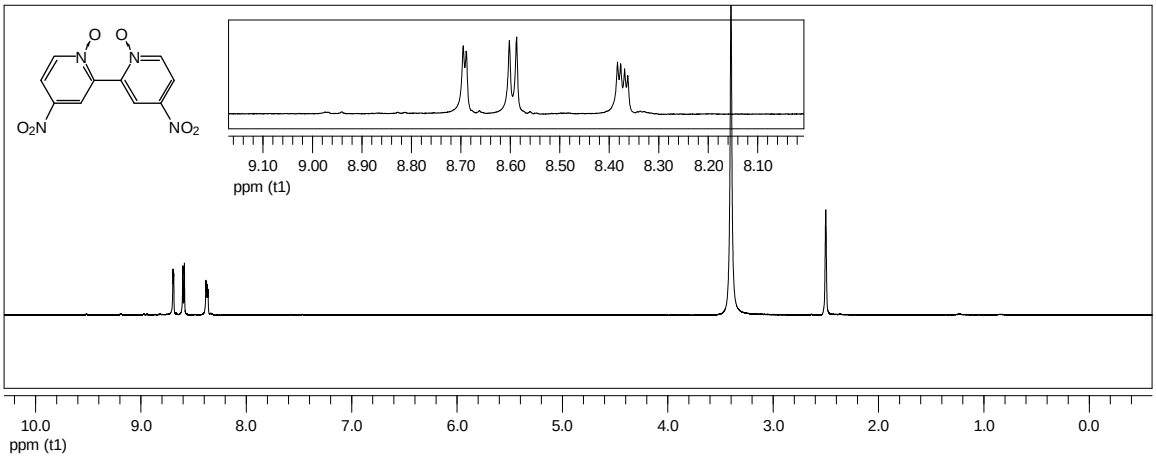

^{13}C NMR (DMSO)-d_6:

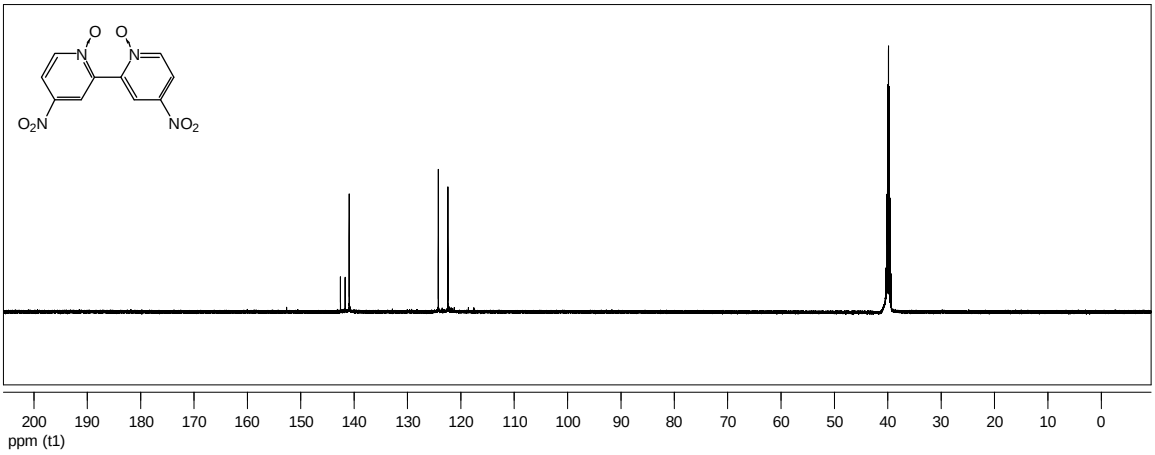

2,2'-bipyridine-4,4'-diamine **7**

^{1}H NMR (DMSO)-d_6:

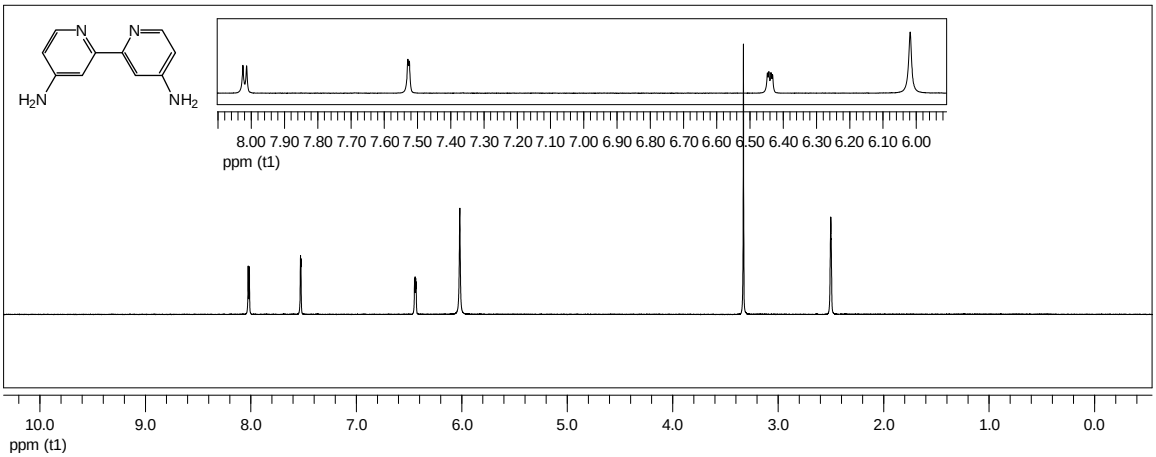

^{13}C NMR (DMSO)-d_6:

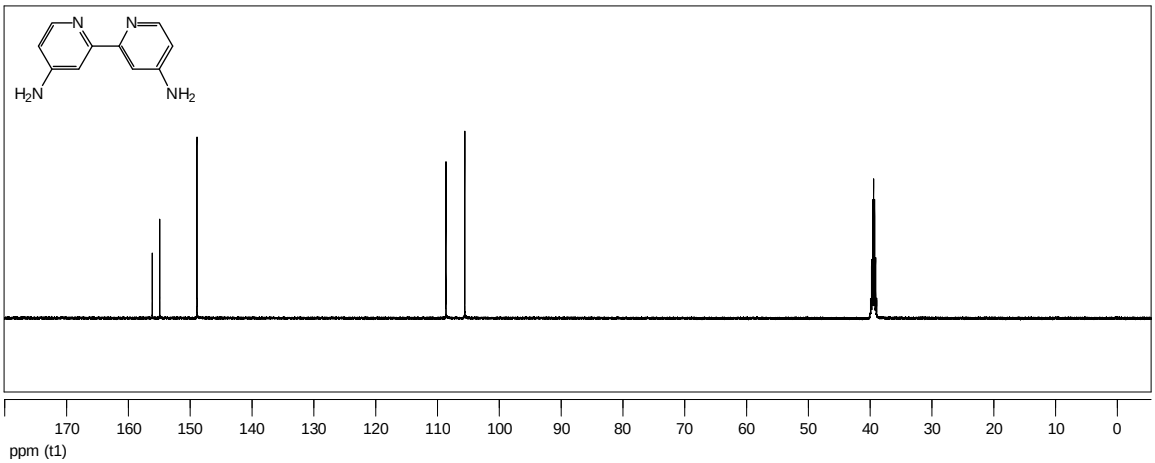

4,4'-diiodo-2,2'-bipyridine **8**

^{1}H NMR (THF)-d_8:

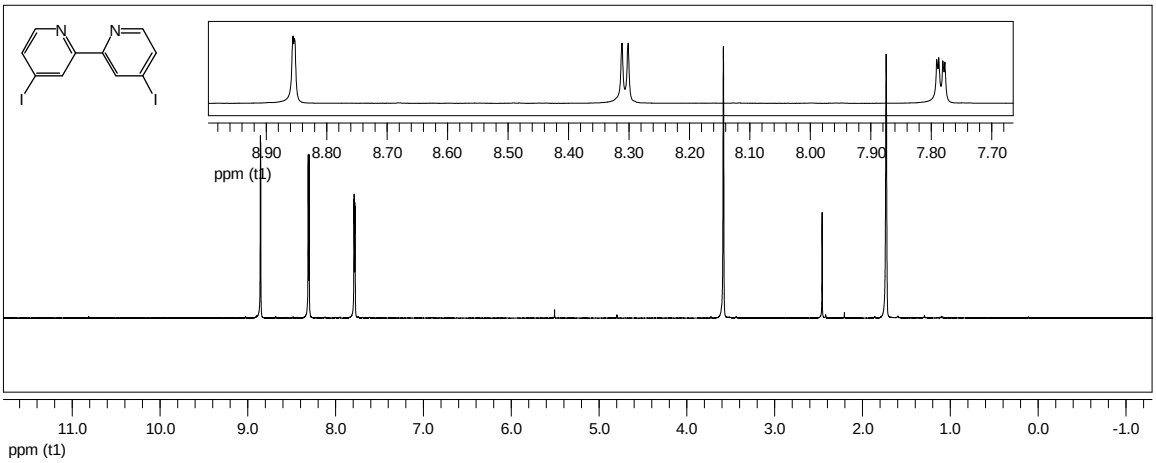

^{13}C NMR (THF)-d_8:

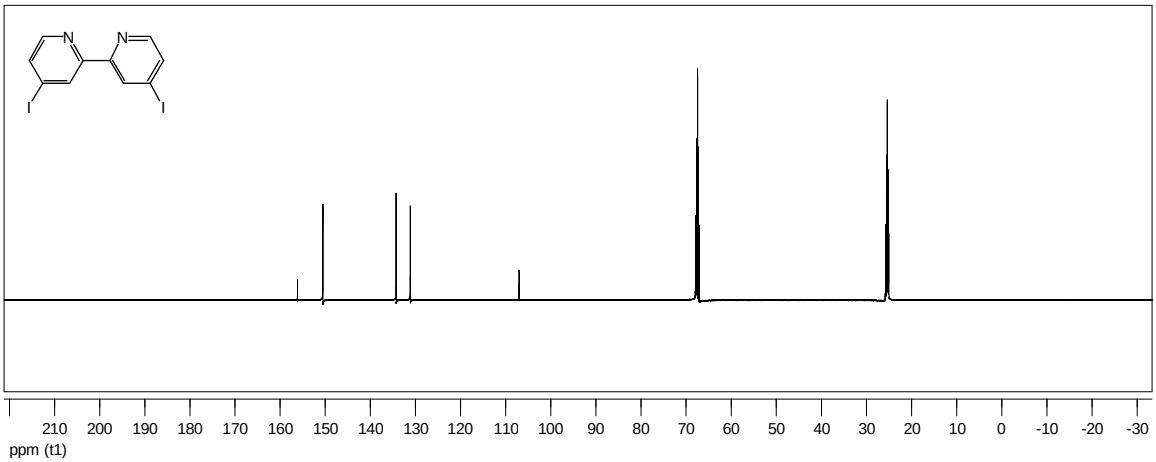

Dimethyl 5-((trimethylsilyl)ethynyl)isophthalate **10**

^{1}H NMR ($CDCl_3$):

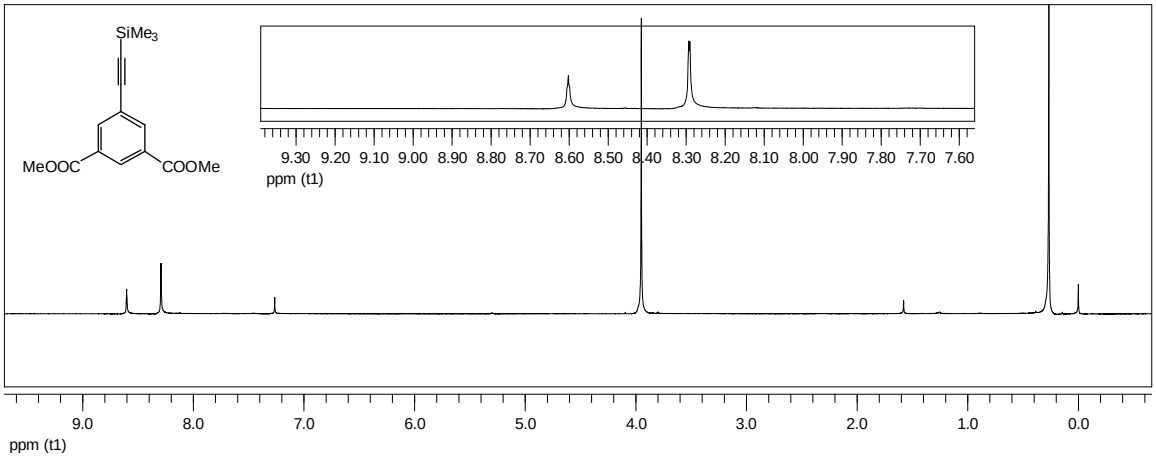

Dimethyl 5-ethynylisophthalate **11**

^{1}H NMR ($CDCl_3$):

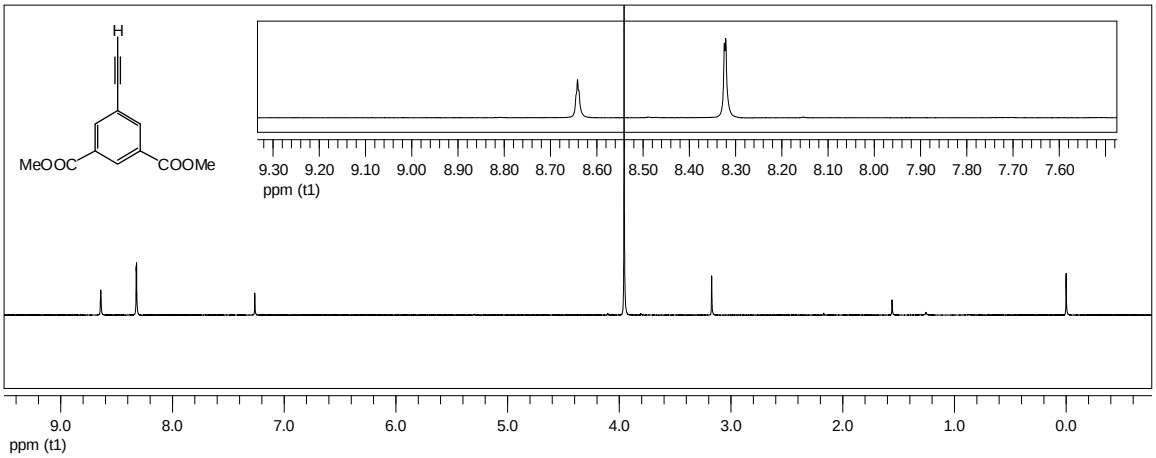

Dimethyl 5-(2,2'-bipyridin-4-ylethynyl) isophthalate **12**

^{1}H NMR ($CDCl_3$):

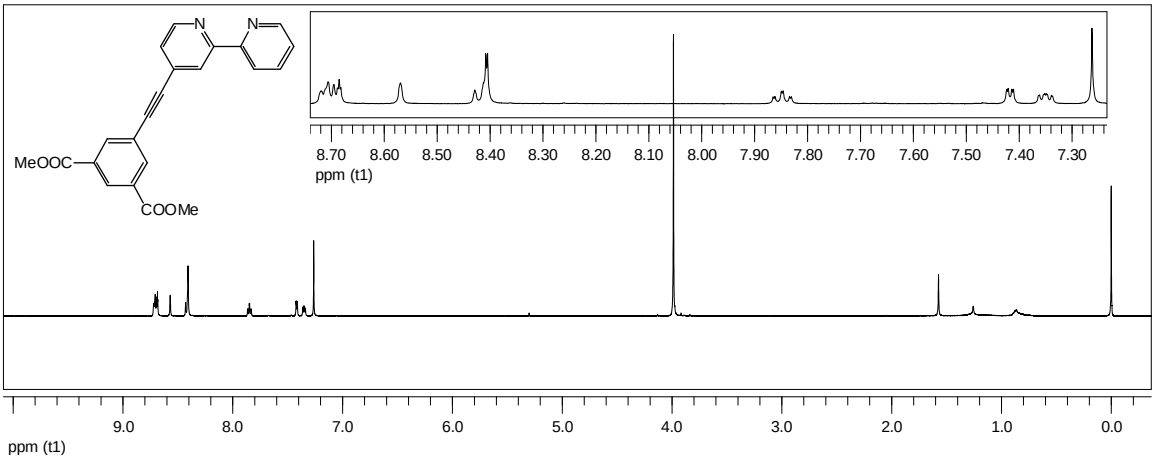

Tetramethyl 5,5'-(2,2'-bipyridine-4,4'-diylbis(ethyne-2,1-diyl))diisophthalate **13**

^{1}H NMR ($CDCl_3$):

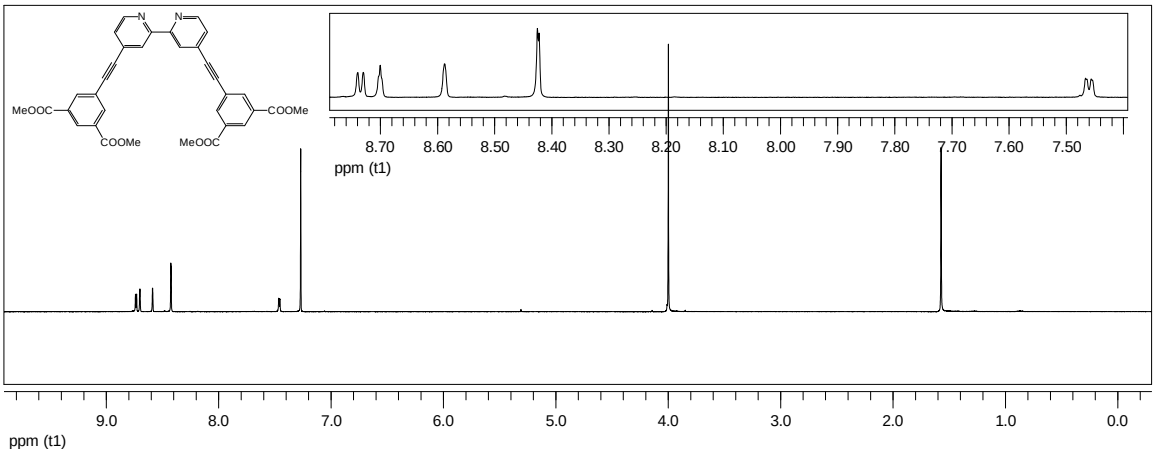

Dimethyl 5-((4-((trimethylsilyl)ethynyl)phenyl)ethynyl)isophthalate **16**

^{1}H NMR ($CDCl_3$):

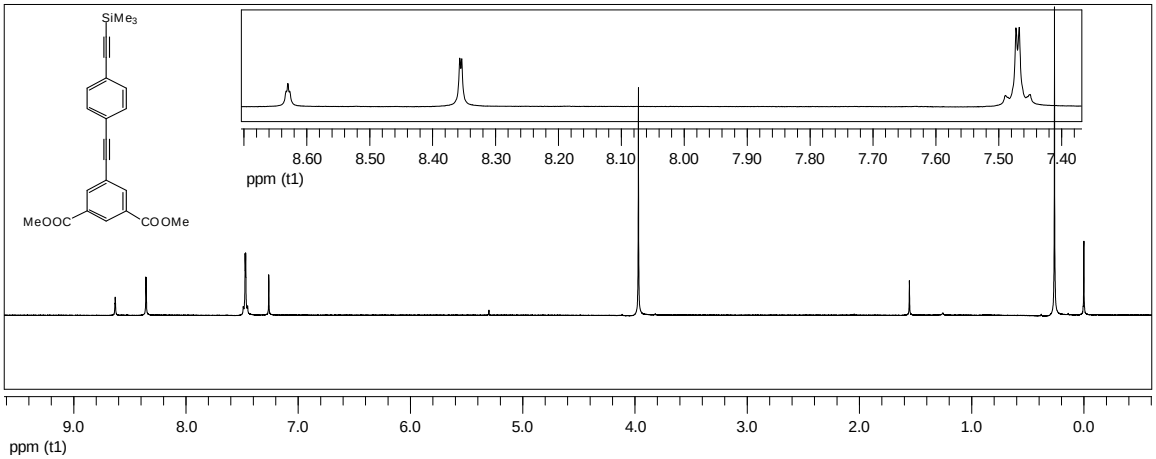

Dimethyl 5-((4-ethynylphenyl)ethynyl)isophthalate **17**

^{1}H NMR ($CDCl_3$):

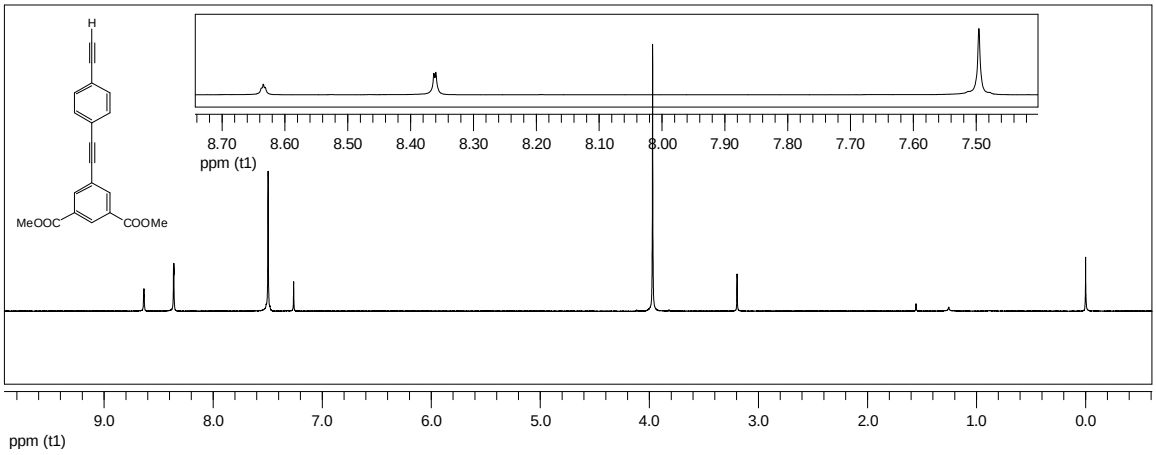

Tetramethyl 5,5'-(4,4'-(2,2'-bipyridine-4,4'-diylbis(ethyne-2,1-diyl))bis(4,1-phenylene)) bis (ethyne-2,1-diyl) diisophthalate **18**

^{1}H NMR ($CDCl_3$):

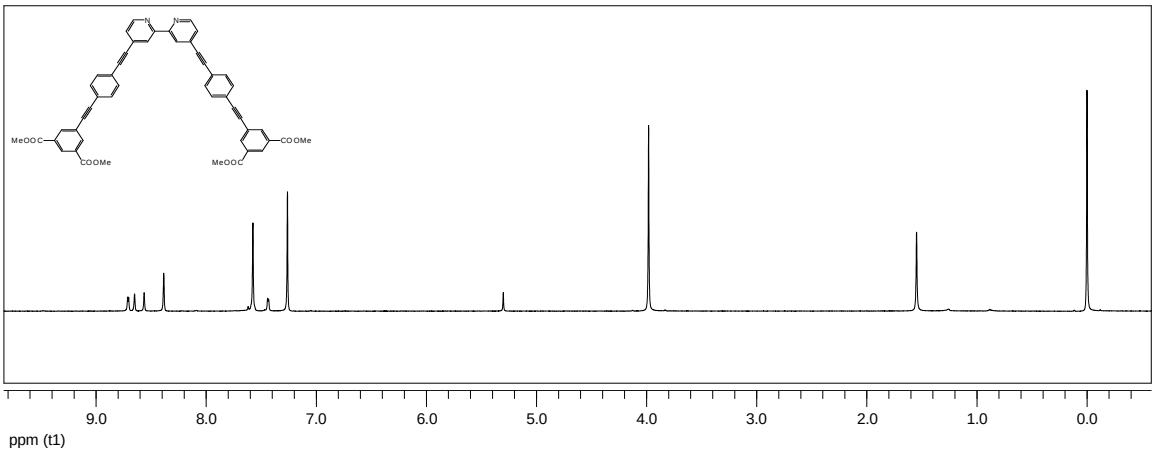

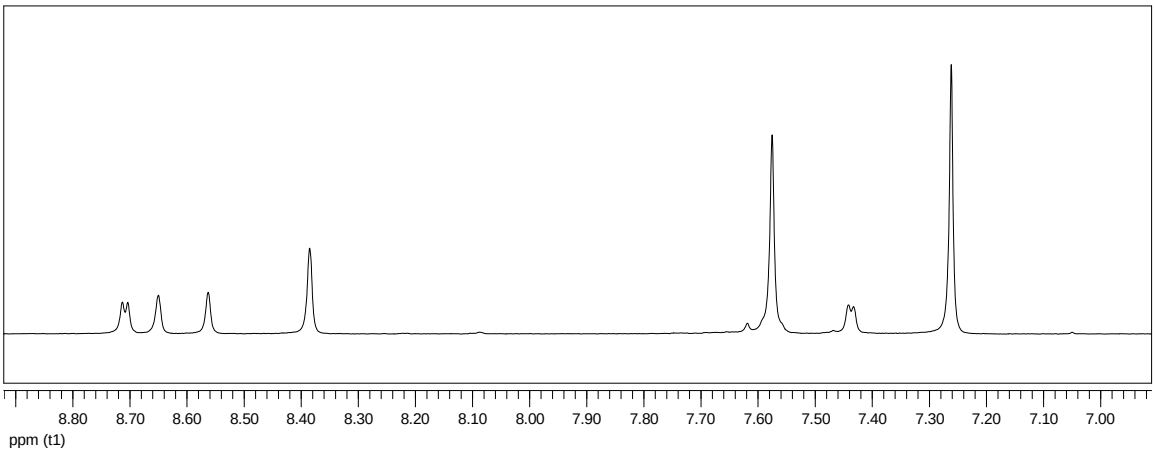

1,4-dibutoxy-2,5-diiodobenzene **20**

^{1}H NMR ($CDCl_3$):

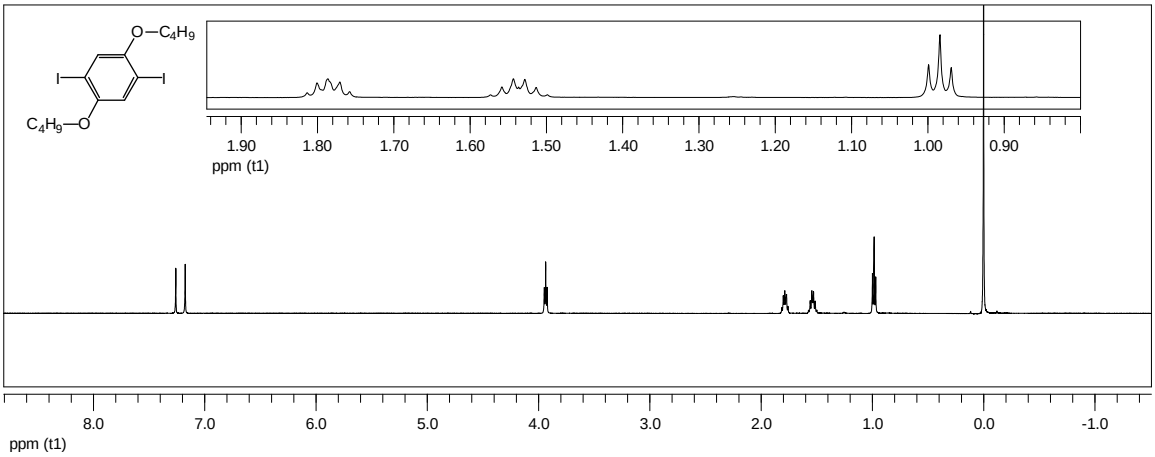

^{13}C NMR ($CDCl_3$):

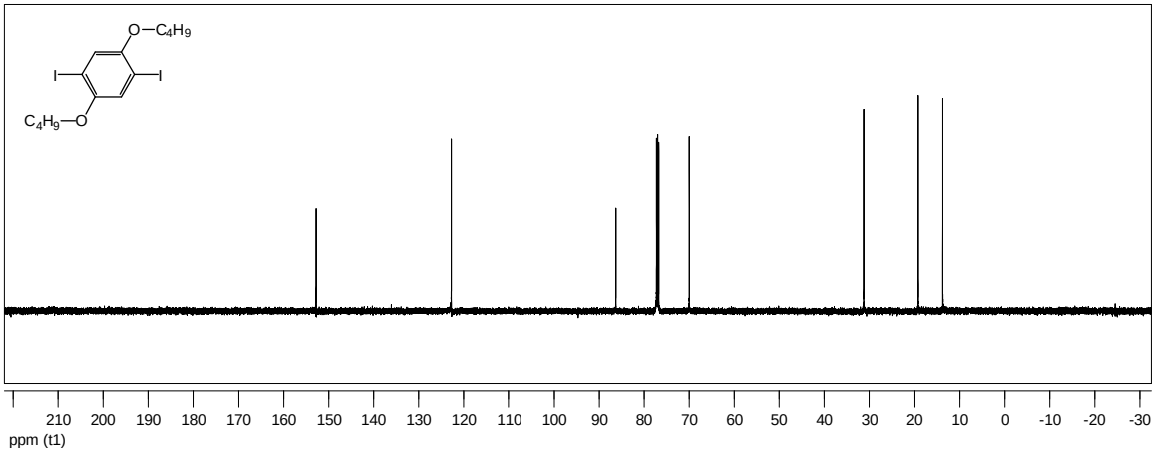

((2,5-dibutoxy-4-iodophenyl)ethynyl)trimethyl silane **21**

^{1}H NMR ($CDCl_3$):

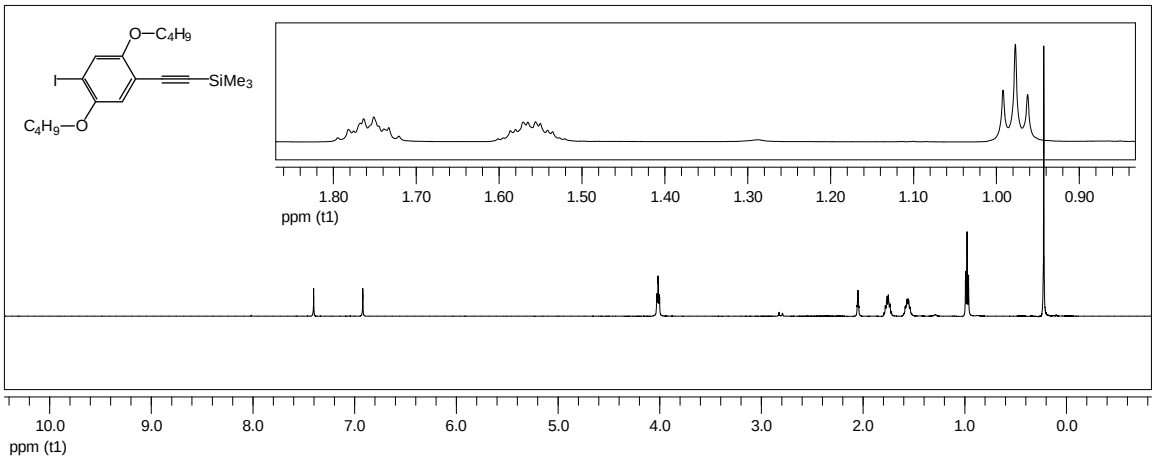

^{13}C NMR ($CDCl_3$):

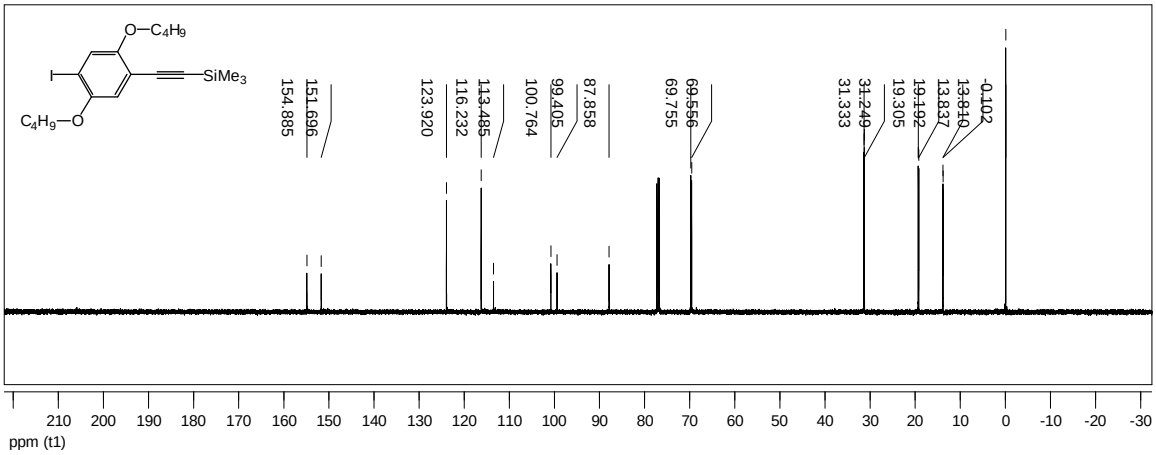

Dimethyl 5-((2,5-dibutoxy-4-((trimethylsilyl)ethynyl) phenyl)ethynyl)isophthalate **22**

^{1}H NMR ($CDCl_3$):

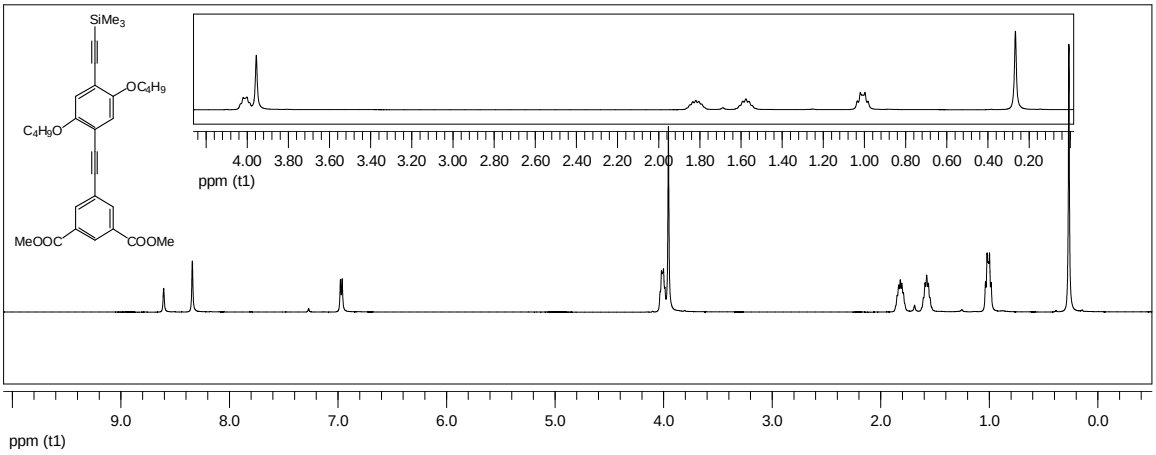

^{13}C NMR ($CDCl_3$):

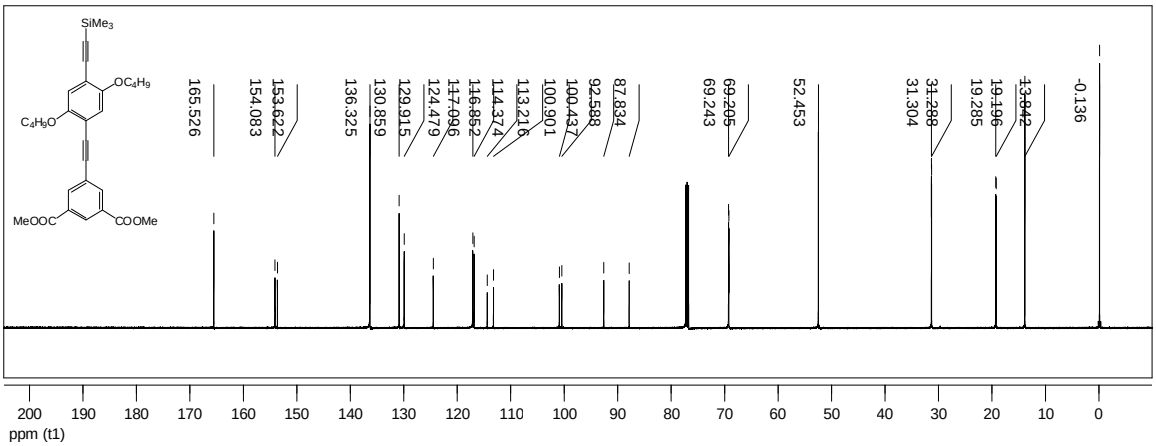

Dimethyl 5-((2,5-dibutoxy-4-ethynylphenyl)ethynyl) isophthalate **23**

^{1}H NMR ($CDCl_3$):

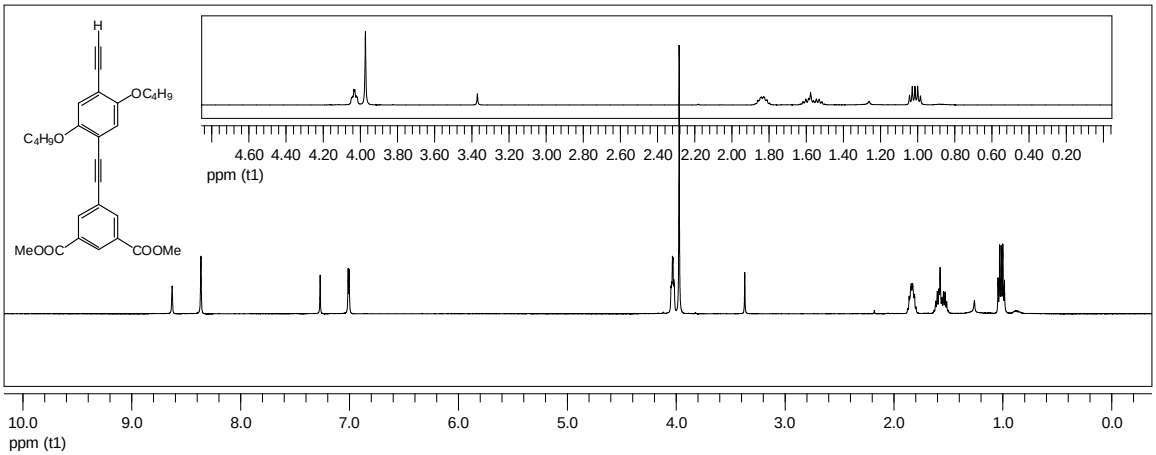

^{13}C NMR ($CDCl_3$):

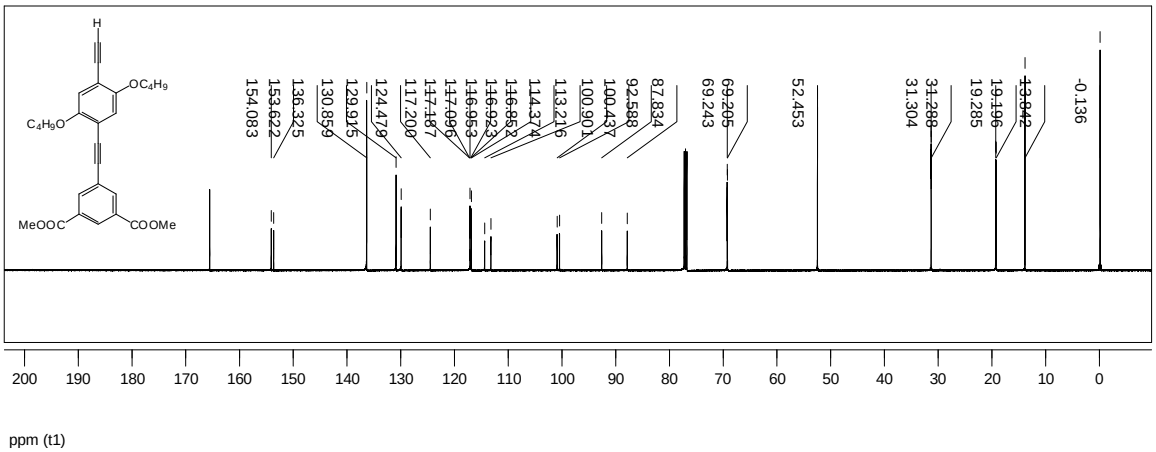

Tetramethyl 5,5'-((([2,2'-bipyridine]-4,4'-diylbis(ethyne-2,1-diyl))bis(2,5-dibutoxy-4,1-phenylene))bis (ethyne-2,1-diyl))diisophthalate **24**

^{1}H NMR ($CDCl_3$):

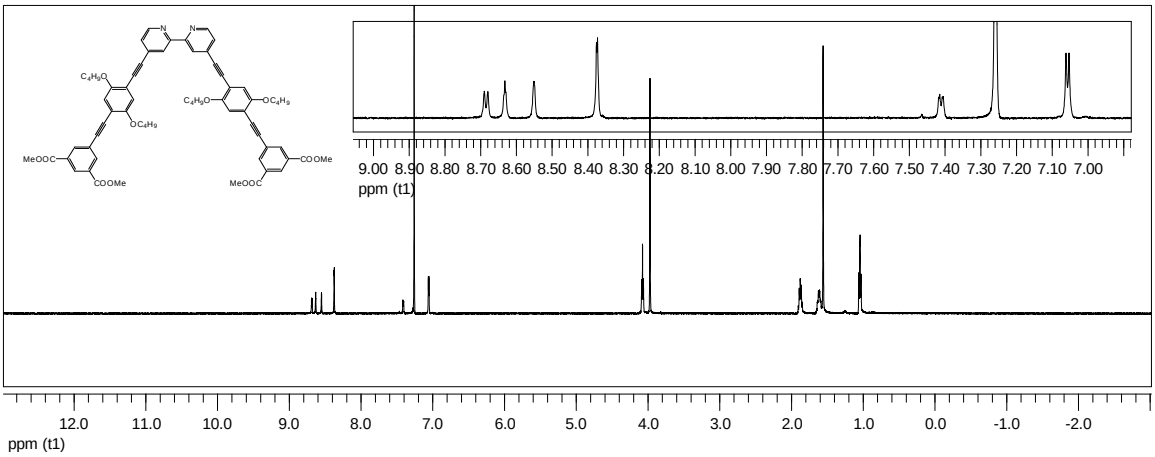

^{13}C NMR ($CDCl_3$):

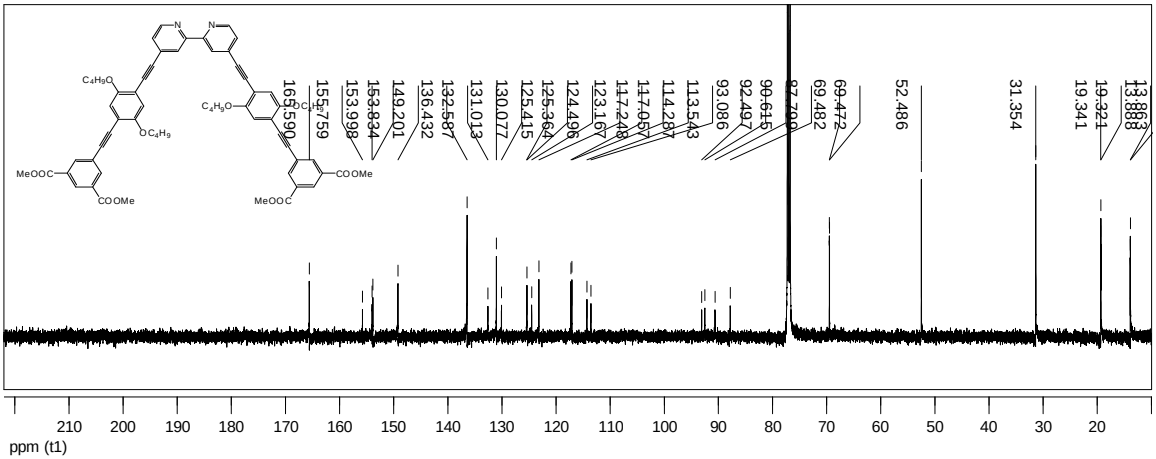

Homoleptic ruthenium complex **3SSC.**

^{1}H NMR (acetone)-d_6:

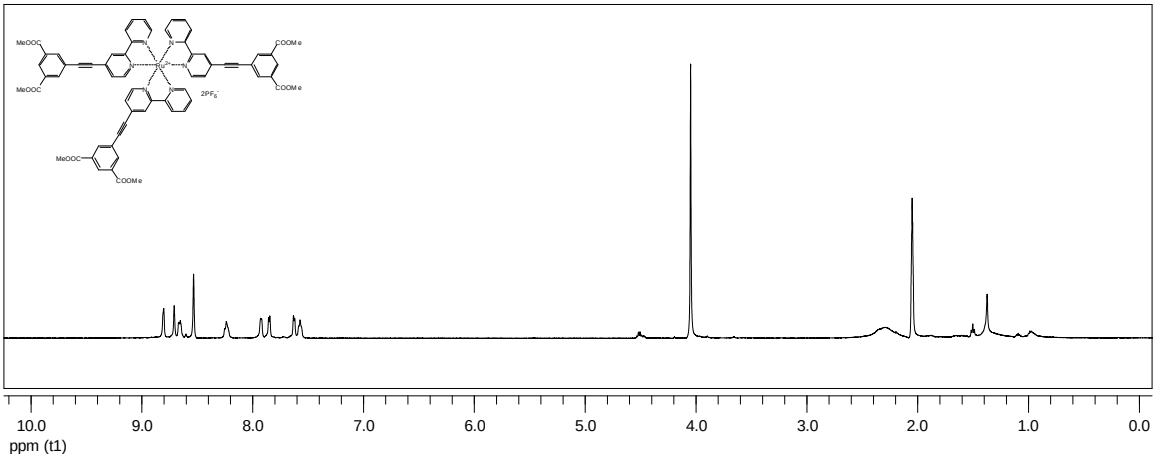

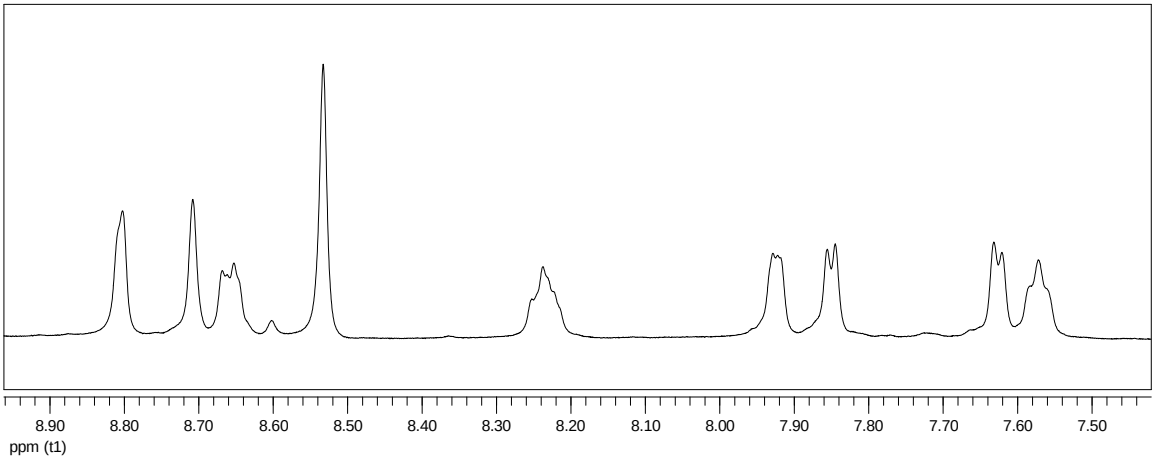

Ruthenium tris(4,4'-dibromo-2,2'-bipyridine) **26**

^{1}H NMR (methanol)-d_4:

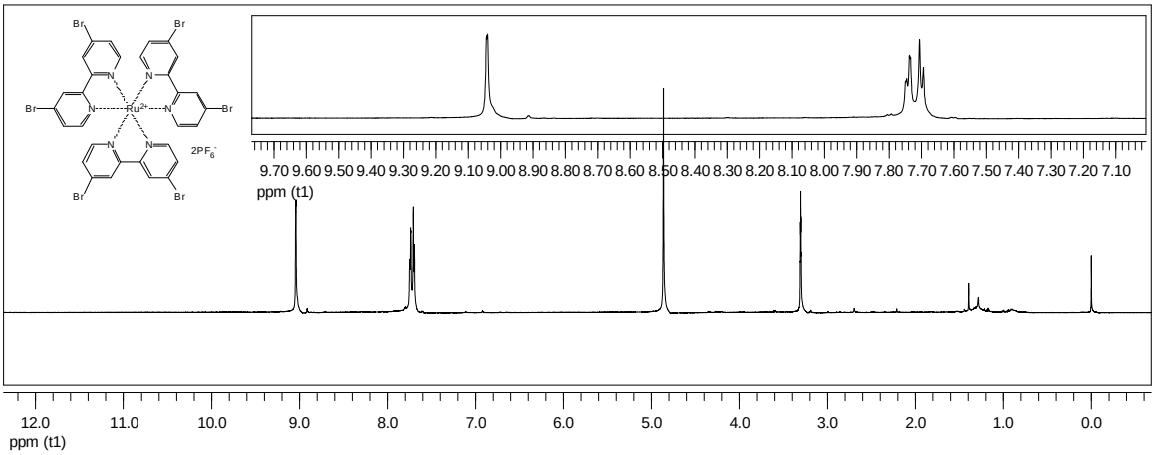

^{13}C NMR (methanol)-d_4:

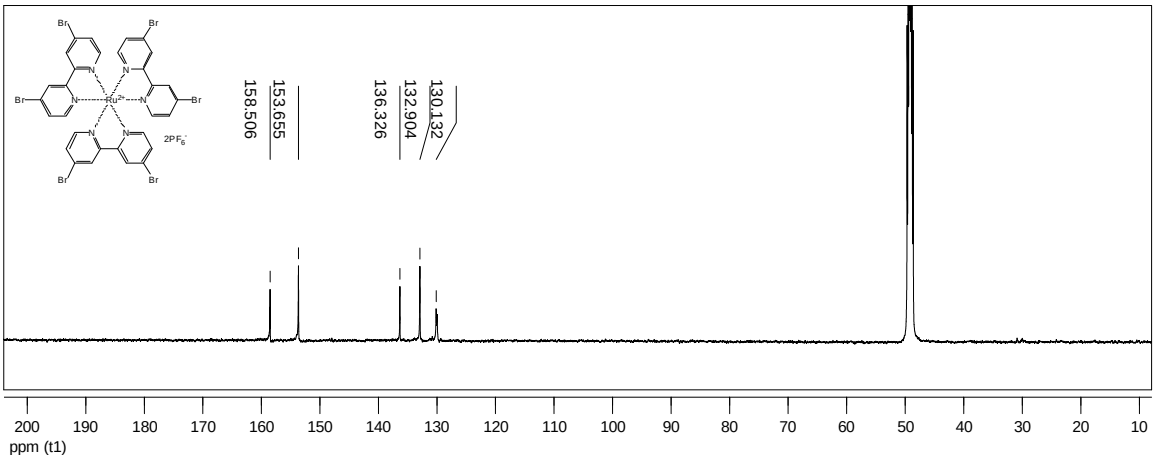

Homoleptic ruthenium complex **SSC**

^{1}H NMR (acetone)-d_6:

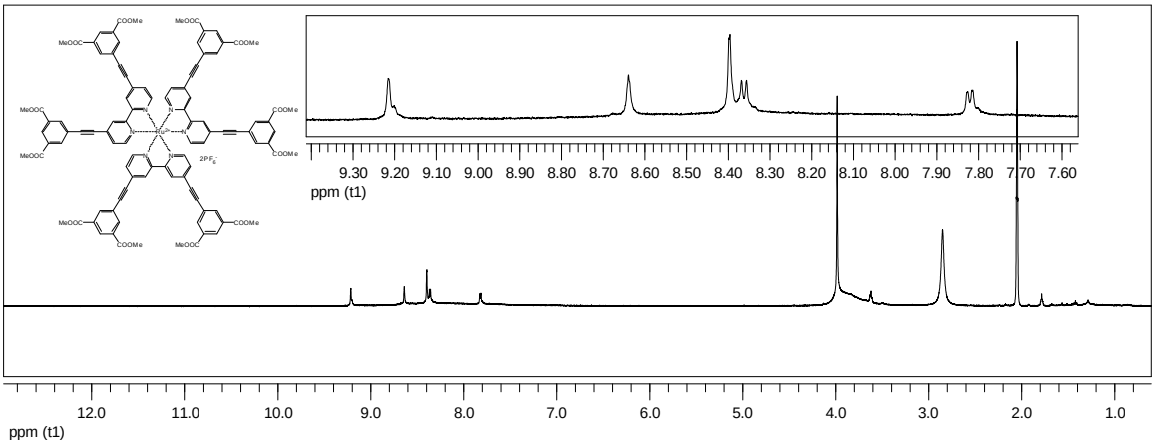

Homoleptic ruthenium complex **LSC**

^{1}H NMR (THF)-d_8:

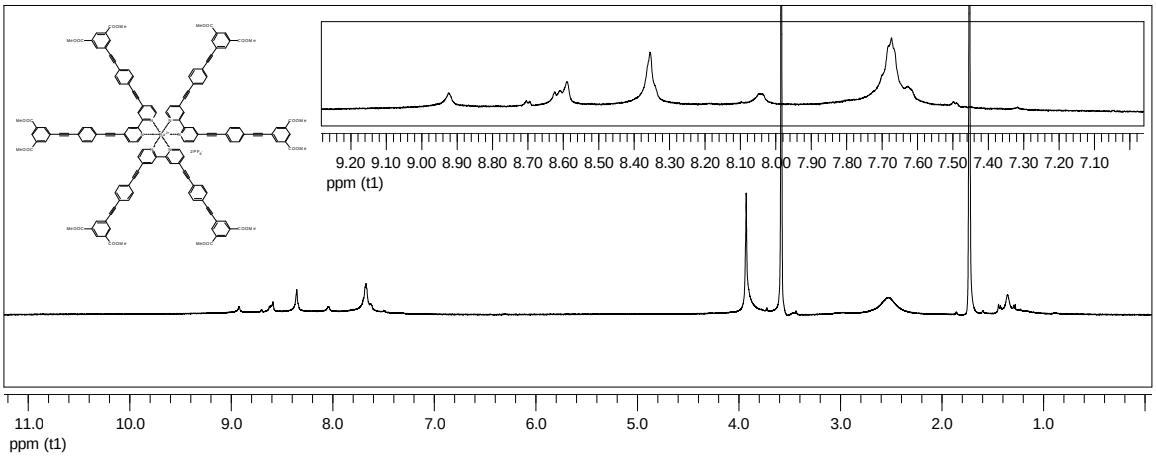

Homoleptic ruthenium complex **SLSC**

^{1}H NMR (acetone)-d_6:

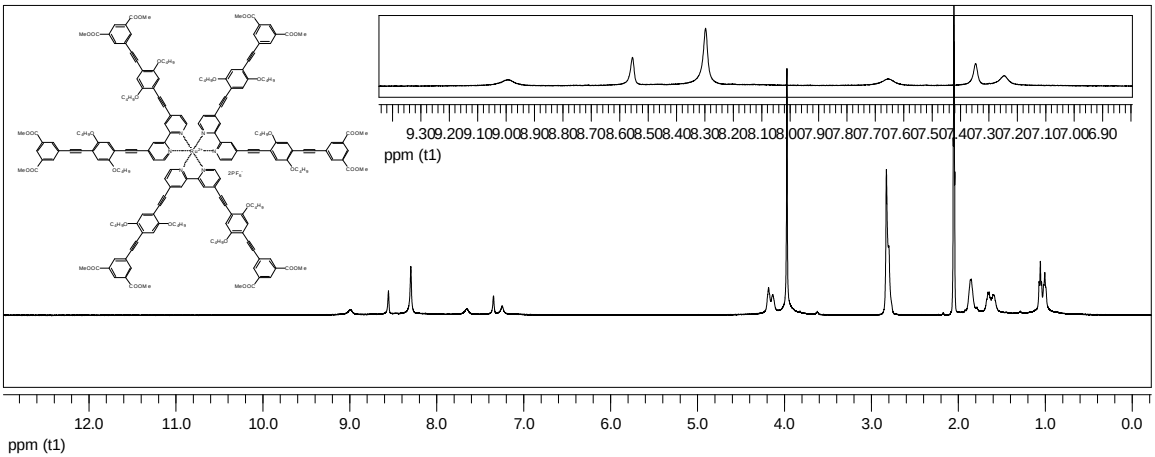

^{13}C NMR (acetone)-d_6:

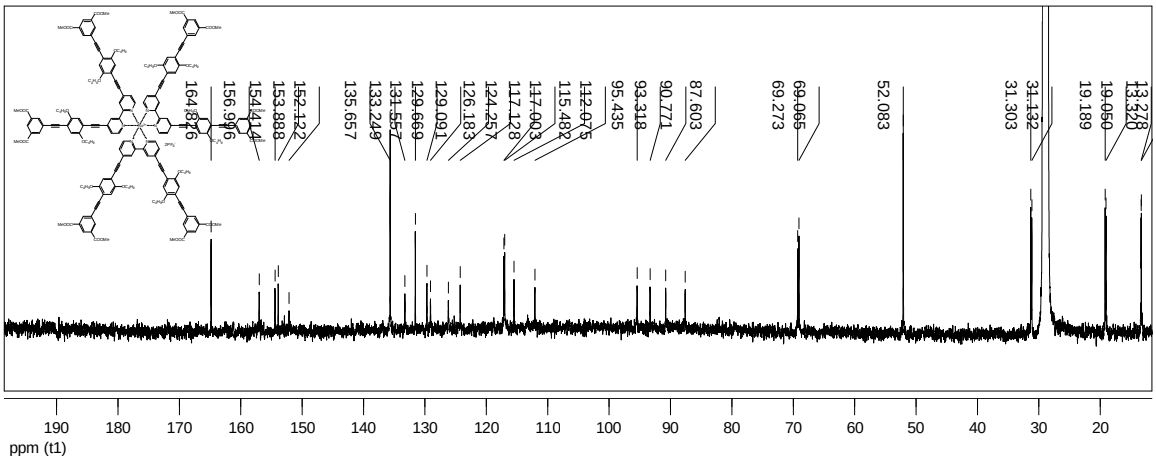

APPENDIX III CYCLIC VOLTAMMETRY

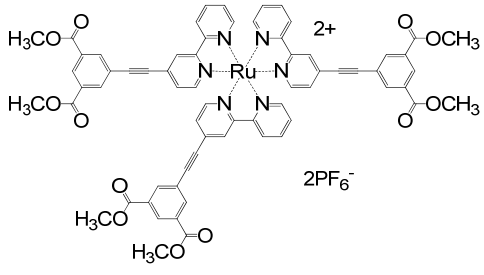

3SSC

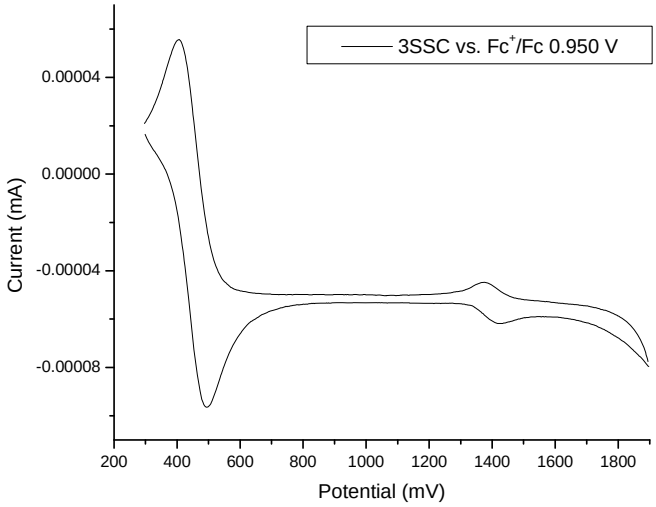

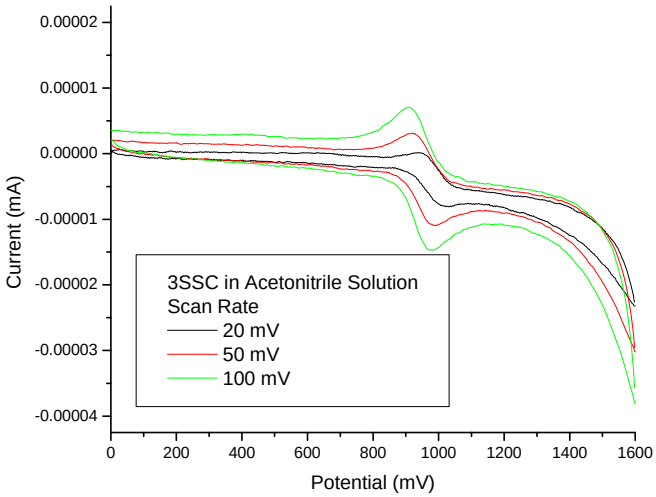

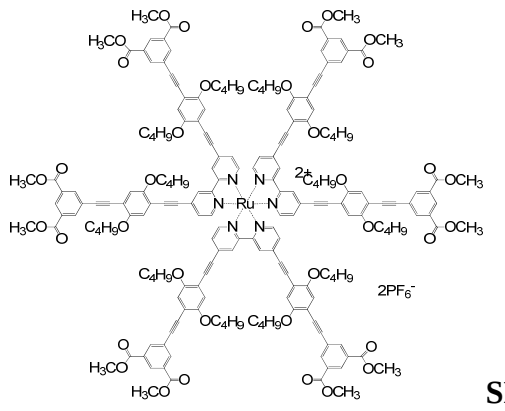
2+
2PF6-

SLSC

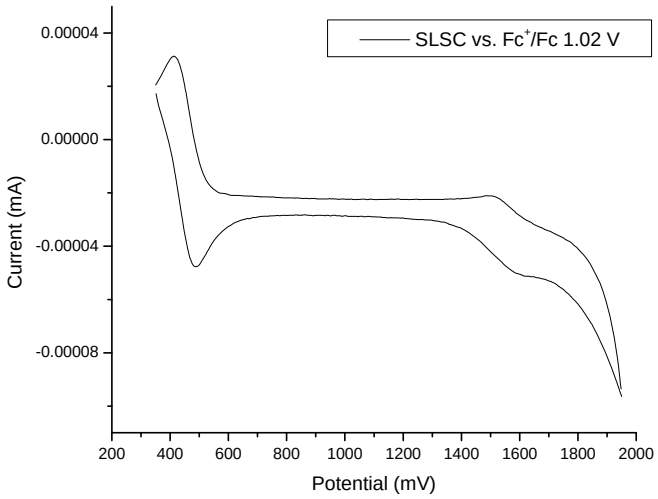
SLSC vs. Fc+/Fc 1.02 V
Current (mA)
Potential (mV)

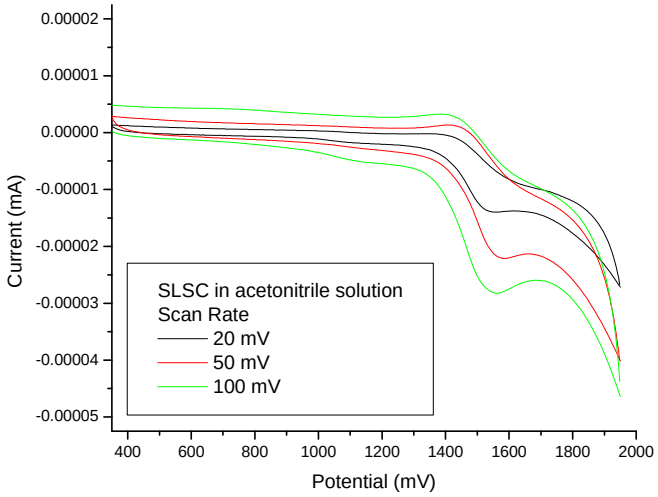
SLSC in acetonitrile solution
Scan Rate
20 mV
50 mV
100 mV
Current (mA)
Potential (mV)

VITA

Yongyi Zhang

Date of Birth	November 14th, 1980
Place of Birth	Bei Jing, P.R. China

Education

1996 – 1998	No. 4 High School, Bei Jing, P.R. China
1999 – 2003	B. S. in Chemistry, Peking University, Bei Jing, P. R. China
2004 – Present	Degree sought: Ph.D., Chemistry, Rutgers University - Newark, NJ, U.S.A.